

· ALMA MATER STUDIORUM ·
UNIVERSITÀ DI BOLOGNA

DOTTORATO DI RICERCA IN:
Automotive per una mobilità intelligente

CICLO: XXXIV

Settore concorsuale: 09/A3

PROGETTAZIONE INDUSTRIALE, COSTRUZIONI MECCANICHE E
METALLURGIA

Settore Scientifico Disciplinare: ING-IND/15 - DISEGNO E METODI
DELL'INGEGNERIA INDUSTRIALE

**Advanced voxel-based CAD
modelling for FSI simulations for
automotive structures design**

Presentata da: Antonio Bacciaglia

Coordinatore Dottorato
Prof. Nicolò Cavina

Supervisore
Prof. Alfredo Liverani

Esame Finale Anno 2022

A Laura, ai miei Genitori e a Valentina
Ai miei nonni A. E. T. e Z.

Abstract

Advanced voxel-based CAD modelling for FSI simulations for automotive structures design

by Antonio Bacciaglia

Additive Manufacturing (AM) is nowadays considered an important alternative to traditional manufacturing processes. AM technology shows several advantages in literature as design flexibility, and its use increases in automotive, aerospace and biomedical applications. As a systematic literature review suggests, AM is sometimes coupled with voxelization, mainly for representation and simulation purposes. Voxelization can be defined as a volumetric representation technique based on the model's discretization with hexahedral elements, as occurs with pixels in the 2D image. Voxels are used to simplify geometric representation, store intricate details of the interior and speed-up geometric and algebraic manipulation. Compared to boundary representation used in common CAD software, voxel's inherent advantages are magnified in specific applications such as lattice or topologically structures for visualization or simulation purposes. Those structures can only be manufactured with AM employment due to their complex topology. After an accurate review of the existent literature, this project aims to exploit the potential of the voxelization algorithm to develop optimized Design for Additive Manufacturing (DfAM) tools. The final aim is to manipulate and support mechanical simulations of lightweight and optimized structures that should be ready to be manufactured with AM with particular attention to au-

tomotive applications. A voxel-based methodology is developed for efficient structural simulation of lattice structures. Moreover, thanks to an optimized smoothing algorithm specific for voxel-based geometries, a topological optimized and voxelized structure can be transformed into a surface triangulated mesh file ready for the AM process. Moreover, a modified panel code is developed for simple CFD simulations using the voxels as a discretization unit to understand the fluid-dynamics performances of industrial components for preliminary aerodynamic performance evaluation. The developed design tools and methodologies perfectly fit the automotive industry's needs to accelerate and increase the efficiency of the design workflow from the conceptual idea to the final product.

Keywords: *Voxelization; Design for Additive Manufacturing; Lightweight structures; Topology Optimization; Additive Manufacturing; Automotive.*

Contents

Abstract	i
List of Figures	v
List of Tables	x
Acronyms	xii
1 Introduction	1
1.1 Voxel-based modelling	4
1.1.1 The main voxelization algorithms	6
1.2 Advanced modelling for AM	7
1.3 3D modelling limitations for AM: how to fill the technological gap	10
2 State-of-the-art analysis	14
2.1 Systematic literature review: Voxels & Additive Manufacturing	14
2.1.1 Additive Manufacturing applications	20
2.1.2 Additive Manufacturing technologies	23
2.1.3 Voxel-based discretization	25
2.2 Limitations and Future developments of Voxel-based mod- elling for AM	27
2.2.1 Limitations of design tools	29
2.3 Scope of the research	30

3	Additive Manufacturing technology	33
3.1	Historical background of AM	34
3.2	The design workflow with AM	36
3.2.1	Reverse Engineering and Additive Manufacturing	37
3.3	Additive Manufacturing advantages	41
3.4	Additive Manufacturing limitations	43
3.4.1	Large-scale Additive Manufacturing framework proposal	46
3.5	Additive Manufacturing applications	50
4	Voxel-based modelling for lattice structures	55
4.1	Periodic lattice structure classification	58
4.2	Lattice structures CAD modelling	62
4.2.1	Ray-tracing intersection method for voxelization	63
4.2.2	1st B-rep modelling method	64
4.2.3	2nd voxel-based modelling method	66
4.3	Voxel-based methodology for mechanical simulations	69
4.3.1	Lattice to 1D (L1D) Methodology	70
4.3.2	L1D numerical simulations	75
4.3.3	Discussion of the results of the L1D approach	77
4.4	Proposal for a 2D representation standard in drawings	82
5	Topology Optimization and DfAM	92
5.1	Vertex-based surface smoothing: state of the art	98
5.2	Optimized HC-SDU algorithm	100
5.2.1	1st version	103
5.2.2	2nd version	107
5.2.3	Discussion of the results	115
6	Voxel-based approach for fluid-dynamics analysis	120
6.1	Fluid-Structure Interaction analysis	120
6.1.1	A solution for the aerodynamic problem	121
6.2	Voxel-based panel methodology	124

6.3	Results	129
6.3.1	The Ahmed body case study	132
6.4	Discussion	138
7	Conclusions	141
	Appendices	144
	Appendix A List of scientific publications	144
	Bibliography	147

List of Figures

1.1	3D geometry modelling approaches (adapted from [3])	2
1.2	Example of CSG approach to model 3D shapes (image source [4])	2
1.3	Example of B-rep approach to model 3D shapes (image source [5])	3
1.4	Example of V-rep approach to model 3D shapes using voxels .	3
1.5	Voxel-based representation applied on a 3D model of a modern car	8
1.6	Topology Optimization application of a benchmark component	9
1.7	Lightweight lattice structures	10
2.1	SLR methodology and filtering flowcharts [30]	16
2.2	Classification of Additive Manufacturing technologies [62] . . .	19
2.3	SLR statistics after the filtering stage [30]	20
2.4	Classification of AM technologies according to ASTM terminology [35]	24
2.5	3D voxels can be seen as close relative to 2D pixels [59]	26
2.6	Exponential computing power increase over the last decades [75]	28
2.7	Relevant topics of the candidate's PhD programme; each numbered topic is the subject of a scientific contribution for indexed International Journals and Conferences available in Appendix A	32
3.1	Manufacturing costs as a function of production volumes [85] .	35
3.2	Approximation of 3D model using STL file format	36

3.3	Photogrammetry workflow to obtain a 3D digital model from a real-life object	39
3.4	Conceptual layout coupling AM and RE to produce spare parts	40
3.5	Additive Manufacturing raw material's classification (adapted from [62])	43
3.6	AM building volume subdivision and definition of common working area; simplified case with $n = 4$ extruders [84]	48
3.7	LSAM CAD handling and subdivision in n subparts	49
3.8	The perfect context where to apply the LSAM developed framework: an aerodynamic wing with a long printing time estimation [84]	50
3.9	LSAM case study applied on an aerodynamic wing [84]	51
3.10	AM applications from the incomes of Companies operating in AM, both metallic and plastics; Adapted from [112]	52
4.1	A 3D model of simple beam filled with uniform strut-and-node lattice structure using a simple cube as unit cell	57
4.2	Periodic lattice structure classification (adapted from [23]) . .	59
4.3	Unit cell topologies taken under consideration in this project [121]	59
4.4	(a) Bending vs (b) Stretching dominated lattice structures [132]	60
4.5	(a) Conformal vs (b) not-conformal lattice structures modelled using the LSWM environment in FreeCAD	62
4.6	Ray tracing along the X dimension to understand which voxels should be activated [122]	63
4.7	Graphic flowchart of the ray tracing voxelization methodology	64
4.8	The intersection of multiple struts need the placement of a sphere (for circular struts) or a cube (for square ligaments) to improve the lattice geometry	67
4.9	The 1D structure obtained through voxel-based modelling of a lattice structure starting from the 3D bulk model saved as STL file	68

4.10	L1D methodology flowchart applied on the aircraft engine bracket of GE [122]	72
4.11	View from different directions of the 3D lattice structures used to validate the L1D methodology	76
4.12	View of strain field of the cantilever beam [122]: a) full 3D model of simple cube lattice with circular cross-section; b) full 3D model of simple cube lattice with square cross-section; c) 1D lattice with circular cross-section and d) 3D equivalent bulk model using the AH method of Vigliotti et al.	78
4.13	Computational time comparison to mesh and solve the lattice structure depending on the approach used	78
4.14	Strain field view of (a) homogenized 3D model using [143] material characteristics and of (b) 1D model using the L1D approach [122]	80
4.15	An evolution in time can be noticed in design/sketching of components	83
4.16	Symbols used to describe the struts and unit cell dimensions for the proposed Standard [121]	85
4.17	Tables used in the proposed representation Standard to describe lattice structures in 2D drawings [121]	86
4.18	Case study to demonstrate the performances of the proposed representation Standard for lattice structure [121]	89
4.19	Case study to demonstrate the performances of the proposed representation Standard for lattice structure: the considered assembly on the left and the resulting 2D drawing on the right [121]	90
5.1	GUI of ToOp framework embedded in FreeCAD: view of the dialog window to insert the main parameters for a Topology Optimization simulation	95
5.2	Visual comparison between a noisy digital model and the equivalent manufactured component after digital post-processing . .	96

5.3	The application of digital post-process techniques is required before the production phase	97
5.4	<i>Optimized HC-SDU</i> flowchart	101
5.5	Pseudo-code of the 1st version of <i>Optimized HC-SDU</i> [157] . .	104
5.6	The case study used to test and compare the performances of the 1st version of <i>Optimized HC-SDU</i> [157]	105
5.7	The 3D smoothed model after 50 iterations	106
5.8	Quantitative comparison of smoothing algorithms after 50 iterations with $\alpha = 0.15$, $\beta = 0.4$ and $\lambda = 0.6307$ [157]	107
5.9	Flowchart of the <i>Optimized HC-SDU</i> 2nd version	108
5.10	Flat surfaces recognized by the <i>detect-flat-surface</i> function, using $L = 2$ [158]	110
5.11	Pseudo-code of the <i>detect-flat-surface</i> function [158]	111
5.12	Methodology flowchart of the <i>detect-holes-edges</i> function [158]	112
5.13	Pseudo-code of the <i>detect-holes-edges</i> function [158]	112
5.14	Pseudo-code of the <i>Optimized HC-SDU</i> algorithm [158]	113
5.15	Visual result of the automatic detection of the <i>no-smoothing-space</i> : (a) detection of flat surfaces (in yellow) and (b) detection of holes' edges (in red) [158]	114
5.16	The 3D smoothed models of GE bracket [158]	115
5.17	Quantitative comparison of the <i>Optimized-HC-SDU</i> smoothing algorithm applied to the GE bracket [157]	116
5.18	Detailed view comparison of the smoothed GE bracket model .	118
6.1	Different approaches to solve the flow can be used at different stages of a typical design workflow	123
6.2	Voxel-based panel method flowchart [184]	126
6.3	Discretization explanation of a Voxel-based model of a flat plate	127
6.4	Sensitivity analysis on voxel resolution for the flat plate lift coefficient at $\alpha = 2^\circ$ [184]	130
6.5	Lift coefficient vs AOA behaviour comparison using $M = 2$ and $vox_{dim} = 0.025$ [184]	131

6.6	Lift coefficient plots for finite wings and the 2D airfoil silhouettes	132
6.7	Sensitivity analysis of voxel resolution for the Ahmed body case study: the computation time (in red) and estimation error (in blue) for the Ahmed body's lift coefficient are shown . . .	134
6.8	Velocity and pressure distribution over the Ahmed body . . .	136
6.9	Comparison of estimation approaches for lift, drag and aerodynamic efficiency	137
6.10	3D voxel-based model of a complete racing car	140

List of Tables

2.1	Relevant contributions coming from the SLR using the <i>Additive Manufacturing</i> and <i>Voxel</i> keywords	18
4.1	L1D computational time changing the voxel resolution for the G.E. benchmark bracket model [122]	73
4.2	Unit cell dimensions for the case studies included in [122]	76
4.3	Comparison of mean % error on the displacements of L1D and AH approaches compared to the 3D full model analysis	79
4.4	Comparison of mean % error on the displacements of L1D and AH approaches compared to the 3D full model analysis	81
4.5	Symbolic image of three different types of periodic structures considered in the proposed Standard [121]	88
5.1	Dimensional and computational results of smoothing approaches applied to the GE bracket; the % refers to a comparison with the original model [158]	117

Acronyms

Acronym	Meaning
AM	Additive Manufacturing
DfAM	Design for Additive Manufacturing
CAD	Computer-Aided Design
CFD	Computational Fluid Dynamics
CSG	Constructive Solid Geometry
B-rep	Boundary Representation
V-rep	Volumetric Representation
TO	Topology Optimization
GD	Generative Design
STL	Standard Triangulation Language
RVE	Representative Volume Element
FEA	Finite Element Analysis
SLA	StereoLithography Apparatus
SLR	Systematic Literature Review
SLS	Selective Laser Synthesis
GDT	Geometric Dimensioning and Tolerances
GPS	Geometric Products Specifications
FGM	Functionally Graded Materials
FDM	Fused Deposition Modelling
SLM	Selective Laser Melting
LENS	Laser Engineered Net Shaping

Acronym	Meaning
PMI	Product and Manufacturing Information
CD	Concrete Deposition
DLP	Digital Light Processing
RTI	Ray Tracing Intersection
ASTM	American Society for Testing and Materials
AMFF	Additive Manufacturing File Format
GUI	Graphic User Interface
CAM	Computer-Aided Manufacturing
RP	Rapid Prototyping
EBM	Electron Beam Melting
LBM	Laser Beam Melting
RE	Reverse Engineering
UAV	Unmanned Aerial Vehicle
LSAM	Large-Scale Additive Manufacturing
PLA	PolyLactic Acid
DED	Direct Energy Deposition
TPMS	Triply Periodic Minimal Surface
ISO	International Standard Organization
AH	Asymptotic Homogenization
SIMP	Solid Isotropic Material with Penalization
ESO	Evolutionary Structural Optimization
BESO	Bidirectional ESO
NURBS	Non-Uniform Rational Basis Spline
SDU	Scale-Dependant Umbrella
HC-algorithm	Humphrey's Classes algorithm
FSI	Fluid-Structure Interaction
AOA	Angle of Attack

Chapter 1

Introduction

To represent 3D models, many geometrical approaches co-exist in the scientific literature (Figure 1.1). For example, the Constructive Solid Geometry (CSG) method employs a set of primitive geometric shapes (i.e. spheres, cuboids, cylinders and so on) that are combined through Boolean operations such as union, intersection and difference (Figure 1.2). Another category of geometry representation technique is the Boundary Representation (B-Rep) methodology, representing the shapes using the limits, namely the boundaries (Figure 1.3). On the one hand, the B-rep method represents a solid by its surfaces and so defines an interior and an exterior; the limiting surface of solid consists of a set of well-organized faces. On the other hand, Volumetric Representation (V-rep) methods, such as the voxelization, is a modelling method for representing shapes using the volumes [1]. Among different techniques, voxel-based modelling is particularly interesting for this research. The voxelization method often supports the tri-dimensional (3D) object's visualization in Computer-Aided Design (CAD) software. This visualization method is based on the employment of elementary volumes called voxels, which can be seen as pixels in 2D images (Figure 1.4). Compared to common 3D representation techniques, such as B-rep, voxel-based modelling is capable to handle a higher amount of data, storing the details of intricate interiors of 3D models and can speed up geometry manipulations and

operations, like boolean operations, rotations and so on [2].

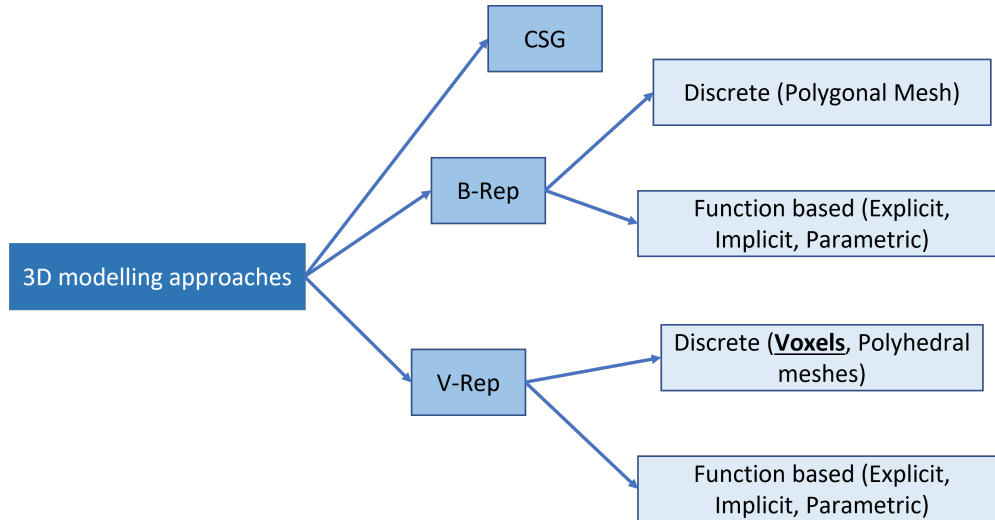


Figure 1.1: 3D geometry modelling approaches (adapted from [3])

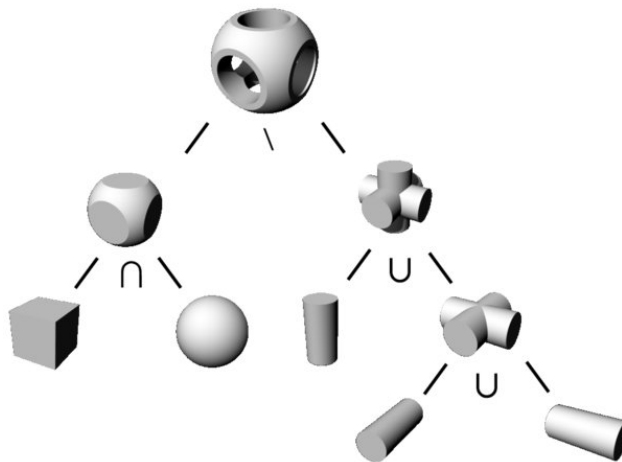


Figure 1.2: Example of CSG approach to model 3D shapes (image source [4])

Voxel-based models are mathematically represented by a 3D logical matrix made of true (1) or false (0) values depending on the belonging of the single voxel to the 3D model's material or the void. Even though voxelization is a 3D discretization, and so an object's discretization, this visual-

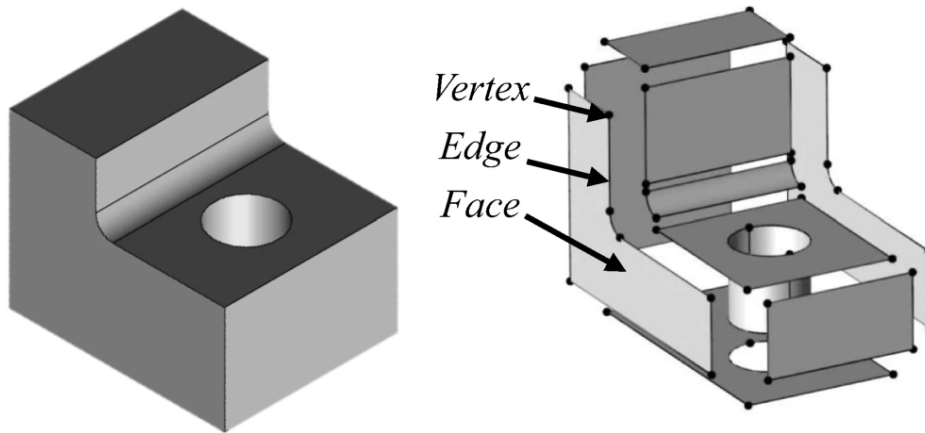


Figure 1.3: Example of B-rep approach to model 3D shapes (image source [5])

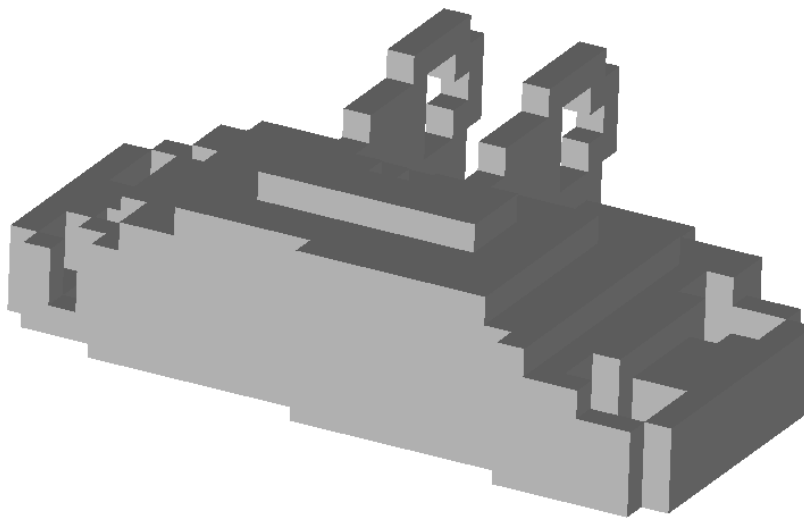


Figure 1.4: Example of V-rep approach to model 3D shapes using voxels

ization methodology can decrease the computational time requirements to analyse, visualise and modify complex 3D models. Moreover, it could also speed up structural and CFD numerical simulations by using the same object's discretization of the volume of interest. For example, [6] describes the application of voxels in the automotive field for structural and thermody-

numeric numerical simulations. The authors reveal a huge decrease of computational timing required to run the simulations thanks to the voxel-modelling that substitute the classic meshing process exploiting tetrahedral elements. Moreover, Torigaki et Al. highlight that voxel-based modelling reveals fundamental when dealing with complex shapes coming from design optimization tools. Indeed, voxelization rarely fails due to the simple unit cell topology, compared to more complex discretization methods. The mentioned advantages amplify when dealing with very complex structures as lattice structures or those optimized through specific routines as the Topology Optimization (TO) [7] or Generative Design (GD) [8]. Furthermore, the 3D model conversion into a Standard Triangulation Language (STL) file format [9], used as a standard in Additive Manufacturing, is more straightforward and hardly falls through.

1.1 Voxel-based modelling

While CSG modelling is a rapid technique to create simple geometries, when the objects to be represented have complicated 3D forms, such as biological systems, the surface representation may not be precise enough. B-rep, on the other hand, uses basic geometric elements to represent linking faces, edges, and vertices locally. As a result, it is more adaptable and frequently produces an accurate 3D depiction. It does, however, need more advanced CAD abilities, and all modelling must be done manually, which is time-consuming [10]. As a result, neither CSG nor B-rep is well-suited to designing bespoke 3D-printed components. This is particularly true in biomedicine, where voxel-based hexahedron meshing is commonly employed because of the absence of geometrical constraints. Indeed, the components are generated straight from the Computer Tomography scans, making it a rapid and fully automated mesh production approach [11].

Voxelization is a numerical process that enables the conversion of a polygonal object into a 3D voxel-based model. The V-representation, using voxels,

is becoming more and more popular in CAD software in the last few years, considering the complexity of the components that is increasing in the last decades, following the manufacturing technology evolution.

The CAD 3D modelling is characterized by the representation of a real object through a mathematical model. A 3D model is constituted by two key stages which are the modelling and the representation. In the former, the computer uses the software to generate the 3D model while in the latter, the object is represented and stored in the computer memory. In the V-rep, a real object is represented using unit elements, called voxels and it is stored as a logical matrix to describe multiple layers of voxels.

In many voxelization algorithms, a 3D grid is superimposed over the 3D model. Thanks to this grid, it is possible to understand if the real object occupies or not a single unit cell, namely a voxel. For each voxel, a binary value is assigned and the 3D logical matrix is populated: 0 if the unit cell is outside the 3D model and 1 otherwise.

Voxelization is a modelling technique that allows to simplify the representation and uniform it for all the 3D models. Compared to other 3D modelling techniques, voxelization allows to achieve faster and more immediate geometry manipulations and to rapidly evaluate the object's properties, interferences, collisions and simulations. Sometimes it is used to evaluate the overall part's volume when it is not possible to evaluate it automatically. The best advantage of a voxel-base representation is the immediate comprehension of the model's interior; a section of the model can be easily obtained by deleting layers of a voxel of the logical matrix. This is extremely important in applications when dealing with complex structures such as aerospace and automotive lightweight components or in biomedicine, to better understand the organ or tissue composition. Moreover, despite higher computational demand, as the voxel resolution increases, more precise and accurate 3D modelling will be achieved. However, the V-rep through voxels has also some limitations, such as an approximated representation and the aliasing.

Currently, voxels are used to accurately determine volumetric data in a

variety of scientific fields. Voxel modelling techniques are frequently used by geologists to simulate geological elements such as topography and elevation. Researchers can compare variations in brain tissue concentration using voxels in V-rep morphometry [12]. More broadly, voxel-based modelling may be used by scientists to visualize and estimate the volume of everything from fluids to green areas in cities.

1.1.1 The main voxelization algorithms

In the literature, there are several voxelization algorithms available that have a sufficient level of fidelity and accuracy. These methodologies can be divided into two main families which are the volume sampling [13] and the implicit function approaches [14]. The former converts a 3D model by occupying the space: a 3D voxel grid is placed over the model and for each voxel, the algorithm decides if the unit cell is inside or outside the object. This kind of approach is easy to be implemented and robust, even if the computational requirements are higher compared to the other approach. The latter uses a voxel grid evaluated through a function of the object's surface; in this way the voxelization occurs only near the object, saving computational power required, but the suffering of issues related to the voxel resolution.

Among the volume sampling techniques, the *parity-count* uses 'V' rays that originate from the centre of a voxel and intersecting the object [15]. An odd number of intersections means that the voxel is inside the object, while an even value means that the voxel is outside the 3D model. A limitation of this approach is the presence of holes in the external surface of the model that could be not considered during the method. To take into account these features, additional rays should be considered in the directions not examined before.

A similar approach is called *ray stabbing* that uses rays as the previous method [16]. However, here the algorithm considers only the first and last intersection points of the object. Indeed, a voxel will be evaluated using only these two information and will be considered inside the model if it is between

the two interacting points, otherwise, it is outside the object.

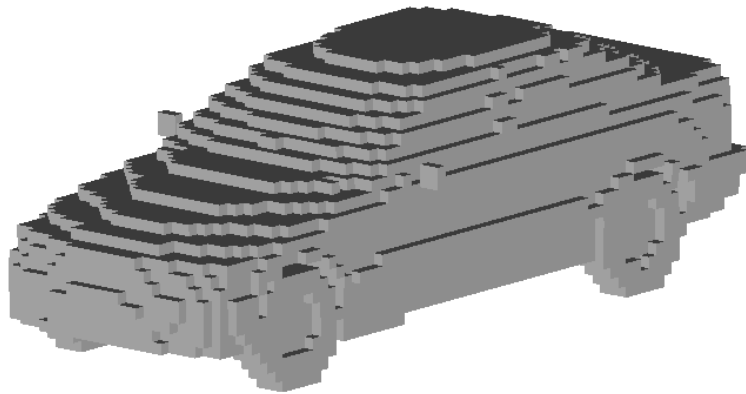
The last strategy, known as *ray-tracing intersection*, is similar to the ray stabbing method [17]. This algorithm will be the reference approach for the entire PhD project due to its robustness and easiness. The algorithm ray-traces in all the three main directions (x, y and z) and combines the results coming from the different dimensions. Specifically, having at disposal an STL file of the 3D model, for each triangle, the voxelization follows the succeeding steps:

- Determine the edges of the triangle;
- Compute the opposite vertex of the selected edge;
- Find the ray relative to the selected edge;
- Check if the relative ray is on the identical side of the selected edge;
- If the check is positive for all the edges of the selected triangle, then it is undoubtedly that the ray flows through the facet and for this reason, the matrix element should be activated.

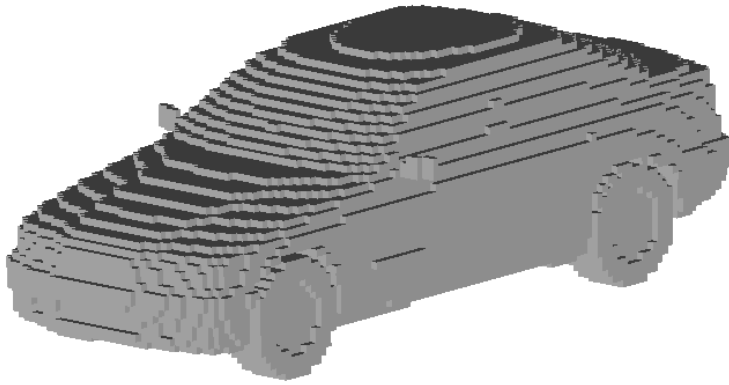
An example of the ray-tracing intersection voxelization applied on a 3D model of a modern car can be seen in Figure 1.5 using three different voxel resolutions (coarse, medium and fine).

1.2 Advanced modelling for AM

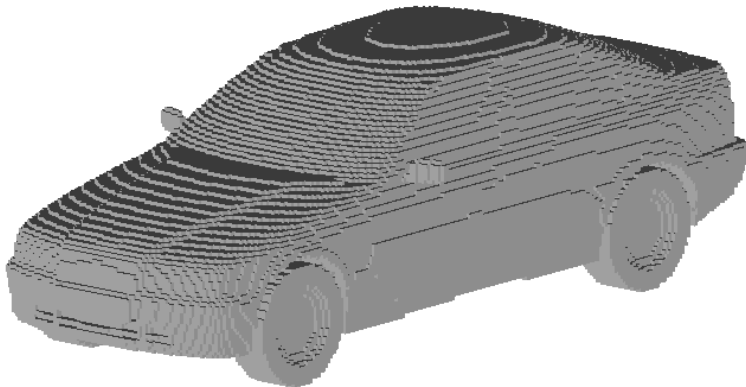
The research for lightweight design is a key factor in industrial applications as high-performance automotive [18], aerospace [19] and even biomedical [20]. Decreasing the overall means of transport weight reflects on high performances, less fuel consumption and lower emissions. In this engineering context, TO is a recurring theme in recent scientific contributions. The Topology Optimization methodology is an optimization approach in which the shape of the component is optimized to minimize a fitness function, usually defined as the structure compliance or in other words, the strain [21].



(a) Coarse voxel resolution (53728 voxels)



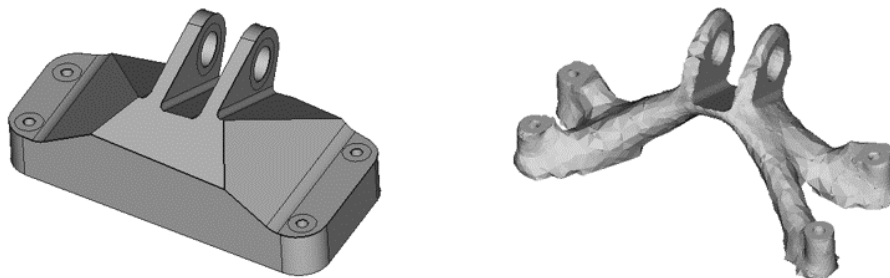
(b) Medium voxel resolution (183120 voxels)



(c) Fine voxel resolution (1422435 voxels)

Figure 1.5: Voxel-based representation applied on a 3D model of a modern car

This optimization occurs according to known boundary conditions, such as the load condition, the constraints and the control volume which is discretized using voxels. The algorithm can understand if the unit voxel should be activated (presence of material) or deactivated (absence of material) to satisfy a volume fraction percentage the designer imposes a priori. In such a way, the overall structure weight can considerably decrease. However, TO algorithms usually return very intricate shapes which are impossible to be manufactured using traditional processes based on casting or material removal by chip removal operations such as turning, milling or drilling (Figure 1.6). In this context, Additive Manufacturing is becoming the leading process to manufacture very complex shapes due to the design flexibility and accuracy offered by AM [22]. With the employment of AM machines, the reduction of component's weight becomes an ordinary distinguishing feature, along with higher structural performances and acceleration of the design-to-manufacturing cycle.



(a) Bulk 3D CAD model of GE bracket

(b) Optimized 3D model of GE bracket
using own programmed TO tool

Figure 1.6: Topology Optimization application of a benchmark component

On the same design direction, namely the weight reduction, bio-inspired trabecular structures, called lattices, have been introduced in industrial applications [23]. These kinds of components are characterized by the repetition of a representative volume element (RVE), of at least one order of magnitude smaller than the full component, that is repeated in the space (Figure 1.7). Such RVE can be associated with a voxel that is repeated in the space for

lattice's design and simulation purposes. Lattices can be made by a combination of several materials or materials and voids revealing unique structural properties. The internal structure can be stochastic or periodic, with the latter revealing higher stiffness compared to the former, making them very attractive for structural applications ([24], [25]). Different parameters describe the lattice structure configuration, such as the pattern, the external surface conformity, the internal progressiveness and the choice of the unitary cell element. Moreover, lattices can be optimized in the highly stressed regions and unloaded where the material is not necessary using the TO process previously described. It is straightforward that such trabecular structures are characterized by high shape complexity making them manufacturable only by additive processes, using AM machines.

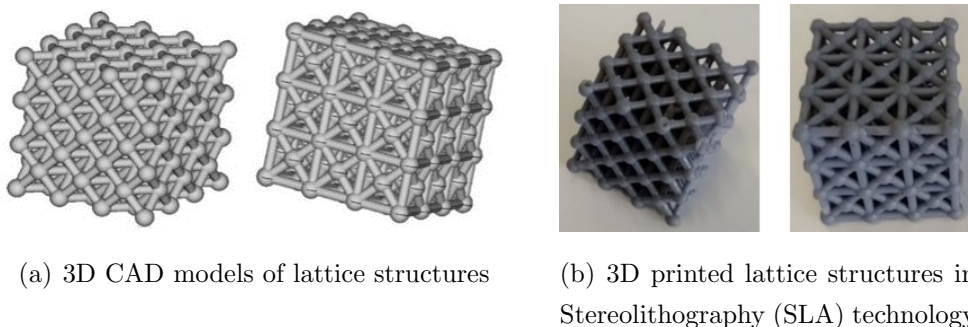


Figure 1.7: Lightweight lattice structures

1.3 3D modelling limitations for AM: how to fill the technological gap

However, there is an important technological gap in the industrial engineering field when highly optimized structures are employed searching for lightweight design, such as topologically optimized components or lattice structures. Indeed, designing them using common CAD software is still challenging because many software still lacks optimized routines for lightweight

structure design, focusing only on common 3D bulk models. Indeed, manually designing and describing very complex shapes as TO structure and lattices is challenging for designers and would require high computational power used in a non-efficient way. Thus, voxel-based CAD modelling could help the users to deal with lattices and TO structures that are very attractive for engineering applications.

Another obstacle for lattice widespread diffusion is their numerical simulation. To predict the mechanical behaviour of lattice structures, Finite Element Analysis (FEA) techniques should be employed. Due to the lattice shape's complexity, huge computational power is required to discretize the structure, if no simplification method is used. Subsequently, traditional FEA solutions are impracticable in a real industrial context, where the design-to-manufacturing cycle is accelerated as much as possible. This comes to the fact that a high-quality mesh that well captures the lattice characteristics, would be made of an enormous amount of elements, slowing down the computations and making the method less effective. To get the structure behaviour in a fast and easy way, the homogenization methodology was developed and treated in many scientific contributions as done in [26] or in [27]. This mathematical procedure allows substituting the complex topology of lattices with an equivalent bulk component with the same volume and equivalent mechanical properties. As the contributions available in the literature show, the results accuracy justifies the simplification method, with a computational time of several orders of magnitude lower compared to the simulation of the full 3D lattice model.

To summarise, it is important to highlight that nowadays the common CAD software and design tools are not able to reproduce and model complex structures, such as the lattice structures or geometries coming from Topology Optimization routines. All the tools are commonly collected with the current terminology *Design for Additive Manufacturing (DfAM)* since all the models have to be manufactured employing AM as the main production process [28]. Moreover, there is still a lack of Finite Element Method (FEM) optimized and

user-friendly integration for the previously cited structures as it happens for common bulk components. This technological gap does not allow us to have a rapid idea of the mechanical behaviour and the stress distributions in the material, slowing down the design process. This is the perfect context where a voxel-based framework for 3D model handling, integrating all the DfAM rules and strategies, could be beneficial to increase the design tools efficiency available for the final user to model highly optimized structures, commonly used in the automotive and aerospace applications. As the reader can understand, the voxel-based modelling, core of the candidate's PhD project, thus, is highly interconnected with Additive Manufacturing, TO methodology, and lattice structures. Indeed, these related research topics will be treated in this dissertation.

As it becomes evident from this brief introduction, the scope of the PhD project is to develop voxel-based design tools and routines for complex structures manufacturable with Additive Manufacturing strategies. This framework, made of different tools, should be capable to support the design, the mechanical and fluid-dynamics analyses of optimized components and could be embedded in open-source CAD software, i.e. FreeCAD, with the help of external software for challenging tasks, such as MATLAB or Nastran/Patran.

The dissertation is structured as follows. In Section 2, the author presents a state-of-the-art review of voxel-based modelling specifically oriented towards AM. Section 3 will briefly describe the Additive Manufacturing technology, its advantages and challenges, along with some applications in the automotive field. In the following, Section 4 will mainly focus on lattices structures, their issues when dealing with FEA and a proposal for 2D representation in technical drawings. Then, Section 5 spotlights the need for external surface post-processing when dealing with Topology Optimization algorithms to make the 3D voxel-based models ready to be manufactured with AM. As the last main topic, in Section 6, the author presents a voxel-based tool for fluid dynamics analyses of simple geometries, very attractive for preliminary design stages, when the designer is asked to find an optimal

solution among a large configuration set in a fast and accurate way. Section 7 will close the work, pointing out the pros and limitations of the research, establishing the main results achieved during this PhD programme. As of last, a brief description of future developments will close the dissertation.

All the research contained in this work is extracted from the contributions published in international scientific journals or presented in international conferences during the PhD programme. The full list of the personal disseminations is available in Appendix A.

Chapter 2

State-of-the-art analysis

As it emerged from the Introduction, in the scientific literature, V-rep and particularly voxel-based modelling are considered more than interconnected topics with the Additive Manufacturing technology. Indeed, voxelization shows its best performances when dealing with complex 3D models which are usually fabricated with AM. Due to this strong coupling, my first concern was to understand how the scientific community deals with voxel-based modelling applied to AM. To fulfil this task, the PhD project started with a literature review to understand the state of the art of scientific contributions dealing with these themes. To obtain an objective and comprehensive review of the available contributions, a Systematic Literature Review (SLR) methodology, developed by Booth [29], was applied. This Chapter collects the main results of this SLR about *Voxel* and *Additive Manufacturing*, and for further details, refer to the own publication [30].

2.1 Systematic literature review: Voxels & Additive Manufacturing

On the one hand, AM is a technology production process with several advantages as higher reliability of one-piece parts compared to assemblies of bolted parts (e.g. time has to be spent to check connections in environments

where vibrations are important). Moreover, higher strength to weight ratio can be achieved because of high design flexibility with few by far limits in shape compared to traditional machining where shape must comply with geometrical and production constraints [31]. Additive Manufacturing application ranges from aerospace to components designed for high-performance racing cars, up to practitioners developing Do-It-Yourself (DIY) projects [32]. On the other hand, voxel-based modelling allows for the management of complex shapes, mainly manufactured with AM, that other geometrical modelling technologies would do with some difficulties. Voxelization is based on the discretization of 3D models with elementary hexahedral volumes, called voxels, to speed up geometry operations, manipulation and interior visualization [33]. Due to this strong interconnection, the scope of [30] is to evaluate the state of the art in voxel-based representation and to discuss the methodology evolution. Particular attention is given to advantages and challenges and the application of voxel-based modelling for AM in the engineering field to understand where we are at the moment and where to focus in future research. The SLR literature methodology can return objective and reproducible results and is particularly suitable to capture literature gaps [34]. The SLR methodology is divided into different steps according to Figure 2.1 (a).

After planning a time window of 5 years from 2013 to 2018 (this SLR comes from my 1st PhD year), and the more famous scientific databases (e.g. Scopus, Web of Science, IEEE and so on), the scope of the literature review was defined to answer to specific questions:

- **Q1:** What is the state of the art of voxel-based modelling applied to complex shapes to be manufactured with Additive Manufacturing?
- **Q2:** What are the potential future developments of voxel-based methodology in Additive Manufacturing?

To answer them, a large set of relevant publications are filtered from the selected database by searching with the string "Additive Manufactur-

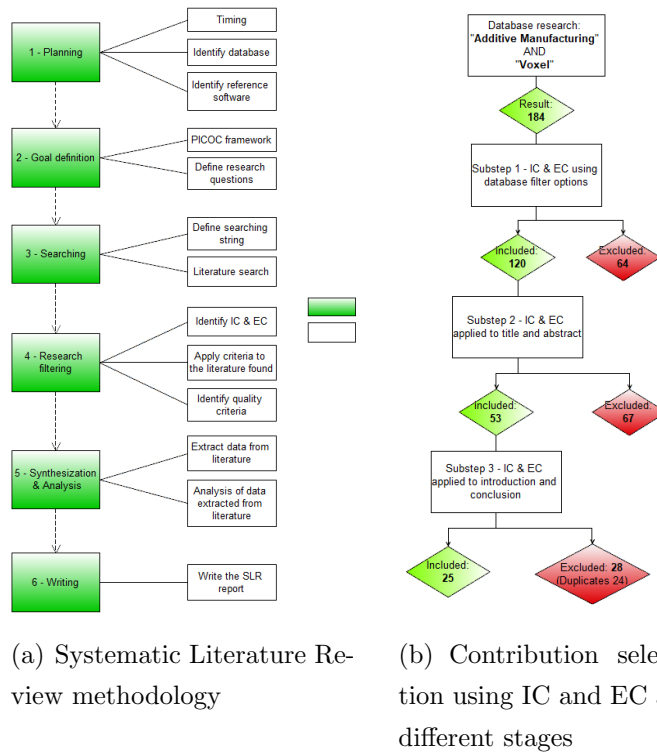


Figure 2.1: SLR methodology and filtering flowcharts [30]

ing” AND ”Voxel” in the contribution’s metadata. The search resulted in 184 publications (duplicates included) on the 10th of December 2018 and in this Chapter, the outcomes from this SLR will be summarized. To filter a large amount of the selected contributions, some inclusion (IC) and exclusion criteria (EC) are applied. These try to select only the specific contributions dealing with recent international research about voxel-based modelling for geometry manipulation and/or discretization in AM as the primary task of the studies. Thanks to the application of these criteria at different stages and deleting the duplicates, 25 out of 184 references have been identified as relevant contributions (Figure 2.1 (b)).

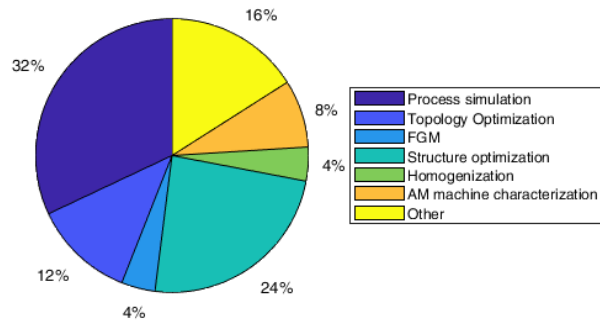
The resulting contributions were deeply analysed and subdivided into five categories to get interesting statistics and recurring topics from each paper (Table 2.1). The categories chosen for the scope of the literature review are:

1. *Engineering field of application*: the applicability sector of the research;
2. *Additive Manufacturing application*: the task or the technology the AM developed algorithm has to fulfil;
3. *Additive Manufacturing technology*: the different AM processes, using the ASTM terminology [35] and according to Figure 2.2;
4. *Software platform*: the programming language or software used to develop the algorithm;
5. *Voxelization use*: the voxel-based final aim.

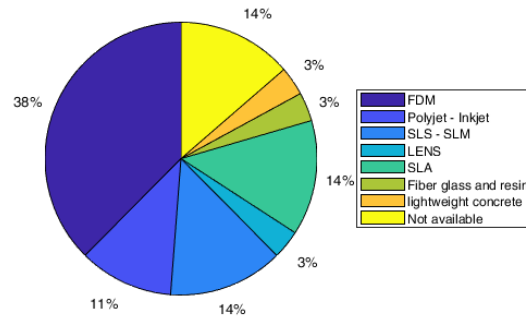
It directly emerged that about 80% of contributions deal with industrial engineering applications, while biomedicine accounts for 12% of the total contributions. Among the industrial engineering areas, the automotive and aerospace industries more than the other relies on AM process due to high design flexibility, high customization and the possibility to adopt lightweight design solutions. Just 8% belongs to niche AM applications, such as civil and exterior design. This trend is also confirmed by recent surveys about the AM fields of applications [36] and it is in complete agreement with the expectations because industrial and biomedical requirements perfectly fit with AM characteristics. Moving to the software platform, many of the contributions use Matlab, Python and OpenCL (an open-source framework based on C) to have the highest level of writing codes and own routines. The other three categories give more interesting results and will be analysed separately, and a graphical preview of their statistics is collected in some charts coming from [30] and visible in Figure 2.3.

Ref.	Engineering field	AM application	Software	AM technology	Voxel employment
[37]	Industrial	Process simulation	not specified	LENS	geometry discretization
[38]	Industrial	Topology optimization	Monolith	Material jetting	Material deposition unit
[39]	Industrial	Process simulation	Lsulpt, Matlab	SLS	geometry discretization
[40]	Industrial	Process simulation	Matlab	FDM	Geometry discretization
[41]	Industrial	FGM	Comsol	MIP-SL	Material deposition unit
[42]	Industrial	Structure optimization	Matlab	FDM-SLA	Geometry discretization
[43]	Industrial	Structure optimization	OpenCL	SLA-SLS	not specified
[44]	Industrial	Topology optimization	not specified	not specified	Geometry discretization
[45]	Industrial	Smart material	Grasshopper	not specified	As matter constituents
[46]	Industrial	PMI	not specified	FDM	Geometry discretization
[47]	Industrial	File format for FRC	not specified	SLM	Material deposition unit
[48]	Industrial	AM machine characterization	Alicona, SPIP	DLP	Material deposition unit
[49]	Industrial	Lattice degradation	Catalyst, ABAQUS	FDM	Geometry discretization
[50]	Biomedical	Structure optimization	Materialize	Material jetting	Geometry discretization
[51]	Industrial-Design	Structure optimization	Grasshopper, Rhinoceros	FDM	Geometry discretization
[52]	Industrial	AM machine characterization	not specified	Fiber glass and resin	Material deposition unit
[53]	Civil	Structure optimization	Grasshopper, Rhino, Ansys	CD	Geometry discretization
[54]	Industrial, Biomedical	Topology Optimization	not specified	SLS-FDM	Geometry discretization
[55]	Biomedical	Process simulation	ImageJ	FDM	Image discretization unit
[56]	Industrial	Process simulation	OpenGL	FDM	Geometry discretization
[57]	Industrial	Homogenization	not specified	FDM	Geometry discretization
[58]	Industrial	Process simulation	Matlab, ABAQUS	FDM	Material deposition unit
[59]	Industrial	Structure optimization	Matlab	not specified	Geometry discretization
[60]	Industrial	Process simulation	C++, OpenCL	not specified	Geometry discretization
[61]	Industrial	Process simulation	Matlab, Android studio	FDM	Geometry discretization

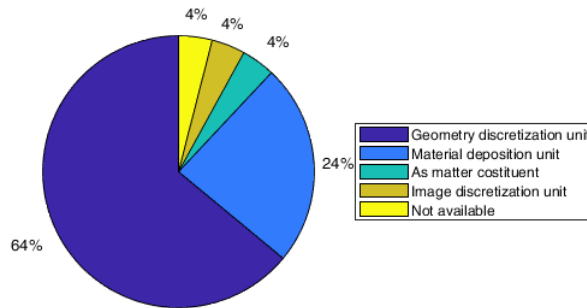
Table 2.1: Relevant contributions coming from the SLR using the *Additive Manufacturing* and *Voxel* keywords



(a) Voxel-based modelling for Additive Manufacturing



(b) Additive Manufacturing technologies



(c) Voxel-based modelling scope

Figure 2.3: SLR statistics after the filtering stage [30]

2.1.1 Additive Manufacturing applications

According to Figure 2.3 (a), one-third of selected contributions employ voxel-modelling to simulate the Additive Manufacturing process to under-

stand the deposition technique, to have a quotation of the overall process and detect possible imperfections.

In particular, from the literature review, it emerges that is important to estimate the time, costs and material consumption during the AM process to optimize it and make AM attractive compared to traditional manufacturing processes. This is done with a developed framework for the Selective Laser Synthesis (SLS) technique to estimate in real-time the building time, the material waste while optimizing the model's orientation to minimize the surface roughness [39]. As a step forwards, [40] and [61] developed a voxel-based algorithm to investigate manufacturing feasibility according to the DfAM rules. Another interesting adoption of voxels, is the development of frameworks for AM process simulation, such as the one described in [37] or in [60] for industrial applications and in [55] for biomedical one. The voxel-based environment is used to simulate the thermal behaviour of the deposition process. This information is useful to understand the solidification rates, voids and residual stresses inside the component which have a big impact on structural applications during the operative life. By simulating the AM process, it is also possible to detect and decrease semantic and printing errors, as done with a voxel-based framework to prevent under and over-extrusion in real-time, analysing layer after layer the model [56] and [58]. A hybrid approach that exploits both quotation and simulation purposes is described in [46] where the 'distance' between the 3D model and the corresponding manufactured part is evaluated in a voxelized environment. Authors combine the Geometric Dimensioning and Tolerances (GD& T) or the Geometric Products Specifications (GPS) standards (based on B-rep visualization) and the voxel-based modelling in a hybrid approach.

Another recurring theme in the selected literature is the development of voxel-based frameworks for TO or structure optimization. Thus, TO could be seen as a subset of structure optimization routines where the geometry is optimized simply by removing material from the domain volume, while TO is more specific in the minimization of a fitness function regarding the mechan-

ical properties of the component. Indeed, TO allows the creation of complex structures knowing the desired volume fraction, the applied forces and the boundary conditions when lightness and material strength should be maximized for specific industrial applications [63]. On the one hand, [38] and [44] developed innovative TO frameworks to optimize the inner lightweight structures of 3D components, even considering the manufacturing uncertainties of AM as anisotropy, defects, concentrated stresses and so on [64]. On the other hand, to minimize the material waste during AM production process, [42] developed an algorithm to optimally hollow the voxelized components in specific regions (not critical from a structural point of view) and meanwhile optimize the AM process parameters. Moreover, [54] developed an algorithm to optimize the infill of complex structures with porous bone-like structures and compare them with the classic TO approach [65] with interesting results in terms of overall compliance.

As stated in Chapter 1, another interesting topic that correlates voxel-based modelling and AM is the design and simulation of lattice structures or more in general of the Functionally Graded Materials (FGM). FGMs are used in biomedicine [50] and in high-performance industrial applications thanks to the gradual variation of structural performances along with the component by varying the inner composition and structure. FGM can be obtained by optimizing local material properties; then the material is translated into a voxel-based model for local composition as it is done in 2D pictures with a half-toning methodology. [41] exploits these interesting characteristics to propose a method to generate FGMs that can be obtained through AM following the DfAM rules.

Lattice structures are components with high shape complexity widely used in aerospace and automotive due to the high stress-to-weight ratio offered. They are made of small elements repeated in space to form the overall component [23]. Lattices can be designed [59] or analysed by exploiting a voxel-based environment [49] better than B-rep due to the inherent structure complexity, especially for interior characterization. However, from the analy-

sis of the relevant literature, it emerged that the structural analysis of lattice structures is a demanding task for designers because FEA would require huge computational power at their disposal. Indeed, the mesh element dimension should be small enough to well capture the behaviour of lattices at the unit cell level, with an exponential increase of required computational power. To overcome this issue, as mentioned in Chapter 1, homogenization algorithms have been developed, such as [57] to extrapolate material properties.

As it was described in this paragraph, several AM applications found in the literature exploit the use of voxelization modelling due to the positive aspects previously highlighted. To summarize, voxel-based frameworks for AM process simulations account for 32%, while the structure and topology optimization references combined are 36% of the relevant contributions. Minor applications involve AM machine characterization, lattice structure analysis through the homogenization method, and FGM design.

2.1.2 Additive Manufacturing technologies

According to the ASTM standard terminology (Figure 2.4), in the selected references it has been found a large variety of AM technology used to fabricate prototypes to validate algorithms. In this section, the author doesn't want to describe in-depth the wide AM technology panorama (the reader should refer to [66]), but he would like just to give an idea of which technologies are more used and why.

Analysing in depth the statistics coming from Figure 2.3 (b), it can be seen that Fused Deposition Modelling (FDM) [67] accounts for 38% due to its low costs for both machines and raw material. FDM uses a plastic filament as raw material, that is fed through a moving extruder head and it is deposited on the printing bed according to the desired path. Moreover FDM has large communities and many research results are available in literature as a benchmark. However FDM suffers of low layer resolution, high stair-effect on the external surfaces, high anisotropy and low strength. For this reason it is widely used to produce aesthetic prototypes or non-structural components.

Just to summarize the SLR results, FDM is used in the following references: [40], [61], [56], [49], [57], [58], [55], [46] and [54].

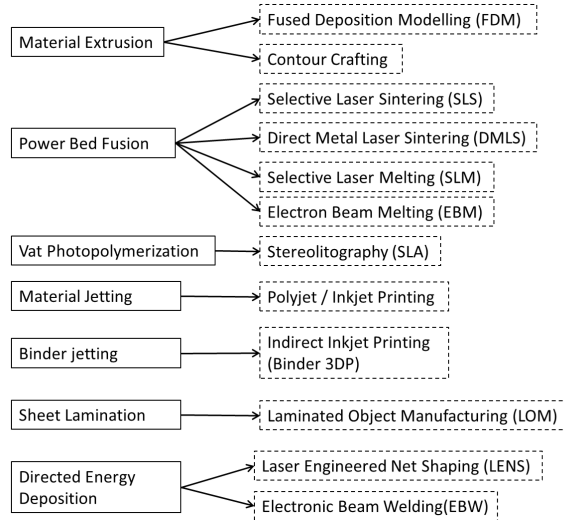


Figure 2.4: Classification of AM technologies according to ASTM terminology [35]

Moving towards more industrial AM technologies, SLS [68] and Selective Laser Melting (SLM) [69] are used when higher accuracy and resolution should be reached. On the one hand, in SLS, a light power source, such as a laser, is used to sinter the powdered plastic material, according to the 3D model shape. On the other hand, SLM employs a high power-density light source to melt and fuse a metallic powder to manufacture the desired shape. For example, [39] developed a quotation framework for SLS when high-level engineering applications are involved. Even SLA returns highly accurate components but with lower structural properties compared to SLM, since a photo-sensible polymer resin is used as raw material instead of metallic powder (SLM) [70]. SLA is used as principal AM technology in the references [42], [41] and [48] and accounts for 14%, obtaining the 2nd place of the more widely AM technologies used in the selected contributions. Other stand-alone contributions employs the Material-jetting technique [50], Laser Engineered Net Shaping (LENS) [37] or Digital Light Processing (DLP) [48].

For further details about these AM techniques, it is recommended to read respectively [71], [72] and [73].

However, what emerges from this analysis is that engineers have a large material and technology portfolio depending on the application, economic budget and project constraints. In the following Chapter, AM advantages and actual challenges will be deeply analysed to understand if industrial companies are ready to substitute traditional manufacturing processes with AM, and if not, which are the niche applications where AM is already mature.

2.1.3 Voxel-based discretization

The last category analysed for the scope of the SLR is the employment of voxelization. From Chapter 1, it is clear that the V-rep using voxels as discretization unit is of particular interest for complex topologies, which are common in Additive Manufacturing applications. Modelling through voxels brings several advantages compared to other methodologies, such as the strength (voxelization rarely fails), the low memory consumption and the possibility to show interior characteristics of 3D models.

As Figure 2.3 (c) shows, in the selected references, voxels are mainly used as a geometry discretization unit (64%) or as a material deposition unit. Starting from the first category, voxels are used to support computational operations due to an efficient way of data storage in a discrete way by using logical matrices composed of 0 and 1 values. Voxels are used as computational unit into Topology Optimization frameworks in [54], and for thermal process simulation tools, as described in [37] and [60]. Voxel-based 3D models are also used to detect critical areas during the manufacturing processes, such as under-extrusion or generic geometrical errors, as described in [40], [57], [56] and in [61]. Voxelization is used in the literature also to optimize the support material required during the AM process if overhangs are present in the 3D model, to speed up the overall production [42]. Moreover, V-rep can be employed also in FEA to evaluate the stress distribution using a logical mesh, exploiting the discretization obtained to represent the model also for

simulation purposes ([44] and [53]). A similar approach is described in [49] where voxels are used to optimize and at the same time discrete the machining toolpath combining neighbour voxels depending on the results coming from FEA in terms of detected stresses.

The more interesting reference that uses voxels as discretization units is described in [59], where lattice structures are modelled through a bitwise way to speed up geometrical operations through a tessellation process. Aremu et al. use the *Ray Tracing Intersection* (RTI) method as a voxelization technique, inspired by [74] due to the easiness of the process that rarely fails, the computational speed and repeatability (Figure 2.5). Indeed, for this research, RTI is used as a main voxelization algorithm in the tools described in the following chapters (further details are available in Chapter 1 and 4).

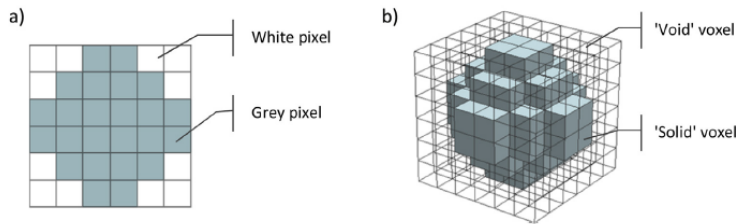


Figure 2.5: 3D voxels can be seen as close relative to 2D pixels [59]

Another interesting use of voxelization is to simulate the deposition process; indeed, voxels can be seen as material deposition units. For example, by using the Material-jetting AM technology, [38] developed a methodology to drive the material placement at the voxel-level (μm) to create complex shapes with extremely high resolution. Moreover, a voxel unit can be used to describe the powder particle or laser beam diameter of an AM process to drive the laser beam for a more accurate process [47] or even the filament deposition in a voxel-based framework for the FDM process [58].

From this brief review, it is clear that the main employment of voxelization in combination with Additive Manufacturing is for geometry discretization purposes. When AM is used, a typical design workflow is usually characterized by the following steps:

1. Design the 3D model (CAD design, FEA simulations, etc.);
2. Find the correct AM technology;
3. Modify and optimize the model according to the DfAM rules;
4. Slice the 3D model to generate the optimal toolpath (gcode generation);
5. Manufacture the component;
6. Post-processing.

Voxels are very useful before producing parts, especially in stages 1, 3 and 4 of the previous numbered list. Indeed, these are the stages of interest when software has to handle very intricate shapes during the design-to-manufacturing cycle. Voxelization enables efficient, strong and fast volume rendering and the model fidelity is not corrupted.

2.2 Limitations and Future developments of Voxel-based modelling for AM

Focusing on the future developments sections of the selected literature contributions, it emerged that many of the described voxel applications in AM are limited by the available computational power ([59] and [46], just to mention a couple of references). Indeed, voxelization is a computational consuming geometrical discretization: to obtain more accurate results, a finer resolution should be adopted, which reflects on longer computational time that is not always possible in a real industrial context. To solve this bottleneck, Information Technology (IT) industries should focus their efforts to produce more powerful processors and chips to accelerate the pace of change and increase the computing power at the disposal of industrial designers and engineers (Figure 2.6).

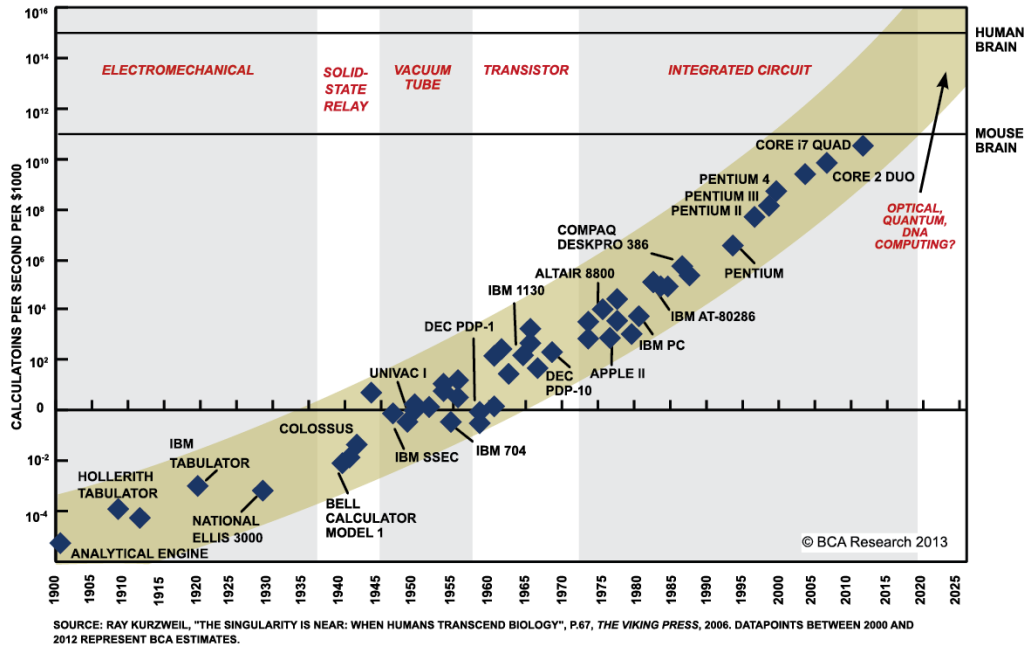


Figure 2.6: Exponential computing power increase over the last decades [75]

With an increase in the computational power, several contributions would like to extend their innovations to wider applications, such as topology optimization models for multi-physics simulations (i.e. combination of thermal, structural and fluid-dynamics optimization [76]) as done in [77] where optimization occurs also to get the best heat exchange. [49] would like to integrate a thermal analysis of the manufacturing process for degradation purposes of lattice structures. A large amount of contributions would like to validate the proposed analytical models with experimental validations to have a complete overview of the described phenomena such as for AM quotation purposes ([40], [42], [39] and [48]) to get more precise information before the actual manufacturing process.

2.2.1 Limitations of design tools

The restriction of current CAD software, and more broadly, design tools available today to obtain ready-to-be manufactured components for AM technology, is the most important result of the analysis of limitations previously discussed. From the SLR it emerges that these relevant contributions could be integrated by using open-source CAD software as a platform with different environments for each task of the classic AM design workflow (e.g. manufacturing quoting, structural analysis, topology optimization and so on) in a user-friendly and coherent way. One of the best solutions could be FreeCAD, free software with a large community behind it, where new macros can be coded in Python and shared with the community, as already done in [78]. Indeed, developed algorithms are very efficient for a specific task, but show important limitations for the other stages of the industrial design workflow. For example, in the literature, there are plenty of efficient TO frameworks that return highly optimized structures. However, these can't be manufactured as they are because some external surface post-processing is needed to delete surface noise, cracks and peaks (called surface smoothing approaches [79]).

Moving to lattice structures, open-source frameworks are optimized only for conventional bulk 3D models and shows important limitations to model trabecular structures [80]. Only in recent years, commercial CAD software developed routines, through the active intervention of the user, to design lattice structures, mainly of uniform type, while large weaknesses are present for conformal lattices. In this technological gap, CAD software, based on V-rep could help designers to treat these structures, very appealing for automotive and aerospace applications by assigning a unit cell to each voxel. Moreover, it emerges that is very challenging to structurally analyse periodic structures due to their inherent topology complexity that reflects on high computing demand for full 3D analyses. To overcome this issue, homogenization numerical techniques are developed, as cited in this chapter, with satisfactory accuracy and a huge decrease in computational time required. Despite that, using homogenization approaches, the designer obtains the behaviour of the

overall structure but loses important information at the unit-cell level.

As of last, but not least, thanks to the SLR emerges a need for alternative representation methodologies and [50] proposes to use new geometry file formats to include more information and to control with more precision the manufacturing process. Indeed, it is well known that the STL file format shows some limitations, especially in the case of lattice structures or FGM. To overcome this issue, the ASTM released the new AMFF to include more information about the material, the colour, the texture and the description of more complex shapes [81]. However, at the moment of this review, this file format is still under development.

2.3 Scope of the research

As it emerged from the SLR, there is a strong connection between voxel-based representation and Additive Manufacturing technology. Moreover, the presence of a technological gap affects the common design tools available to designers in research and industry contexts to obtain complex and highly optimized shapes, such as ready-to-be-manufactured TO models or lattice structures. TO and periodic structures are extremely interesting and appealing for aerospace and automotive industries and for all those applications where the lightweight design is fundamental. More coherent and user-friendly tools should take advantage of AM flexibility to manufacture lightweight components. Moreover, international Standards should take the pace of the Additive Manufacturing technological innovations available nowadays.

To overcome these actual limitations, the scope of the candidate's PhD project is to design and programme procedures and codes, based on V-rep through the Ray Tracing Intersection method, to easily design complex structures following the DfAM characteristics. A non-exhaustive list of innovative approaches could contain:

- Modelling lattice structures using voxels;

- Integrating FEA tools to rapidly analyse lattices and TO structures, as it is done with conventional bulk models;
- Developing an improved methodology for lattice structure mechanical analysis to understand the unit-cell behaviour;
- Proposing a 2D representation Standard for lattice structures in technical drawings;
- Developing an external surface smoothing algorithm for topologically optimized structures to obtain 3D models following the DfAM rules;
- Accelerating the design-to-manufacturing cycle of spare parts by using AM;
- Using AM for large-scale components in the automotive and aerospace industry;
- Developing fluid-dynamics tools using voxel-based representation to accelerate the meshing process.

All these innovative methodologies can be programmed in Python and Matlab language to be included in the future in a single open-source voxel-based software, through a user-friendly Graphic User Interface (GUI). In this way, the designer could have at his disposal a coherent and well-integrated tool that can improve the efficiency of the design workflow, decreasing the human effort.

To fill the highlighted technological gaps, the candidate examined in depth these topics and developed new methodologies to solve the limitations proposed in this Chapter. In the following, the candidate will describe these topics which are also proposed in all the scientific contributions submitted and published in different indexed International Journals and Conferences (in Figure 2.7, each bold number refers to a precise candidate's publication).

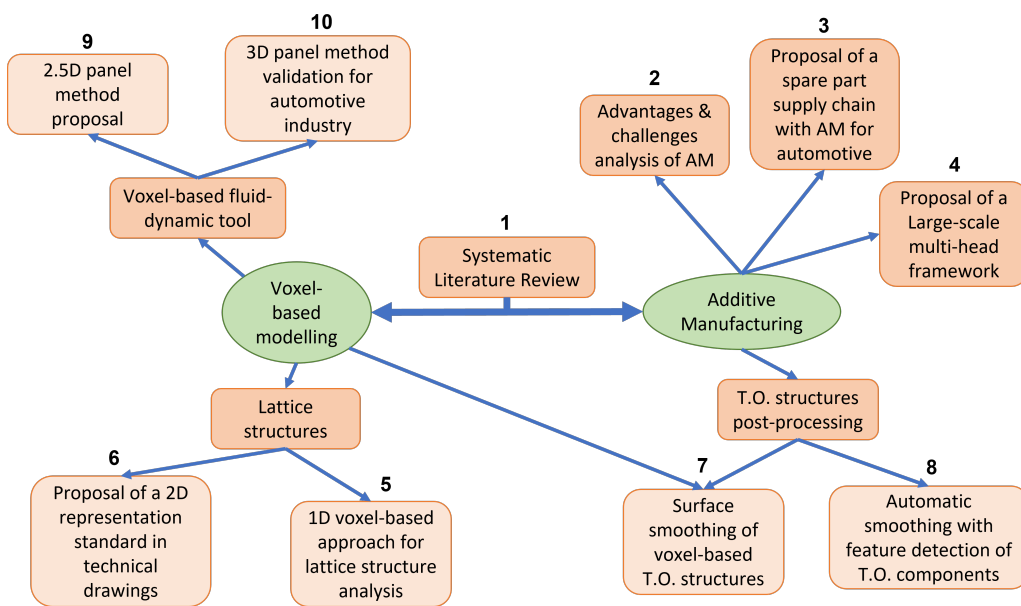


Figure 2.7: Relevant topics of the candidate’s PhD programme; each numbered topic is the subject of a scientific contribution for indexed International Journals and Conferences available in Appendix A

Chapter 3

Additive Manufacturing technology

In this chapter, a detailed description of Additive Manufacturing, the available techniques and the application fields are included along with a comparison with traditional manufacturing processes. The information included in this Chapter comes from own publications [82], [83] and [84].

In industrial engineering companies, the manufacturing processes can be subdivided into 3 main categories: formative manufacturing, subtractive manufacturing and additive manufacturing. The formative processes, such as injection moulding, casting, stamping and forging, typically shape the raw materials through high pressure or heat to the mould. In the case of high production volumes, formative manufacturing has no rivals considering the costs per unit. Tooling the mould is very expensive, but it has to be done once and can be considered effective at high volumes. Design constraints affect this production process, namely draft angles and uniform wall thickness to help the forming process.

The subtractive processes, i.e. CNC, turning and drilling, use a block of raw material (usually metallic) and through the employment of cutting tools, the exceeding material is removed to get the desired shape. The obtained components are characterized by an excellent surface finishing and high ac-

curacy. However, trained designers should prepare in advance the tool path using Computer-Aided Manufacturing (CAM) software, adding costs and time to the overall process. Overhangs and other geometrical restrictions limit the opportunity to generate complicated forms using subtractive methods. Moreover, a consistent amount of raw material is wasted to produce the final geometry.

The Additive Manufacturing process, known to the large audience also as Rapid Prototyping (RP) or 3D printing, is characterized by an additive process of joining layers of raw material. There is a wide panorama of AM techniques using specific materials with each having advantages and limitations. The main advantage is the total design flexibility offered by AM and there are no start-up costs due to the absence of expensive tooling processes, allowing the development of fast and low production volume supply chains. For this reason, the costs per unit of AM can be seen as constant as the volumes increase and AM is very attractive for low batches of products (Figure 3.1). However, AM is limited by the poor mechanical properties of the final product compared to traditional manufacturing, due to strong anisotropy for most of the AM techniques. Another main limitation affects the production repeatability: often, object's characteristics have slight modifications due to raw material properties, changes in the printing settings, different cooling processes or warping during curing.

3.1 Historical background of AM

The first AM technique that was developed in 1983 by Charles Hull is Stereolithography (SLA). This production methodology is based on the idea to create 3D models adding raw material (a liquid photo-sensible polymer) layer by layer thanks to a computer-controlled energy source, such as a laser beam, used to harden the raw material. However, there was a huge technological gap in the communication between the AM machine and the innovative design tools (CAD and CAM software) available at that time. To fill this

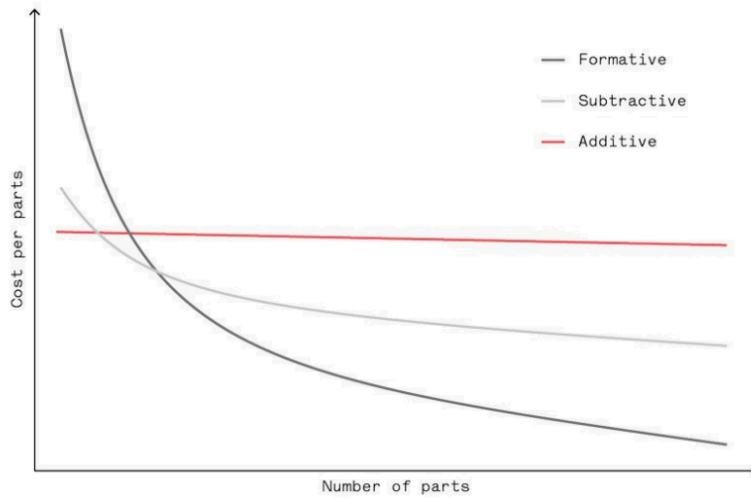


Figure 3.1: Manufacturing costs as a function of production volumes [85]

gap, Mr Hull and the 3D System developed the Standard Triangulation Language (STL) file format in 1987, to transfer the component's topology from the CAD software to the AM machine [86]. The STL file format is still in use due to its large compatibility with all the CAD software even if it is not the ideal format for AM since it does not include information about the colour or texture of the model. The STL file describes an unstructured triangulated surface mesh of the 3D object by using unit normals and vertices of the triangles of the mesh (Figure 3.2). The file lists each triangle as follows:

```
facet normal  $n_i n_j n_k$ 
  outer loop
    vertex  $v_{1_x} v_{1_y} v_{1_z}$ 
    vertex  $v_{2_x} v_{2_y} v_{2_z}$ 
    vertex  $v_{3_x} v_{3_y} v_{3_z}$ 
  end loop
endfacet
```

Thanks to this important step forward, a huge effort from the research

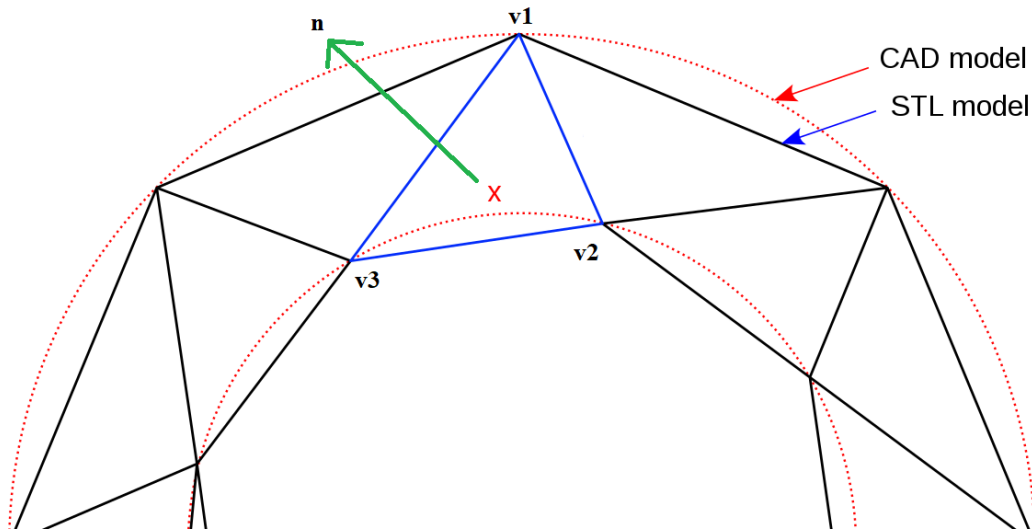


Figure 3.2: Approximation of 3D model using STL file format

community was oriented towards the innovation of AM techniques. The 1990s can be remembered for the development of innovative additive manufacturing techniques involving metal powders, such as the Electron/Laser Beam Melting (EBM and LBM) that facilitates the manufacturing in AM of metal raw materials, such as titanium, Inconel and steel parts for structural applications [87]. The 2000s are remembered as the years where the main attention was focused on the development of supporting software tools for AM, e.g. primitive TO software, due to the increase in computational power and lower prices of personal computers. As the last step, in recent years, AM became more affordable, especially the polymer-based techniques, not only for industrial companies but also for hobbyists and small research groups.

3.2 The design workflow with AM

Even if a wide range of AM techniques are available nowadays (see as a reference Figure 2.2), it is possible to rough out a common design workflow that is constant across all technologies. The design steps can be divided as follows:

1. Design a 3D model: using CAD tools, the designer is asked to obtain a 3D model of the desired object. A 3D model can be also obtained through Reverse Engineering (RE) techniques, such as laser scanners or photogrammetry;
2. STL model conversion: the 3D model is converted into a compatible file format (i.e. STL, OBJ, 3DP) to be imported into slicing software;
3. Manipulate the geometry and generate the gcode: the STL file is imported into a slicing software in which the designer can choose the printing settings (layer height, % of infill, the velocity of the material deposition and so on) to generate the gcode file. This file contains a list of numerical control instructions used in CAM to automatically control CNC and AM machines;
4. AM process itself: the gcode is uploaded into the AM machine and the manufacturing process takes place according to the different technologies available nowadays;
5. Printed object's removal: the 3D component is extracted from the AM machine by an operator and can be extremely easy or complicated depending on the AM technique used;
6. Post-processing: the 3D component is post-processed to remove support materials or to externally finish it to obtain the desired surface roughness. Post-curing may be required for some AM techniques using UV ovens.

3.2.1 Reverse Engineering and Additive Manufacturing

The Reverse Engineering (RE) techniques are used to obtain a conversion from a real object into a digital 3D model. RE can be coupled with AM to print an existing object to understand its functionality, its geometry or to

detect its defects [88]. RE algorithms generate a cloud of points that fits the surface of the model to create a surface mesh and a solid 3D model. RE techniques can be divided into touching methods, more expensive and accurate processes, and optical methods, less accurate but more affordable. The more common optical methods are the 3D laser scanners or photogrammetry. RE techniques and in particular photogrammetry can be used as a process to generate 3D models as a starting stage in the AM design workflow.

To better understand the capabilities of the AM-RE coupling, the candidate analysed the idea of producing automotive spare parts through AM with the use of photogrammetry to create spare parts when the digital model is not available, such as for classic or highly customized luxury cars. An innovative methodology involving both Additive Manufacturing and photogrammetry for decentralized spare part production in the automotive industry is described in detail in own contribution [83]. Here some interesting previews are discussed.

It is well known that the supply chain of spare parts for the automotive industry is a very complex environment characterized by an extremely high number of spare components ([89] and [90]), the need to support both new and former generation products with a heterogeneous spare part demand [91]. This reflects on high management costs, due to the magnification of shelf keeping parts in after-sales inventories [92]. To lower the costs, companies can take advantage of AM process, by manufacturing the spare parts only when necessary through RP techniques, and storing the component information in a 3D digital model. A hybrid solution between an in-situ production and a centralized supply chain can be the best option to optimize the entire supply chain based on an entire AM factory installed at the central distribution centre and some located at local service stations [93].

Thanks to the photogrammetry technique, affordable and easy to be implemented, 3D models can be computed starting from a series of high-resolution snapshots taken from a different point of view [94] (Figure 3.3). This RE technique has been applied in several contexts, such as in medicine,

archaeology and the industrial field. The photogrammetry workflow can be divided into five steps:

1. Image matching for each snapshot using recurring points. These points are saved, while each snapshot is oriented;
2. Triangulation occurs to evaluate the coordinates of previously cited points;
3. Creation of the cloud of points;
4. Densification of the cloud;
5. Surface mesh creation.

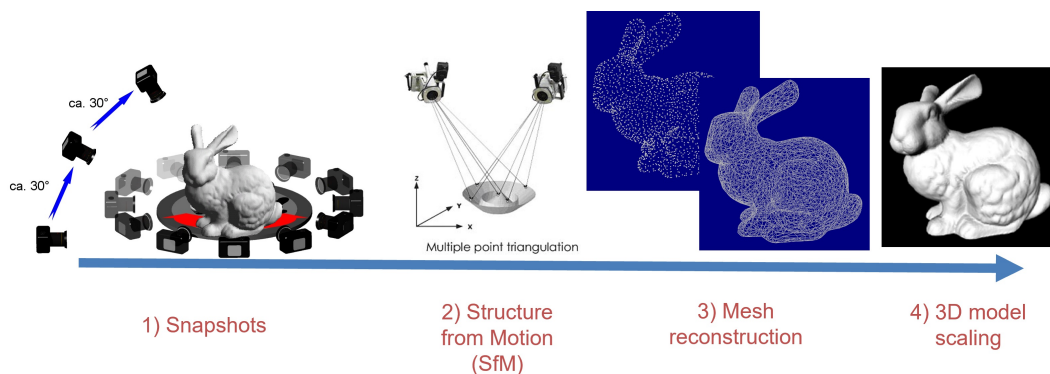


Figure 3.3: Photogrammetry workflow to obtain a 3D digital model from a real-life object

3.2.1.1 Conceptual supply chain proposal for the automotive industry

The candidate proposes a conceptual supply chain for spare part production for the automotive industry by coupling AM with photogrammetry. In particular, a customer that needs a spare part can contact a local service and ask for the component. On the one hand, if the 3D digital model is already stored in the company database, the product can be manufactured with AM

and sent to the consumer. However, if the 3D digital model is not accessible, for example, owing to a previous generation automobile or a luxury car, the local service may ask the customer to take numerous photos from various angles using a smartphone, which currently has a strong camera system, and transmit them to the local service. Thanks to photogrammetry, a local operator can comfortably recreate the 3D model without the need to reach the consumer with a bulky 3D scanner or other apparatus. Then the 3D model can be sent to the nearest local service, where an AM machine produces the component which is sent to the consumer, as shown in Figure 3.4.

This methodology proposal exploits the photogrammetry advantages such as affordable prices and can be easily used in a remote context without the need for a skilled operator and expensive apparatus while maintaining a sufficient level of accuracy. From a simple case study included in [83], the can-

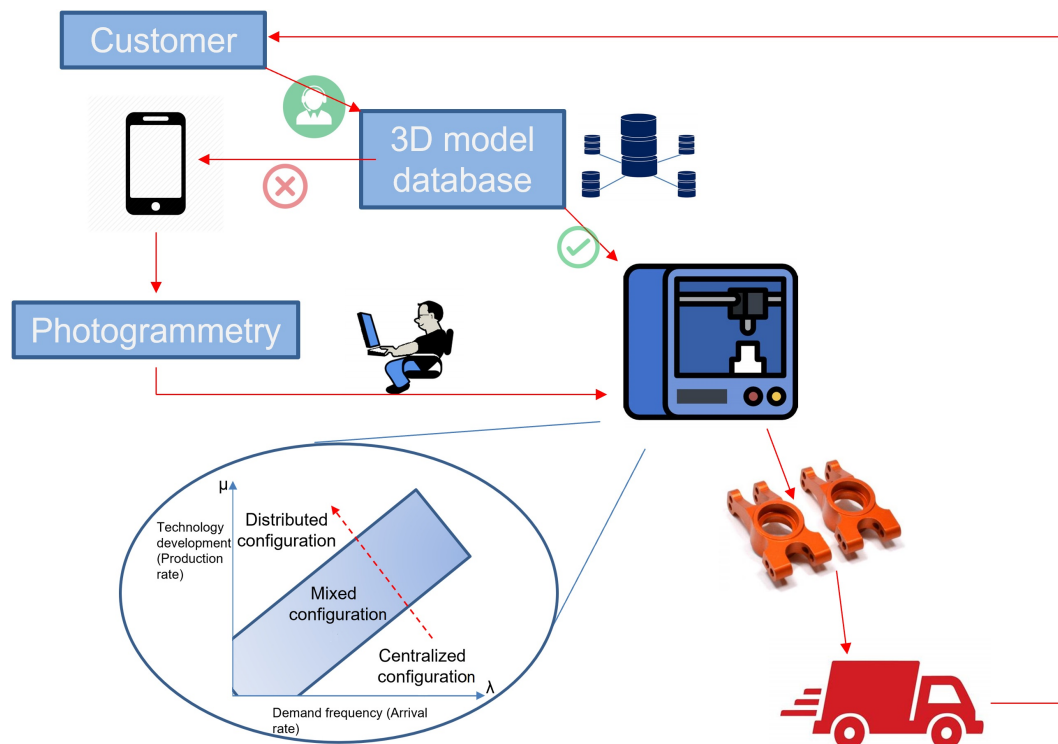


Figure 3.4: Conceptual layout coupling AM and RE to produce spare parts

didate shows that a maximum error of 1.86% is noticed in the digital model obtained through Autodesk Recap Photo compared to the real component, demonstrating that the technology is still not mature due to low resolution of nowadays camera and not enough efficient computations from the available software. Due to slight mistakes, the object's characteristics should be adjusted for couplings or interferences, and no information regarding geometric dimensioning and tolerancing from photogrammetry can be provided currently, necessitating human involvement to set them correctly. However, this conceptual methodology proposal can be seen as a case study to show the possibilities AM offers to industrial companies.

3.3 Additive Manufacturing advantages

In this section, the description of the advantages of AM processes that have facilitated its diffusion in industrial applications will be listed and briefly analysed. Further considerations are contained in a candidate's Conference paper [82].

The main advantage of AM is the possibility to produce almost whatever shape the designer wants, offering extreme flexibility and the absence of geometrical constraints that affect traditional manufacturing processes. This flexibility is given by the synergy of CAD software and RP machines following the DfAM rules. Thanks to the high design flexibility, the AM products can be customized following the customer requirements, very important in the biomedical and in automotive industries to create spare parts for classic or luxury cars and for all the applications where high customization and small batches or even a single piece should be manufactured. Furthermore, topology optimization tools can be used to design efficient and lightweight structures obtaining far from common shapes designed by hand by human designers and impossible to manufacture using conventional processes. AM and TO provide significant benefits in terms of lowering waste material, design time, and structural weight, all of which are important variables in the

construction of transportation vehicles, since lower mass means less power is used and fewer pollutants are produced. For example, in aerospace, the SLM process is often coupled with TO and lattice structures to manufacture complex and lightweight structural components, gaining all the advantages offered by AM design flexibility [95].

Moreover, the time needed for the design-to-manufacturing cycle is drastically reduced by minimizing the internal process logistics due to fewer operations, such as tooling, drilling, assembling and so on [96]. Moreover, rapid changes can be done to the product before commercialization without wasting time and money. AM offers also the possibility to manufacture prototypes for preliminary tests well before the production, becoming a key factor to decrease the cost of changes in the products' design cycle. AM shows even important advantages by limiting the number of connections, by generating complex assemblies in a single piece, thus reducing the time needed to properly connect different components by bolts or welding and so reducing the overall weight. Moreover, connections are critical in vibrating environments such as helicopters making AM extremely attractive especially due to limited maintenance and inspections to detect failures.

AM offers also the possibility to customize the material used to fabricate the component by mixing different raw materials, embedding fibres in the structure or modifying the material density along with the object as it is done in the FGM or in non-uniform lattice structures to achieve the required material properties by changing the internal porosity [97]. Moreover, different raw materials are available in the AM portfolio, such as polymers used in FDM, SLA and SLS, or metal powder employed in SLM or EBM (Figure 3.5). Furthermore, organizations may make all of the required parts with a single AM machine, employing a variety of materials and geometries. It is also feasible to manufacture tools in-house, which is becoming increasingly important for small businesses looking to enter the manufacturing sector without making large upfront expenditures, as is the case with traditional manufacturing production chains. As of last, with the arrival of the AMF

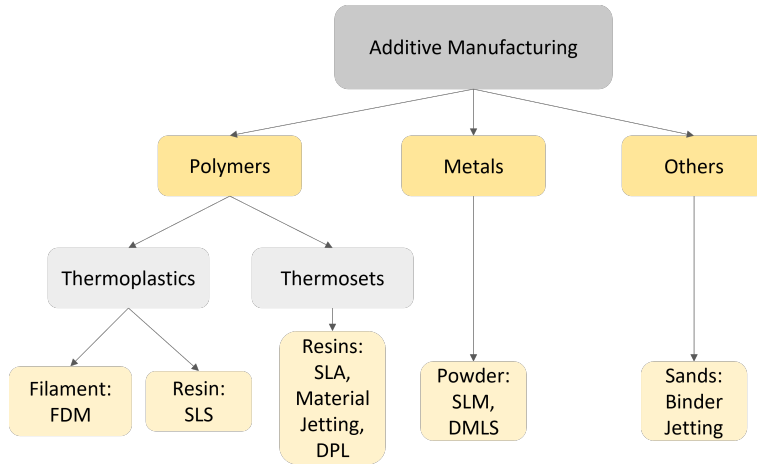


Figure 3.5: Additive Manufacturing raw material’s classification (adapted from [62])

format, the multi-material capability combined with the multi-structure freedom will be used to create competitive products compared to those coming from traditional processes.

3.4 Additive Manufacturing limitations

On the one hand, AM shows extremely attractive advantages, described in the previous section, but on the other hand, this manufacturing technology still suffers from important limitations that slow down its widespread diffusion in all industrial contexts.

The main drawback of AM, especially valid for the FDM technique, is the highly anisotropic material behaviour due to the manufacturing process itself: the object grows in the z-direction during the manufacturing layer after layer and possible voids between layers may occur. For this reason, the structural properties are comparable in the XY plane and lower in the Z direction [98]. Moreover, if the layer height is not sufficiently small, the external surface of 3D printed objects may suffer from the known phenomenon called *stair effect*, namely high surface roughness. This issue can be mitigated by post-

processing to increase the external finishing of the components.

As it emerges from the literature review proposed in Chapter 2, nowadays there is still a gap between the manufacturing process capabilities and the limitations of actual design tools, especially for complex structures due to the implementation of B-rep [99]. The voxel-based method could be advantageous to obtain fast geometry manipulation, get information on the components and carry out topology optimization on large structures. However, efficient surface smoothing algorithms with automatic and intelligent feature recognition should be applied to the geometry before the manufacturing processes to get a more appealing shape. The design tools optimized for AM are still fragmented into the design, topological optimization, STL export and manipulation, surface smoothing, slicing, and AM simulation, thus introducing inefficiencies in the design process. Furthermore, designers and operators should be trained to handle in a correct way the DfAM criteria to completely exploit the AM advantages.

While producing complex assemblies in one piece reduces the number of connections and overall weight, it may cause issues when the component needs to be inspected or repaired regularly because the as-printed assembly cannot be disassembled, resulting in a higher cost in case of overall assembly replacement. Moreover, metallic AM is associated with high costs for both machine and raw material compared to traditional processes (powder metals can be up to 200 times as costly as sheet metal and a study demonstrates that nowadays AM titanium powder is competitive only if machining waste is 50-75% of initial volume). Nowadays, in AM the cost per unit is constant when the production volume increases, while for traditional processes, exponentially decreases, making AM attractive only for small production volume applications.

The low repeatability offered by 3D printed components results from the effect of lots of batches of powders from the same producers, the effects of powders/resins/wires conservation and the manufacturing settings on the component. This low repeatability contributes to a slow or even unavailable

certification process along with a lack of historical data from AM structures. For the applications where repeatability is a must, AM structures can't still be certificated and AM application is limited to non-safety-critical components [100].

To increase the number of industrial applications, international Standards and regulations should be published to facilitate wider adoption of the technology, allow technical exchange and guarantee the process consistency. However, few Standards are available to date specifically for AM purposes. In particular, the American National Standards Institute (ANSI) identified 93 technological gaps for AM, meaning that Standards do not respond adequately to industry needs [101]. Indeed, just a few Standards, dealing with AM, can be here recalled. For example, the ISO/ASTM52900-15 defines the basic nomenclature and processes commonly used in AM, while few Standards provide guidelines for material characterization, such as the ASTM F3049-14 and the AWS A5.01M/A5.01:2013. Moreover, few Standards deal with DfAM, such as the ISO/ASTM 52910:2017(E) published in 2017 or the ASME Y14.46-2017 that treat the dimensioning and tolerances for lattices and topologically optimized structures. Other Standards deal with specific AM processes, such as PBF and Direct Energy Deposition (DED) for process definition and metal AM inspection and qualifying training.

Furthermore, the application of Standards in the AM field has very slow dynamics and appears as a vicious loop cycle. In particular, on the one hand, industries need Standards to use AM for critical and structural components, moving from prototypes and mock-up parts. On the other hand, International Standards Organizations and Associations are waiting for historical data and experience to understand the AM structures during the operative life in critical applications such as aerospace and automotive.

Last, but not least, AM machines are characterized by a limited building volume and slow production rates: as a matter of fact, is extremely rare to find 3D printers with more than $1m^3$ of printing chamber, thus limiting strategic applications such as building entire car's chassis or entire aircraft

wings which could come from topology optimization tools. A candidate's contribution focuses on these aspects and proposes a collaborative multi-head large-scale Additive Manufacturing machine, trying to solve this limiting factor [84]. Some details are discussed in the following paragraph.

3.4.1 Large-scale Additive Manufacturing framework proposal

Application of AM to large-scale components is still an open challenge, because of limited printing volume, slow manufacturing process and low production rates even if some applications could benefit from the research and development of a fast, accurate and large scale AM framework. For example, in the literature, there are some Unmanned Aerial Vehicles (UAV) manufactured with AM as a multitude of parts which are assembled in a second moment [102]. TO has been applied to satellite's chassis such as Cube-Sat, but not on large-scale satellites. Moreover, in the automotive industry, the reference length of a car's chassis is $4.5m$ to manufacture it as a single piece [103].

However, available technology is still not able at the same time to allow accurate, fast and big dimensions during the AM processes. There are some examples of large-scale AM frameworks, for civil [104] and industrial application [105], composed of robotic arms with single extrusion heads that allow the creation of large components. Yet, the manufacturing resolution is very high (in the order of millimetres) which is unacceptable in highly accurate applications such as automotive and aerospace. Moreover, if the accuracy level could be adjusted in some way, the production times needed to manufacture large-scale components with a single extruder head could reach even weeks which is not permissible in a real industrial context.

Multi-head extruder AM machines could be the solution to the mentioned issue. Nowadays, there are AM machines with conventional dual extruder mainly used to extrude hydro-soluble support material [106], in order to decrease the post-processing efforts, or to exploit the multi-material advantage

offered by AM ([107] and [108]). Furthermore, an interesting technology, called IDEX, developed by BCN3D, allows using two independent extrusion heads in the same machine, by splitting the X-axis, while sharing the Y and Z axes [109], allowing to produce simultaneously two copies of the same object, doubling the production volumes. However, there is no multi-head technology that solves the limited building volumes and slow manufacturing velocities that affect AM.

To overcome these limitations, the candidate proposes a collaborative multi-head large-scale Additive Manufacturing (LSAM) framework. In particular, the idea is to create a large-scale AM with multiple extrusion heads that work simultaneously on the same piece to lower the manufacturing time while maintaining sufficient accuracy. The overall building volume could be divided into n subvolumes, where a single extruder works. Neighbour subvolumes are related to each other with common working regions, where both neighbour extruders may work, with a control system software that avoids dangerous collisions between them (Figure 3.6). The common working regions are necessary to create overlapping regions between the n subparts to connect them to create the desired component. An optimized design of the overlap region is required to better homogenize the boundary working area of each extruder and bond together the subparts avoiding glueing or assembling operations [110]. The large-scale component obtained through the proposed methodology could be manufactured in a reasonable time and could be similar to the same component manufactured with a single extruder.

In the proposal for a LSAM framework, particular attention was given to the geometry file handling of large-scale components before the printing process itself, acting directly on the 3D digital model, by an optimized subdivision. Existing literature contributions dealing with AM machine customization, usually customize the gcode file, increasing the complexity of tasks. On the contrary, the proposed methodology can be easily programmed in a macro and integrated into common CAD software decreasing the designer's effort in the design workflow. Moreover, the CAD subdivision is applied

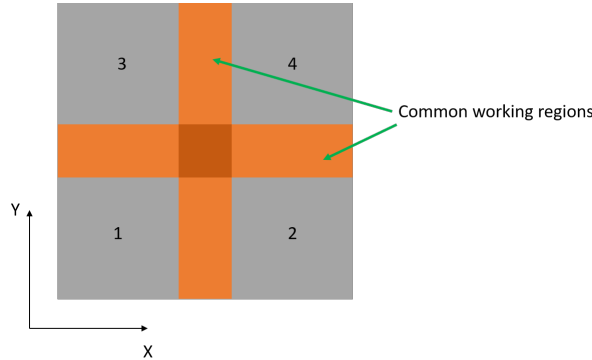
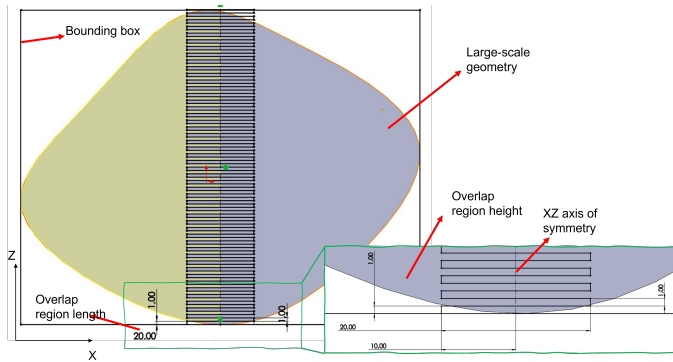


Figure 3.6: AM building volume subdivision and definition of common working area; simplified case with $n = 4$ extruders [84]

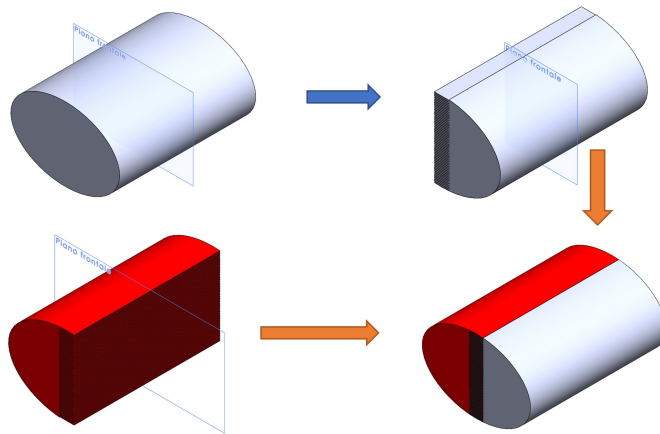
through simple Boolean subtractive operations to create a serrated tool for alternately overlapping regions between adjacent subparts which can be easily adapted and reproduced to every framework that follows the proposed philosophy. The serrated tool is characterized by a square wave geometry designed to obtain the best bonding between layers extruder from different heads, limiting weak spots in the overall structure (Figure 3.7). Applying the proposed methodology, it is possible to obtain n STL files that can be imported into common slicing software and assign a single extruder-head to each subpart.

The proposed CAD handling methodology is easy to be reproduced, limiting the designer's effort during the design workflow. The mechanical characteristics of the final component are not downgraded, thanks to the design of the overlapping region that does not affect even the external surface of objects. Moreover, using the same hardware and software, industries could also produce copies of a single small-scale object by following the IDEX methodology, dramatically increasing the production rates.

A simple case study, applied on an aerodynamic wing, such as a race car wing, is included in [84] to demonstrate the effectiveness of this approach. To manufacture a wing of $1m$ length in span-wise direction and a $0.5m$ chord, using standard FDM printing settings for the PLA raw material ($0.25mm$



(a) The 2D sketch of the serrated tool using a square wave line



(b) Overall component subdivision in two different subparts; by assembling together the two subparts, it is possible to obtain the initial component

Figure 3.7: LSAM CAD handling and subdivision in n subparts

layer height, 30% of tri-hexagonal infill [111]), the slicing software estimates two weeks, an unacceptable amount of time, to manufacture a single wing (Figure 3.8). By applying the proposed methodology, the wing is subdivided into $n = 4$ subparts using a square wave line to design the overlapping region. The estimated printing time using the same settings is more than halved for a single subpart assigned to an extruder (Figure 3.9).

In the near future, this methodology should be supported by further re-

search focusing on the development of the prototype of an LSAM machine with multi-heads and to design a control system software that can simultaneously start the print of the subparts and avoid possible collisions between the extrusion heads. Moreover, structural weak spots could be limited by the optimization of the overlapping region topology through numerical and experimental tests. These topics will be considered for future research and for scientific contributions.

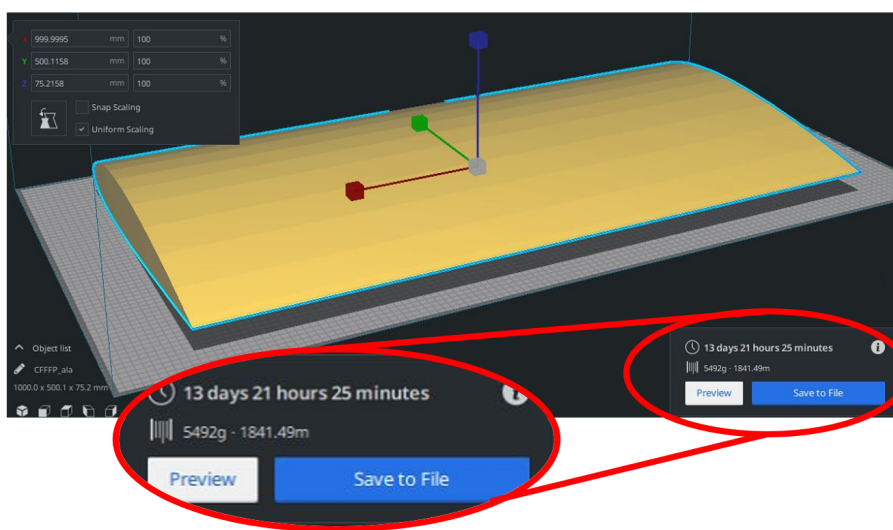
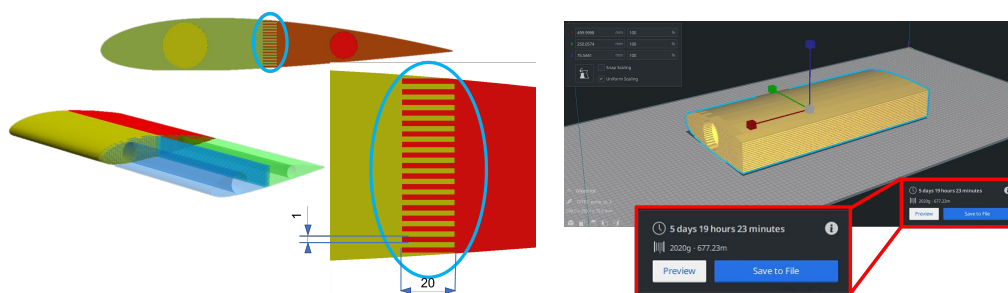


Figure 3.8: The perfect context where to apply the LSAM developed framework: an aerodynamic wing with a long printing time estimation [84]

3.5 Additive Manufacturing applications

Thanks to the aforementioned advantages discussed in the previous sections, the interest in AM skyrocketed in the last couple of decades and is becoming to be widely used as a principal manufacturing process in many industrial contexts. Wohlers Associates, powered by ASTM International, provides technical, market, and strategic advice and reports on the worldwide trends in AM. It is fascinating to collect some findings from studies of Wohlers Associates on AM developments in industrial applications, to under-



(a) The wing subdivision into four different subparts; by assembling together the subparts, it is possible to obtain the initial component
 (b) The subpart printing time estimation; by applying the LSAM framework, the printing time is more than halved

Figure 3.9: LSAM case study applied on an aerodynamic wing [84]

stand where the technology is going and to depict the worldwide protagonists of new developments and trends of this manufacturing technology. According to the research of Wholers, it emerges that the highest AM impact on the production of goods has been recorded in the consumer/electronic products, followed by automotive, biomedical and aerospace industries, which together account for more than 65% (Figure 3.10). It is clear that in all these contexts, the possibility to highly customize the product in small batches is a key factor to prefer AM compared to traditional manufacturing processes.

AM is becoming crucial for customized medical devices that imitate the human body, using, for example, lightweight and periodic structures that mimic bone's inner topology that can be manufactured only with AM technologies, reaching more than 30,000 prosthetic limbs produced worldwide [113]. Moreover, AM is considered the dominant technology for manufacturing in-the-ear hearing aids, following the design workflow previously described (scan through RE techniques, manipulate the digital model and manufacture it). Other applications in the biomedical industry include dental implants and the manufacturing of skin tissues and human body parts using ad-hoc raw materials. Last, but not least, low-cost plastic models are widely used to train surgeons or to simulate interventions.

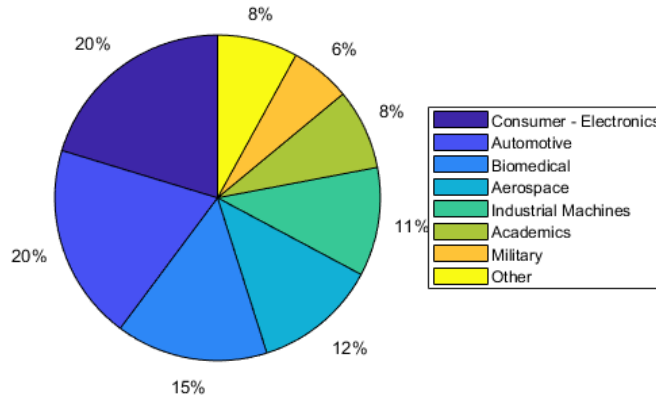


Figure 3.10: AM applications from the incomes of Companies operating in AM, both metallic and plastics; Adapted from [112]

Moving to the aerospace sector, AM is widely used to manufacture lightweight, strong and geometrically complex components which are usually produced in small batches. Thanks to its advantages, AM is aiding aerospace companies to reduce the costs of prototypes and components manufacturing due to low production rates that are common in aerospace industries. Moreover, the employment of RP is pushing a material shift from aluminium and steel to titanium and plastic in structural and non-critical components. Furthermore, Topology Optimization and Generative Design tools are widely used in aerospace components to obtain a high stress-to-weight ratio product that is essential in such an industrial context, where each gram weighs on the overall mission costs. Just to mention some key industrial players, Boeing and Airbus are already using AM parts for non-critical applications such as wind tunnel models, flight test parts, UAVs, propulsion system parts, air ducts and internal commercial aeroplane furniture [114]. AM technology was employed in the GE9X General Electric engine for the B777ER aircraft where more than 300 parts manufactured with traditional processes were

substituted with components manufactured in SLM, increasing of more than 10% the efficiency compared to the previous model [115]. The helicopter engine from Safran has been recently redesigned with more than 30% of components coming from the AM supply chain [116]. However, the AM's limited dimensions and the slow certification process, linked to standards not up with the times, are still limiting the diffusion of AM in aerospace and defence applications.

The automotive sector is the more interesting field for this PhD project and most of the solutions and algorithms proposed in this dissertation are focused on this industrial field. Even if characterized by very high production capacity compared to biomedicine and aerospace, AM products are increasing year after year specifically in low production rate applications such as special, luxury, racing and classic cars [22]. Latest trends report that AM is mainly used to build prototypes and small custom parts in plastic materials such as wind tunnel models using FDM technology. Moreover, metals AM (aluminium alloys) are used in niche applications such as motorsport to manufacture lightweight and optimized components [18]. For example, the Light Cocoon vehicle, designed by the German company EDAG is the first concept car with the entire chassis manufactured in SLM [117]. Furthermore, big companies, such as Ford are prototyping cylinder heads, brake rotors, and rear axles manufactured with AM in less time than traditional manufacturing would require. Indeed, AM could save a high amount of production time with prototypes of complex assemblies such as cylinder engine head that includes multiple parts.

Nowadays, AM is used also in architecture to build 3D scaled models or even to manufacture entire buildings [104]. This manufacturing technology is also used in the art & design sector to produce complex and intricate shapes, such as jewels that should be customized to satisfy the customer's needs. Moreover, AM is also used in niche applications such as musical instruments to manufacture customized single-piece components to achieve unexplored sounds [118], a theme investigated by the candidate in off-topic

research, whose results are contained in two distinct scientific contributions ([119] and [120]).

To summarize, this Chapter aimed to collect and discuss the AM technology, the possible applications, along with its advantages and challenges that still affect this technology nowadays. Minor topics were discussed in more detail to report some interesting results coming from own contributions. Now, it is clear the key role of Additive Manufacturing in the industrial context, especially for Automotive applications, is to build highly optimized and lightweight components exploiting the design flexibility offered by AM. These components, namely lattice structures and topologically optimized models are the same complex geometries cited in Chapter 2 for which a volumetric representation using voxels could bring enormous benefits in terms of model handling and visualization. For this reason, in the following Chapters, these two categories of interesting structures will be analysed in-depth showing important achievements obtained during the PhD programme.

Chapter 4

Voxel-based modelling for lattice structures

In this chapter, a detailed description of lattice structures characteristics, their classification, and the application fields are included along with a description of how they can be modelled by exploiting the voxel-based representation. The information included in this Chapter comes from own publications [121] and [122].

Thanks to the design flexibility offered by AM processes, in the last decades the employment of cellular complex structures has dramatically increased in several industrial applications where lightweight, stiffness and high strength-to-weight ratio are needed. Nowadays, lattice structures are replacing other types of cellular materials used in structural applications both in automotive and aerospace due to the enhanced capability to absorb sound waves and mechanical vibrations or to increase crashworthiness. For example, the Boeing 360 Helicopter is designed using sandwich structures and lattices in many structural components to achieve high strength-to-weight ratios and to reduce the number of joints in a highly vibrating environment [123]. Another interesting application can be found in the automotive field where it is common to topologically optimize structural components of high-performance cars. To increase the component performances and reduce

its weight, lattice structures can be used as an infill of optimized structures, as described in [124]. Other interesting characteristics of lattice structures are:

- The capability of absorbing thermal energy thanks to the high porosity between the unit cells which makes them attractive for thermal insulation;
- The high electrical and thermal conductivity that allows reaching high temperatures without structural degradation;
- The interesting property of controlling the flow of fluids, attractive for filters and tanks thanks to the unit cell dimensions that can reach micrometres.

Cellular structures span a broad range of structures that may be classified as foams (stochastic framework) and non-stochastic structures that can be separated into 2D frameworks, such as honeycombs, and 3D periodic bodies, such as lattices (body with periodic characteristics) [23]. Among the periodic 3D structures, the Triply Periodic Minimal Surface (TPMS) mimics the structures available in nature and has acquired large approval for specific applications such as enhanced thermal exchange or wave sound absorption due to their high external surface [125]. TPMSs are characterized by zero mean curvature, allowing enhanced properties such as mechanical response without stress concentrations and fluid-dynamics behaviour, very important in biomedical applications to allow organic fluid exchange [126]. However, the main achievements obtained during the PhD project deal with the so-called *Strut-and-node* lattice structures and in the following, the lattice structure terminology will refer to this kind of periodic configuration. Strut-and-node-arrangement better fits optimized voxel-based modelling and analysis, which will be described in this Chapter, better than other lattice topologies, because the eight vertices of a single voxel can be linked together following different schemes to obtain a widespread lattice unit cell portfolio. Indeed, these

periodic frameworks are characterized by a network of elementary entities, namely nodes, which are interconnected with rectilinear structural elements, called struts or ligaments [127]. Lattices are usually characterized by a unit cell, made by struts linked strategically, that is repeated in space a hundred or thousand times, as shown in Figure 4.1. For further details on a complete overview of general cell patterns, please refer to [128].

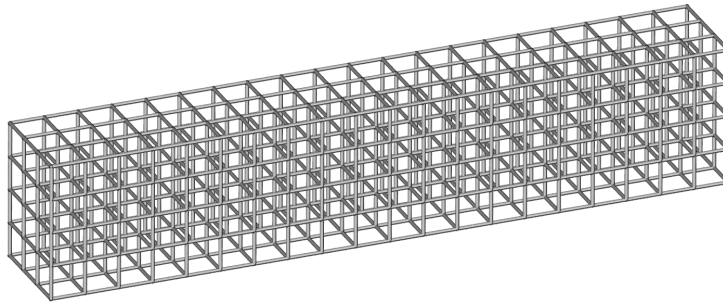


Figure 4.1: A 3D model of simple beam filled with uniform strut-and-node lattice structure using a simple cube as unit cell

When dealing with lattices, an issue not to be underestimated is their design: even if the advantages of lattices are clear, nowadays, current design tools, such as CAD software, still present large limitations due to the employment of B-rep. Indeed, lattices are very complex and intricate structures characterized by challenging boundary surfaces that should be modelled by common CAD software [129]. This challenge was investigated in the literature in the last years and some solutions were proposed to facilitate the 3D modelling of lattices through some automation but these solutions can be considered stand-alone and not embedded in CAD software [130]. Moreover, there is a lack of a user-friendly FEM solver interface as it happens for bulk models, where the design workflow is more straightforward. To fill these gaps, this Chapter will describe a voxel-based approach to model and structurally analyse strut-and-node lattice structures developed by the candidate and integrated into the open-source CAD software called FreeCAD with the support of some functions coded in MATLAB. FreeCAD is chosen because a

workbench called LSWM has been developed at the University of Bologna to design lattice structures and it is still in the development phase [78]. Thanks to the gained experience, this design environment has been chosen to implement the proposed automation. Before going in deep with the voxel-based modelling, it is important to briefly summarise the characteristics and classification of strut-and-node lattices, depending on their topology.

4.1 Periodic lattice structure classification

Lattice structures have gained the interest of many researchers and engineers because of the combination of dense and void spaces periodically arranged with properties not available with a single material. Strut-and-node lattices can be classified according to the following geometrical parameters (graphically collected in Figure 4.2):

1. Pattern, namely the unit cell topology that describes the connection configuration of the eight vertices of a single cubic unit cell;
2. Structural performances that describe the unit cell behaviour under stretching or bending loads;
3. Strut cross-section geometry, such as square, circular, triangular and so on;
4. Progressivity of unit cells that describes the changing in the geometric characteristics of lattices inside the structure;
5. Conformity, describing the way the structure is filled with hierarchic structures.

The first main distinction is based on the unit cell topology, namely the way the eight vertices of a cubic cell are linked. The single cubic cell is usually described as the Representative Volume Element (RVE) of the structure and many scientific contributions try to deeply analyse the RVE to understand the

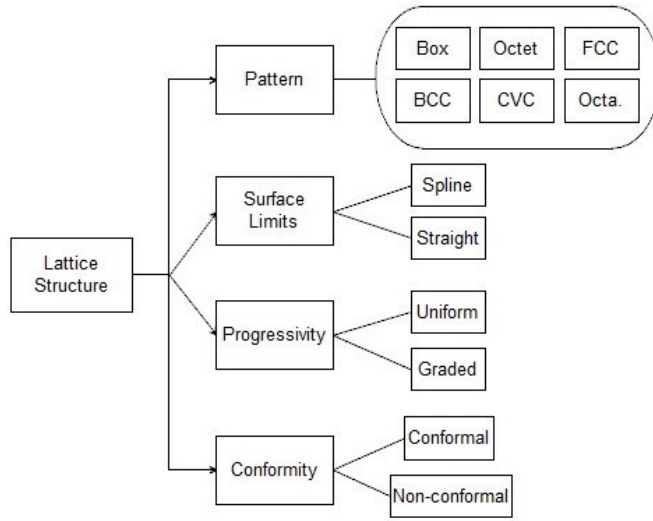


Figure 4.2: Periodic lattice structure classification (adapted from [23])

mechanical characteristics before analysing the entire structure. There are several ways the eight vertices can be linked, but for the aim of this project, only the more commonly used topologies will be taken under consideration (Figure 4.3).

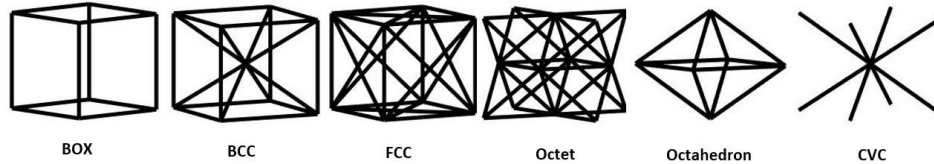


Figure 4.3: Unit cell topologies taken under consideration in this project [121]

Cubic cells are convenient because of the easiness of implementation and the close link with a voxel-based representation. Indeed, it can be assumed that each cubic unit cell is represented by a single voxel. Compared to the TPMS which has a fixed geometry, the strut-and-node cell has different variables that can be meticulously chosen by the designer, such as the length of the struts, the angles between them and their cross-sections shapes. For the scope of this project, only the square and the circular shapes will be considered.

The unit cell topology is closely linked with the structural behaviour of a single cell under external loads. In the literature, the unit cells have been divided into *stretching dominated*, structures with high connectivity that reflects on higher stiffness and *bending dominated*, structures with low connectivity and lower stiffness but higher strain values can be achieved [131]. On the one hand, the stretching dominated cells have a higher elastic limit compared to the bending ones at the same structure density. For this reason, the stretching dominated is the perfect choice in the case of lightweight and stiff applications. Looking at the stress-strain behaviour (Figure 4.4), the stretching dominated has an initial linear elastic behaviour up to the yield point; then there is the post-yield softening region, meaning that it is necessary a lower load that continues to deform the structure up to a point called densification, where the opposite struts of a cell get in touch and the stress becomes to increase again. On the other hand, the bending dominated, due to lower connectivity, reaches a lower yielding point; after the linear elastic point, a plateau describes increasing deformation under constant load up to the densification level. The bending dominated cells are optimal to absorb a high amount of energy in crashes exploiting the plateau region of the stress-strain curve.

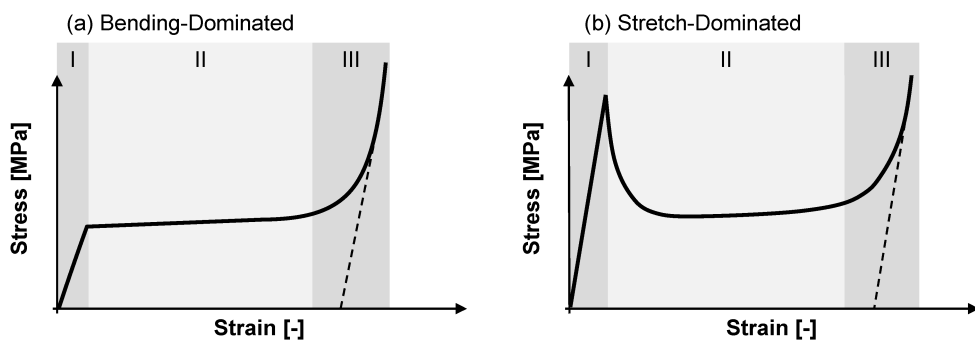


Figure 4.4: (a) Bending vs (b) Stretching dominated lattice structures [132]

To understand if a unit cell belongs to a stretching or a bending dominated behaviour, the Maxwell Stability Criterion can be used [133]. The criterion

evaluates Maxwell's number m that for 3D lattices is:

$$m = b - 3j + 6 \quad (4.1)$$

where b is the number of struts, j is the number of joints of the lattice unit cell. If $m < 0$, it is possible to say that the unit cell is bending-dominated due to the low connectivity, while if $m \geq 0$ then the unit cell has a stretching dominated or over-stiff behaviour. For example, considering, on the one hand, the simple cubic unit cell, the number of struts is $b = 12$, while the number of joints, namely the vertices, is $j = 8$; for this reason $m = -6$ and it is possible to say that the simple cubic unit cell is bending dominated. On the other hand, considering the FCC unit cell of Figure 4.3, it is true that $b = 36$ and $j = 14$, so $m = 0$ and the FCC is a stretching dominated unit cell.

Another important characteristic of lattices is their progressivity, namely how the geometric properties of the hierarchic structure may change along with the component. Indeed, graded lattice structures have gained the interest of many engineers due to the possibility to modify the lattice geometry in specific and limited regions, such as the more stressed of the overall structure. In this way, the lattice is optimized and its lightweight characteristics are even more prominent. Few design tools give the possibility to design graded lattices and they operate by increasing the lattice density in two alternative ways: decreasing the unit cell dimensions or increasing the cross-section of the struts.

The last important parameter for which the hierarchic structures are categorized is conformity. This parameter determines how lattices are filled, and conformity can have two different qualities: uniform and conformal. On the one hand, a non-conformal periodic structure is characterized by the easiest way to fill a component without taking into account the external surfaces. Indeed, the filling operation has a fixed unit cell orientation, completely independent from the body's shape. On the other hand, a conformal lattice is filled with distorted unit cells that follow the external surface curvature of the body. In the conformal lattices, the design is oriented to maintain

the unit cell integrity obtaining a stiffer structure due to a redistribution of external loads that do not occur in uniform lattices if an external shell is not included, as shown in Figure 4.5.

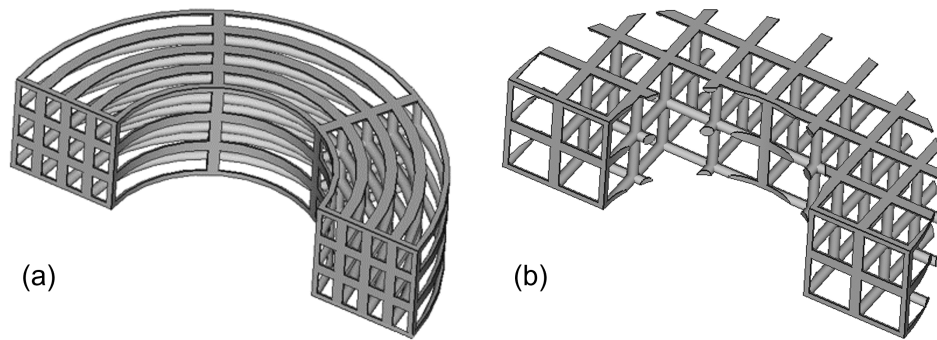


Figure 4.5: (a) Conformal vs (b) not-conformal lattice structures modelled using the LSWM environment in FreeCAD

4.2 Lattice structures CAD modelling

As previously mentioned, among the wide panorama of periodic lattice structures, those that have a cubic cell are convenient because of the easiness of implementation and because they perfectly fit a voxel-based representation, the core of the PhD project. The methodology behind the modelling of lattices structures has been implemented in FreeCAD as a set of coded functions in Python language. Supporting codes were developed using MATLAB software for easiness. Two ways of 3D modelling lattice structures have been implemented. Both approaches aim to obtain a 3D model that is ready to be manufactured with AM techniques. For this reason, the conversion into the STL file format is mandatory and an intermediate step, with the 3D lattice modelled using B-rep, should be considered, even if at first glance it could be not efficient. However, voxel-based representation, using the ray-tracing intersection algorithm, is used to speed up the entire 3D modelling. Indeed, in the following section, the voxel-based methodology will be introduced and then two smart ways of 3D modelling lattice structures will be described.

4.2.1 Ray-tracing intersection method for voxelization

Among the available voxelization algorithms in the literature, the candidate chose the ray tracing intersection method due to its simplicity and robustness compared to other approaches, as discussed in Chapter 1.

The ray-tracing intersection algorithm was own programmed in the MATLAB software. As a starting point, the algorithm asks for the 3D model of the object the designer would like to voxelize and the bounding box dimensions of the 3D model are automatically evaluated. The user needs to have at his/her disposal the STL model of the component and to establish the voxel resolution d . This choice directly affects the voxel's spatial grid (S_{x_i}) and as a matter of fact, the lattice structure density. Knowing the voxel grid, it is possible to initialize the logical matrix *VOXELmatrix* with all null values. As a second step, the algorithm automatically ray-traces in all the three main directions (x, y and z) and combines the results coming from the different dimensions to understand which elements of the logical matrix should be activated (Figure 4.6).

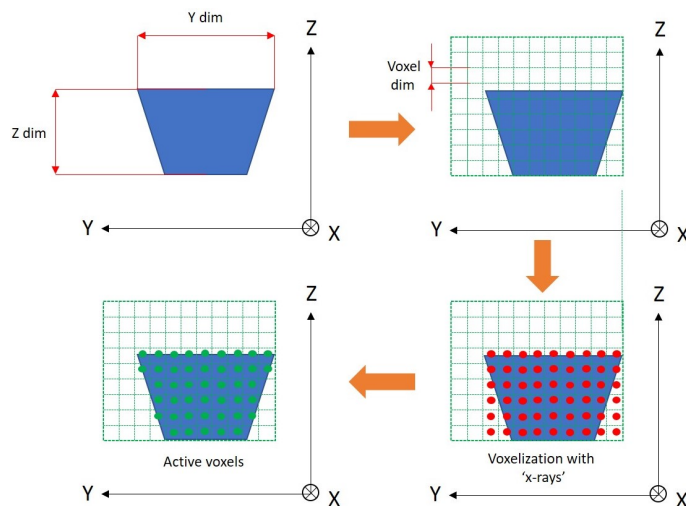


Figure 4.6: Ray tracing along the X dimension to understand which voxels should be activated [122]

Specifically, for each triangle of the STL file, the voxelization follows the

succeeding steps:

- determine the edges of the triangle;
- compute the opposite vertex of the selected edge;
- find the ray relative to the selected edge;
- check if the relative ray is on the identical side of the selected edge;
- if the check is positive for all the edges of the selected triangle, then it is undoubtedly that the ray flows through the facet, and for this reason, the matrix element should be activated.

The overall process can be graphically seen in Figure 4.7.

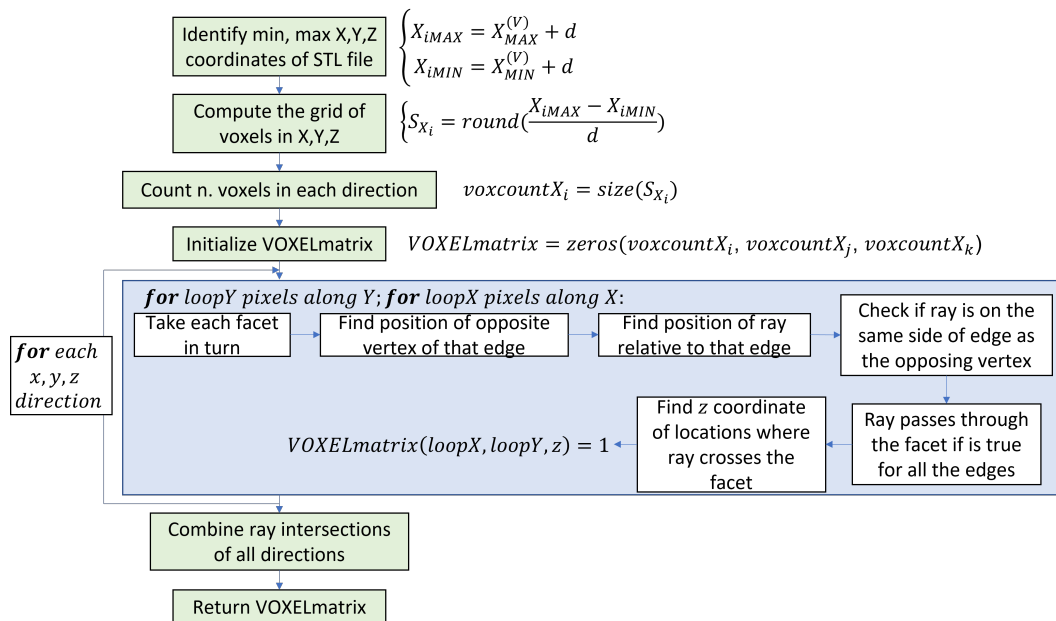


Figure 4.7: Graphic flowchart of the ray tracing voxelization methodology

4.2.2 1st B-rep modelling method

A first method has been written in Python to generate a full 3D model of a strut-and-node uniform and non-conformal lattice that does not include

the voxelization process before populating the structure with struts. In particular, this simple method generates a cloud of equally spaced points, which can be assimilated as a voxel grid. Such a grid is properly connected using struts knowing the unit cell topology. This generates a parallelepiped shape filled with a uniform lattice structure that is drawn exploiting the B-rep; then the designer is asked to perform a Boolean intersecting operation between the desired 3D model shape and the parallelepiped lattice model. As the last step, the desired 3D lattice model is ready to be exported in STL file format and manufactured with AM. The steps are described in more detail in the following list:

1. The designer chose the unit cell type (Refers to Figure 4.3), the struts topology (square or circular), the length and its characteristics, namely the cross-section dimensions;
2. The designer passes to the function the dimensions of the parallelepiped lattice model;
3. A file matrix is generated containing the struts type, the number of nodes and ligaments of the overall parallelepiped lattice, the cross-section dimensions and the sphere dimensions at the end of the struts;
4. The algorithm evaluates the coordinates of nodes belonging to the RVE of a single unit cell;
5. The coordinates are duplicated along the 3 dimensions to create a cloud of equally spaced points;
6. Duplicate nodes are deleted;
7. Only neighbour nodes with exact spacing from one node to another are connected (i.e. in the FCC unit cell, consider ligaments with length L and $\sqrt{2}L$);
8. Duplicate ligaments are removed;

9. Create a matrix $\mathbf{N} = n \times 3$ containing the list of nodes coordinates;

Node 1: $x_1 \quad y_1 \quad z_1$
 Node 2: $x_2 \quad y_2 \quad z_2$
 \vdots
 Node i : $x_i \quad y_i \quad z_i$
 \vdots
 Node n : $x_n \quad y_n \quad z_n$

10. Create a matrix $\mathbf{M} = m \times 2$ containing the ligaments topology between nodes;

Strut 1: $P_1 \quad P_2$
 Strut 2: $P_2 \quad P_3$
 \vdots
 Strut j : $P_i \quad P_{i+1}$
 \vdots
 Strut m : $P_{n-1} \quad P_n$

11. Place a sphere or a cube over the intersection of multiple struts to improve the overall geometry (Figure 4.8);
12. At turn, extrude a j strut between point i and $i+1$ of the grid contained in the $j - th$ line of \mathbf{M} matrix where the coordinates of both points are contained at lines i and $i + 1$ of \mathbf{N} matrix;
13. Intersect the obtained parallelepiped lattice structure with the desired component previously modelled as a bulk model.

4.2.3 2nd voxel-based modelling method

The second method employs the voxel-based ray tracing intersection algorithm to transform a B-rep bulk model into a voxel-based one and then

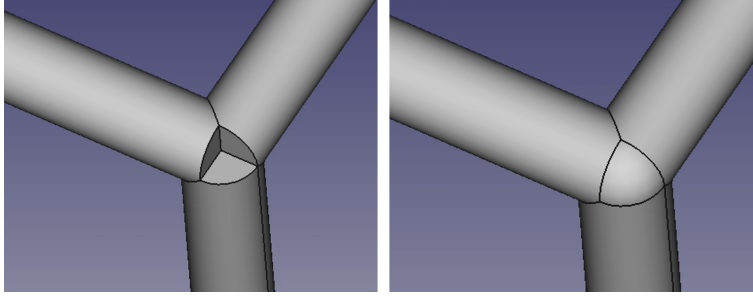


Figure 4.8: The intersection of multiple struts need the placement of a sphere (for circular struts) or a cube (for square ligaments) to improve the lattice geometry

assigns to each voxel a cubic unit cell. In this way, the Boolean's intersection operation of the previous method is avoided, speeding up the entire modelling phase.

Going into more detail, the process starts with an STL file of the 3D bulk model written both in ASCII or binary format. The triangular exterior surface discretization is stored and the triangles' vertices, facets, and normals are retrieved using a function that reads the STL model. Knowing the coordinates of the vertices, it is possible to evaluate the bounding box of the overall 3D model, essential information for the voxel grid computation. Then the designer is asked to give the desired voxel resolution in *mm* and the unit cell geometric characteristics. The algorithm automatically evaluates the number of voxels in each direction. A null logical matrix is initialized and then the ray tracing intersection method takes place to activate elements of the logical 3D matrix that belongs to the bulk model.

In the following, just the active voxels are considered as belonging to the desired lattice model. Using 3 nested *for* cycles along the 3 dimensions of the logical matrix, for the active cells, the algorithm distributes the nodes of the unit cell over the edges of each voxel depending on the unit cell type, computing the \mathbf{N} matrix. As done in the previous method, duplicate nodes are deleted, and the remaining ones are interconnected through ligaments, contained in the matrix \mathbf{M} . Duplicate ligaments are removed and the \mathbf{N}

and M matrices are given to the FreeCAD environment that produces the 3D lattice model using the B-rep just to export the final STL lattice model, needed for production purposes.

Compared to the previous method, the voxel-based approach could be further optimized by skipping the modelling of the 3D B-rep shape. Indeed, by knowing the node's coordinates and the ligament topology, a 1D simplified structure can be built (Figure 4.9). This simplified model can be of terrific interest for structural analysis purposes as will be shown in the next sections. Moreover, from the 1D structure, it could be possible to reconstruct the external surface made of triangles as similarly done in [134]. This task will be considered as the future development of the codes programmed for the aim of this thesis.

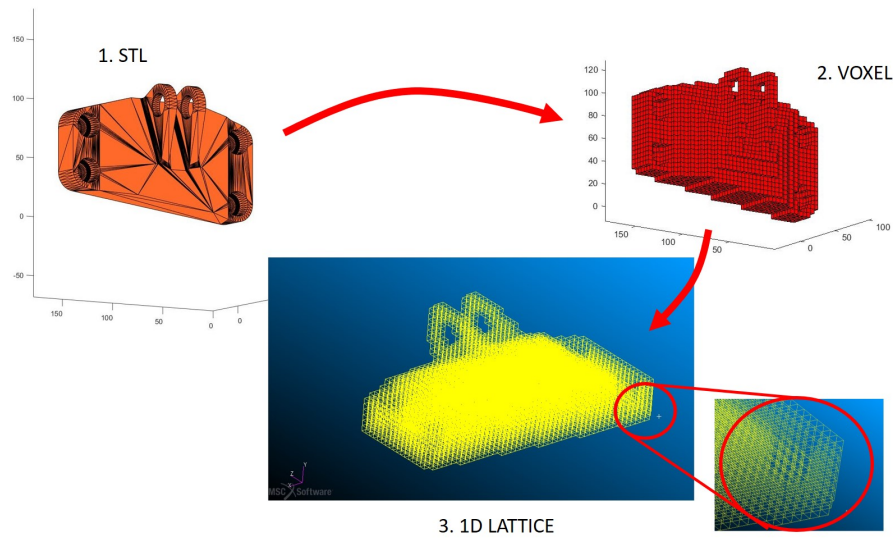


Figure 4.9: The 1D structure obtained through voxel-based modelling of a lattice structure starting from the 3D bulk model saved as STL file

4.3 Voxel-based methodology for mechanical simulations

Another significant issue of lattice structures emerges when a numerical analysis is used to analyse their mechanical behaviour. Due to the high structural complexity of real-life components, FE analysis requires a large amount of computational power to discretize the structure in billions of meshing elements, making traditional FEM less appealing. Alternative methods, such as homogenization algorithms, have been developed in the literature to address this issue. A non-exhaustive list of approaches for reducing the time required for structural analysis can be found in the literature:

- Closed-form expression based on the Euler-Bernoulli beam [135];
- Matrix-based techniques based on Bloch's theory [136];
- Micropolar elasticity theory [137];
- High-frequency homogenization [138];
- Discrete homogenization technique [139];
- Asymptotic Homogenization (AH) [140], [141].

Because of the stress distributions prediction reliability in the lattice structure without limits on unit cell topology, AH performs well in validation testing for a variety of applications. The AH method proposes to accelerate mechanical analysis by replacing a lattice structure with a completely dense homogeneous solid with equal mechanical characteristics, the same occupied volume, and the same loads and application points. The computer power required to calculate numerically the mechanical behaviour of periodic structures is reduced exponentially in this way. The reader is directed to Section 2.10 of source [7] for a more extensive exposition of the mathematical model of AH, which is beyond the scope of this thesis.

Using AH, it is feasible to get a closed-form formula for the equivalent stiffness matrix for a variety of unit cell topologies, based on published results. The meshing and analysis procedures are less computationally intensive, and the results closely resemble real-world behaviour.

The primary disadvantage of the AH method is its high computing cost in the case of complicated forms, which is related to a multi-scale issue that must handle a large number of variables in the event of non-closed-form solutions. This is why, in the case of complicated unit cell topologies, researchers must continue to create various simplification approaches to speed up material analysis. Furthermore, by adopting a bulk component instead of a periodic structure, this technique moves away from the real structural behaviour, and the designer may lose the geometrical lattice properties at the unit cell level.

To overcome these issues, the candidate proposes a voxel-based 1D methodology to analyse lattice structures, whose description is contained in an own journal article [122]. The research compares three ways of doing Finite Element Method (FEM) assessments on lattice structures: classic 3D analyses of the entire lattice structure, AH, and a novel creative 1D representation and simulation called Lattice to 1D (L1D). The last solution attempts to tackle the periodic lattice simulation problem by simulating a 3D strut-and-node lattice using 1D components. The ligaments, in particular, are approximated with their beam axis, resulting in roughly 90% less computing effort than the entire 3D model, with modest estimation error (around 15–20%) and the ability to provide the designer with a visual picture of the periodic lattice. Light computing efforts, superior lattice geometry comprehension at a preliminary design phase when multiple possibilities must be studied quickly with reasonable results, and less estimation error compared to real 3D lattice behaviour define this technique.

4.3.1 Lattice to 1D (L1D) Methodology

To apply the L1D approach, at first, a dense 3D model of the component in a lattice structure is drawn and stored in STL format to produce the mono-

dimensional lattice structure. Following that, an algorithm has been designed to fill the dense region with a periodic structure produced using 1D wireframe modelling: the direction and size of this 1D modelling are equivalent to the parameters of the lattice cell. Through a voxel-based technique, the 3D dense component is turned into a 1D lattice utilizing the axis of ligaments; the geometrical cross-sectional data and material parameters are sent to the solver in a second phase. Only mono-dimensional geometrical elements, such as lines connecting two different points according to the unit cell geometry, are used to create the resultant geometry. The voxel-based algorithm used in this approach is the same described in Section 4.2.3. The code's final step is to create a .out neutral file. The neutral file comprises the coordinates of the lattice points and the index of vertices connected together [142]. Several types of geometry file formats were studied, but the Patran software's neutral file format was determined to be the best owing to its ease of importing geometrical description, and formatting. Figure 4.10 shows a flowchart of the methodology established to get 1D geometry, with successive steps of this approach applied to a model of an aircraft engine bracket using a lattice.

Preliminary numerical studies are done using Patran/Nastran software with a tensile load scenario, imposed on a cantilevered rectangular beam filled with uniform lattice for validation purposes, to examine the viability of this alternative technique. Patran/Nastran is adopted as a software platform because of its great stability when compared to low bandwidth open-source frameworks like FreeCAD. To begin, the L1D method is verified to see how certain design characteristics (unit cell type, cross-sectional type) impact the results. The L1D method is then used to simulate a real-world item, such as an aircraft engine bracket with a uniform and periodic lattice. The cubic form, assimilable to voxels, of the periodic structure's unit cells, is used. In the cantilevered beam example, two separate unit cells are used: the basic cube unit cell and the face-centred cubic unit cell (FCC) to test the L1D's efficiency for bending (simple cube) and stretching dominated (FCC) lattice unit cells. Furthermore, the ligaments that make up the lattice are modelled

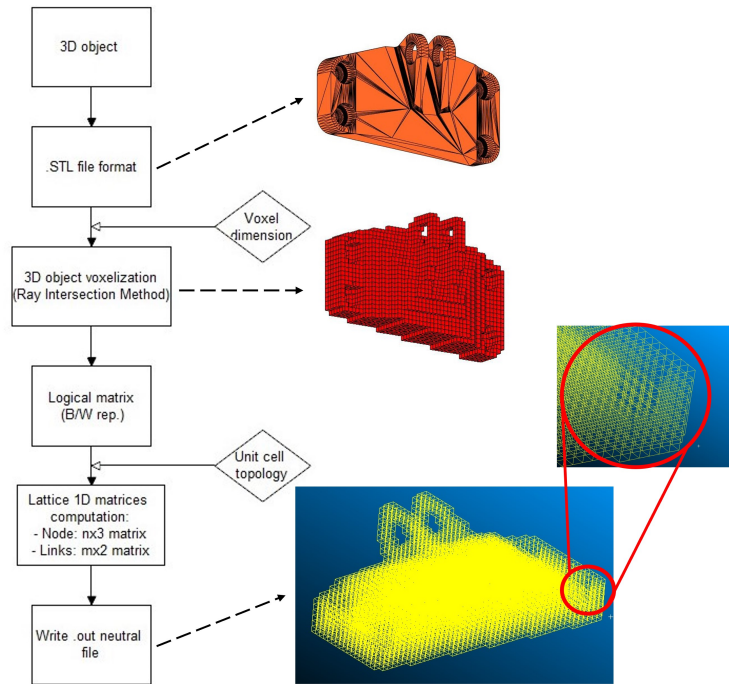


Figure 4.10: L1D methodology flowchart applied on the aircraft engine bracket of GE [122]

using both square and circular beam cross-sections for the sake of this study to evaluate all of the various settings that may affect the lattice design. In the engine bracket simulation, just the simple cubic unit cell is employed for simplicity.

On a workstation equipped with 32 GB RAM and an Intel Zeon CPU @ 3.50 GHz, the L1D approach is performed to voxelize and write the neutral file. Table 4.1 shows the total time required to convert the sample component provided by the aircraft engine bracket changing the voxel resolution.

After importing the resulting mono-dimensional lattice geometry as a .out format file into Patran/Nastran, the material characteristics, which are the effective ones rather than the corresponding properties derived via AH techniques of a hypothetical completely dense object, can be provided to the program. Furthermore, because the neutral file lacks this information, the user can define the beams cross-sectional properties in the solver using

Voxel resolution [mm]	Computational time for L1D	N. of voxels
7	22.4	1576
6	33.2	2560
5	52	4207
4	104	8136

Table 4.1: L1D computational time changing the voxel resolution for the G.E. benchmark bracket model [122]

the Patran "Properties" menu. The "beam" 1D attribute was chosen to characterize all of the ligaments that make up the lattice for the sake of this study. The bending effects would be ignored if you used a rod option.

To demonstrate the effectiveness of the L1D technique, additional simulations involve a 3D bulk model with equivalent mechanical properties evaluated through AH methodologies. The 3D completely dense homogenized material stiffness matrix is filled with AH closed-form data from two of the most relevant literature contributions on the topic. In particular, on the one hand, in [143] the macroscopic stiffness of several lattice topologies is determined using an asymptotic homogenization multi-scale technique. The stiffness matrices are determined by geometrical unit cell properties such as ligament length (L), cross-sectional dimension (t), the moment of inertia (I) and cross-sectional area (S), as well as material characteristics such as Young's modulus (E) and Poisson ratio (ν). These results can be implemented only if a slenderness ratio (ligament length over cross-sectional dimension) of at least 10 is guaranteed to validate the slender beam assumption at the basis of this approach.

On the other hand, based on Andreassen and Andreassen's process [144], in [145] the researchers created a MATLAB tool to examine alternative unit cell lattice topologies using a voxel-based approach. Knowing the unit cell dimensions, the unit cell topology and the material parameters, the algorithm may provide the lattice stiffness matrix entries. However, in terms of cross-

sectional topologies, this technique is restricted, and only circular topologies are represented.

The resultant lattice stiffness matrix for both specified contributions has a varied scheme compared to typical isotropic materials and sees the lattice structure as an orthotropic material. The stiffness matrix \mathbf{K}_{latt} may be represented in a closed-form as a function of three parameters α , β , and γ (eq. 4.2) for periodic structures if the geometric properties of the unit cell topology are known. The matrix parameters for the simple cubic unit cell are evaluated thanks to eq. 4.3.

$$\mathbf{K}_{latt} = \begin{pmatrix} \alpha & \beta & \beta & 0 & 0 & 0 \\ \beta & \alpha & \beta & 0 & 0 & 0 \\ \beta & \beta & \alpha & 0 & 0 & 0 \\ 0 & 0 & 0 & \gamma & 0 & 0 \\ 0 & 0 & 0 & 0 & \gamma & 0 \\ 0 & 0 & 0 & 0 & 0 & \gamma \end{pmatrix} \quad (4.2)$$

$$\begin{cases} \alpha = \frac{S}{L^2} \\ \beta = 0 \\ \gamma = \frac{6I}{L^4} \end{cases} \quad (4.3)$$

The eigenvalues of each unit cell type will be different, resulting in various mechanical properties. Moreover, if the Euler–Bernoulli beam assumptions are incorrect, local compressive loads may cause instabilities, as reported by Vigliotti and Pasini [146]. Then, the results coming from AH are compared to those of 1D analysis for the scope of the research.

The goal of this study was to see if the L1D technique may be a viable alternative to the AH method for lattice structural analysis. To accomplish so, a series of simulations were run in Patran/Nastran software, comparing maximum and mean displacements, mesh size, meshing time, and solution time for three different situations (AH, 1D, and fully 3D model).

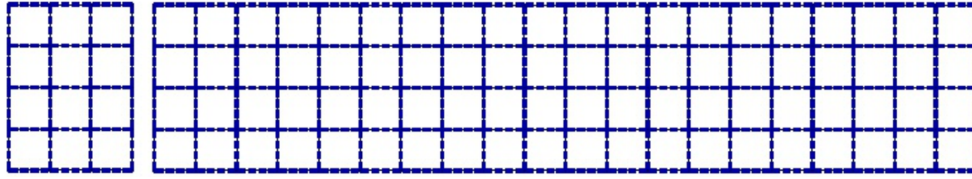
4.3.2 L1D numerical simulations

A cantilevered beam with a rectangular cross-section is utilized to test the L1D methodology's capabilities, with a 500 N axial load applied to the free extremity as nodal forces on the overall surface. The parameters of the beam are 30 mm in thickness, 40 mm in height, and 200 mm in length (Figure 4.11 (a)). Furthermore, the unit cell characteristics are chosen to provide a slenderness ratio of 10 to comply with the Euler–Bernoulli assumption. The size of the unit cell is chosen to keep the computing power required to create and simulate the 3D lattice structure to a minimum. The L1D technique is tested with two distinct unit cell topologies to see if it can describe both stretching and bending dominating lattices. Both squared and circular cross-sections are modelled for each unit cell type, allowing the cross-sectional variable to be explored for the study.

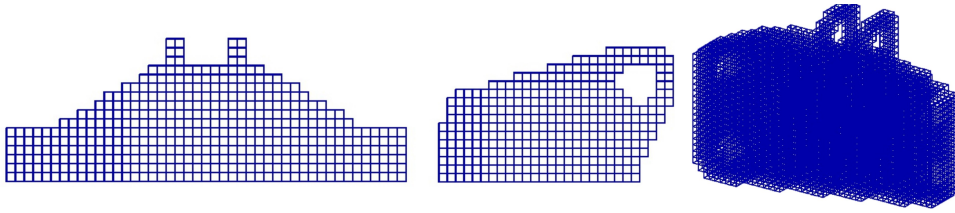
To comprehend the L1D performances in a substantial industrial engineering scenario, an additional set of simulations involves an aircraft engine bracket that was designed with a uniform and periodic lattice. For the purposes intended, the bracket's constraints are four holes on a base that are fully limited for all six degrees of freedom. There are two vertical holes in the opposing section of the bracket where a tensile load is provided in the form of nodal force dispersed over the cylindrical hole surface. A vertical component of 200 N and a horizontal component of the same amount make up the simulated load. The bracket is filled with uniform and non-conformal lattice, with the simple cubic unit cell topology being used for simplicity (Figure 4.11 (b)).

In Table 4.2, are reported the unit cell topology features for the cantilever beam case study, used to validate the methodology and for the aircraft engine bracket from GE [95].

Equation 4.2 is used to represent the 3D homogenized component with an orthotropic material, using matrix entries derived from [143] and [145]. The whole 3D lattice and 1D wireframe are modelled using an isotropic material with bulk properties. The change in unit cell dimensions between



(a) Beam geometry



(b) Bracket geometry

Figure 4.11: View from different directions of the 3D lattice structures used to validate the L1D methodology

the beam and bracket case study is done for computational purposes. In the engine bracket voxel-model, in the support region where the tensile stress is applied, such unit cell dimension has been selected to have at least two layers of lattice cells: a trade-off has been carried out using a voxel size that is not very demanding for the computational resources available to us. The material employed in these calculations for the cantilevered beam is Ti6Al4V ELI-0406 powder for AM applications, which has a Young's Modulus of 126

Dimensions [mm]	Cantilever beam	GE engine bracket
Ligament length	10	4
Cross-section dimension:		
Square edge	1	0.4
Circular radius	0.5	0.2

Table 4.2: Unit cell dimensions for the case studies included in [122]

GPa and a Poisson ratio of 0.3 [147].

A mesh convergence study, applied to the cantilever beam case, has been set for the whole 3D model simulation since it is the most important because it provides benchmarking data for comparing other techniques to study periodic structures. It was discovered that a mesh size of 0.5 mm (half the cross-section dimension) is precise enough to capture the mechanical behaviour of the component with low computing costs (less than 0.5 % inaccuracy and 89 % time savings compared to 0.125 mm average mesh size). After the mesh convergence study has been fixed, the whole set of simulations for the cantilever beam has been carried out: two simulations using the 3D complete model (one for circular cross-section and one for square shape), two simulations using the 1D model from the L1D approach (respectively for circular cross-section and square), and three simulations using the 3D fully dense beam (two simulations using the results from [143] for square and circular topologies and one simulation using the research outcomes of [145] for the circular configurations) (Figure 4.12).

4.3.3 Discussion of the results of the L1D approach

The tables with the full results of the cantilever beam can be found in the own contribution [122], while here just the more significant outcomes are collected and discussed in this subsection. Table 4.3 contains the evaluation of the relative errors on the maximum and mean displacements compared to the full 3D model results for each unit cell topology. In the Table, the mean relative error value for square and circular cross-sections has been considered.

Moreover, a further analysis involves the mean computational time required to discretize and numerically solve the entire lattice structure for both the involved topologies. In Figure 4.13 it is shown a tower chart with a visual comparison of the full 3D approach versus the L1D and AH approaches.

From these results, it is straightforward that both L1D and AH approaches decrease about 90% of the time required for meshing and more than 80% time needed for the software to converge to a solution no matter

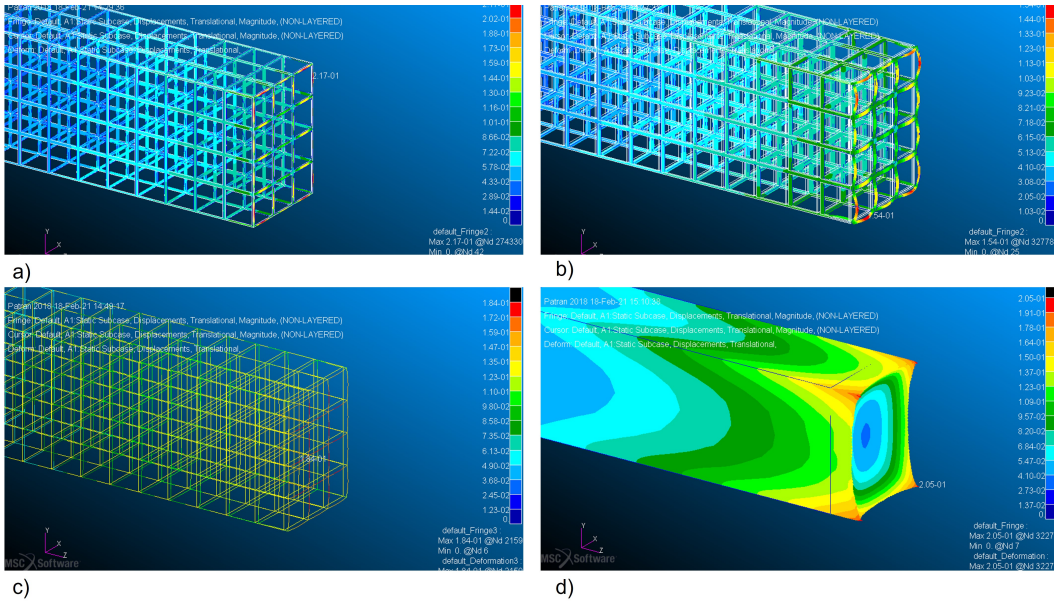


Figure 4.12: View of strain field of the cantilever beam [122]: a) full 3D model of simple cube lattice with circular cross-section; b) full 3D model of simple cube lattice with square cross-section; c) 1D lattice with circular cross-section and d) 3D equivalent bulk model using the AH method of Vigliotti et al.

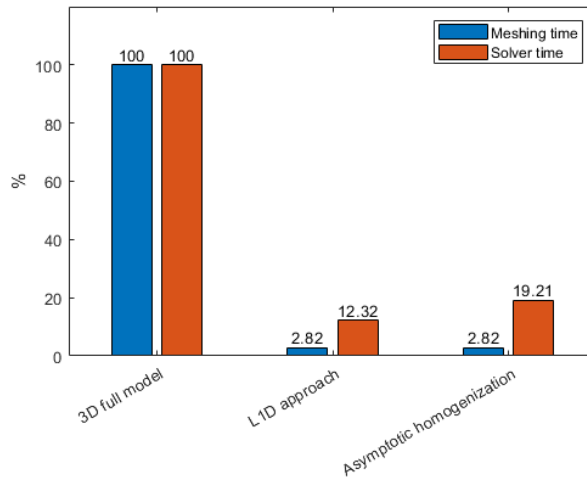


Figure 4.13: Computational time comparison to mesh and solve the lattice structure depending on the approach used

Numerical approach	% error on U_{max}	% error on U_{mean}	Lattice topology
L1D	12.5	23.5	simple cube
	21	13.5	FCC
AH [143]	4	1	simple cube
	49	25	FCC
AH [145]	13	20	simple cube
	52	27	FCC

Table 4.3: Comparison of mean % error on the displacements of L1D and AH approaches compared to the 3D full model analysis

is that the unit cell or the cross-sectional sort. This result's extraordinarily vital within the context of conceptual/preliminary design once many configurations got to be investigated in a very quick manner. Moreover, from this research, it's also viable to recognize that the cross-sectional topology does not affect the computational fees and the accuracy of the outcomes for each AH and 1D approach, confirming the effects received with-inside the study of Cook [148]. The most effective distinction is that, once the square topology is used, the computational price will increase for the full 3D model analysis.

Focusing the attention on the accuracy of the proposed L1D approach, it can be seen that the error on the displacement estimation is about $15 \div 20\%$ which is an encouraging result, especially for the possible application context for this methodology. Moreover, the AH approach proposed by Vigliotti and Pasini estimates with greater accuracy the lattice deformations for the bending ruled unit cell for both maximum and mean displacement, whilst worse deviations are depicted for the stretching ruled unit type as compared to the L1D technique. The AH technique by Dong is restricted to the cross-section topology and the accuracy is withinside the order of magnitude of the 1D methodology.

The main advantage of the L1D approach is that the designer can rapidly understand the behaviour associated with individual beam elements, which

is not possible with the AH methods while maintaining the same level of accuracy in terms of displacement estimation.

In the example study represented by the GE bracket, the same strategy was used to compare the L1D methodology against AH approaches and the 3D complete model. However, we ran into some computational problems when simulating the 3D entire model of the engine bracket filled with uniform lattice. The computer resources at our disposal were insufficient, and the meshing technique ultimately failed. Because of the restricted computer capability, alternative methods must be utilized to model the mechanical behaviour of a complicated lattice structure in a real-life scenario. Due to good findings from the cantilever beam simulations, the AH techniques were used as a benchmark to evaluate the L1D capabilities used on a real-life item, since the results from the 3D complete model were not accessible. The engine bracket is simulated utilizing AH techniques with the same design using a basic cube unit cell with both circular and squared shapes while the L1D technique is used on the same object's 1D model (Figure 4.14).

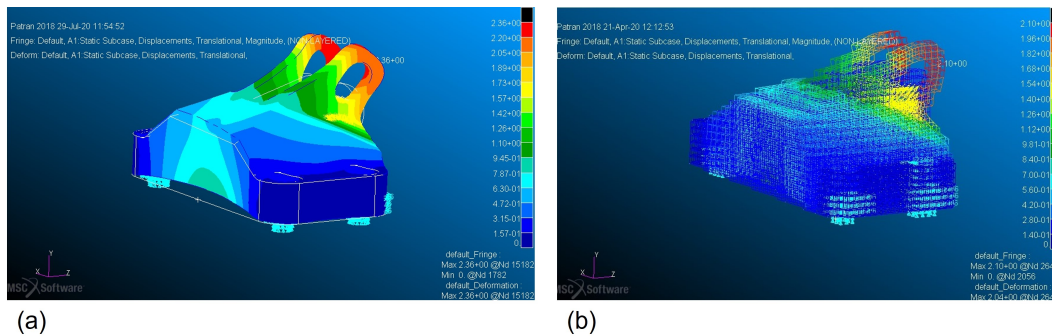


Figure 4.14: Strain field view of (a) homogenized 3D model using [143] material characteristics and of (b) 1D model using the L1D approach [122]

However, just to have a quantitative reference for the 3D model, a linear trend for the displacement estimate error was assumed using the values of the relative errors determined with the cantilevered beam example. Knowing the maximum displacements of the AH models, it was feasible to extrapolate the maximum displacement of the 3D whole model, using eq. 4.4.

Numerical approach	% error on U_{max}	Meshing time [s]	Solver time [s]
3D model	-	2817	$\rightarrow \infty$
AH [143]	6	5	25
AH [145]	13	5	25
L1D	15	35	28

Table 4.4: Comparison of mean % error on the displacements of L1D and AH approaches compared to the 3D full model analysis

$$\frac{U_{max_{3D}}}{1} = \frac{U_{max_{[143]}}}{1 - err_{[143]}} = \frac{U_{max_{[145]}}}{1 - err_{[145]}} \quad (4.4)$$

Thanks to this assumption, it is possible to estimate the deviation from the 3D model simulation of the alternative investigated approaches. The main outcomes of this comparison are collected in Table 4.4.

From these results, it emerges that to reduce the computing time and power required for mechanical simulations, simplification methods such as AH or L1D must be utilized for items with complicated geometry, such as the GE engine bracket. On the one hand, the simulation failure was caused by the 3D complete lattice model being too intricate and computationally intensive. Both the AH and L1D techniques, on the other hand, reduce meshing time and element count by up to 99 % while keeping a sufficient level of accuracy ($\simeq 10 \div 15$ % deviation on maximum displacement), which is essential in the context of conceptual/preliminary design.

To summarize, the 1D approach can estimate maximum and mean deformations with low computational power while still providing a designer with an overview of the lattice geometry and behaviour, even at the ligament level, for both stretching and bending dominated unit cells, whereas AH approaches are more precise for bending dominated topologies compared to stretching ones. When compared to the 3D object, both AH and 1D techniques have equal processing needs for meshing and convergence. Furthermore, the

L1D technique may be considered a good alternative to homogenization approaches since it can produce equivalent results, or perhaps better, while still providing the designer with a quasi-real geometric perspective. However, because only node-strut arrangement lattices can be represented, the suggested technique has certain restrictions that will be investigated in further studies in the future. The proposed approach, with further improvements, could be used in the conceptual design stage to understand the mechanical behaviour of complex automotive structures filled with a lattice structure, like those described in [149], and lowering the designer effort to analyse structurally components through traditional approaches.

4.4 Proposal for a 2D representation standard in drawings

By reviewing the interesting literature about lattice structure modelling, the candidate found an interesting gap among the available Standards related to the DfAM of lattice structures. In particular, a large number of contributions deal with the optimization of 3D modelling of lattice structures ready to be manufactured with AM. In this way, the STL or the AMFF file can be generated, so that for manufacturing purposes there is no need for 2D part drawings. However, 2D sketches are still widely used in industrial companies and the workshops for assembly/disassembly sequences, maintenance manuals, bill of materials and spare part nomenclature because they contain GD&T symbols and tooling details. Thus 2D drawings still play a key role even if Augmented Reality and 3D manuals have been gaining ground in recent years (Figure 4.15). Indeed, a digital revolution makes sense only for high-value maintenance operations, such as in aerospace [150]. Moreover, they can be used to rapidly exchange data between technical offices and operators without the need for technological support. 2D drawings can also preserve intellectual property better than 3D models by hiding information and using simplified representation.

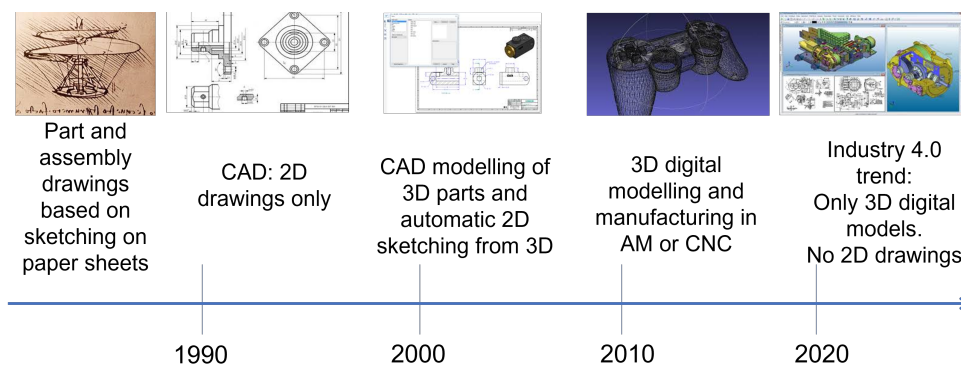


Figure 4.15: An evolution in time can be noticed in design/sketching of components

In the common design workflow, 2D drawings are automatically produced by CAD software from the 3D bulk models to support workshops, manufacturing, illustrated parts catalogues and maintenance manuals. However, if the 3D part has small size features that are repeated thousands of times such as the lattice structures, the representation in drawings could be hardly understandable, due to the enormous amount of small detail. In this context, 3D components usually related to the AM field are still not considered in the available Standards and their representation could be a challenging task. For this reason, International Standard Organization (ISO) should be pressed by companies to develop new Standards dealing with all the design, production and maintenance stages of products coming from the AM supply chain.

To overcome this technological gap, the candidate proposed a new representative Standard for periodic structures based on the use of conventional symbols to describe their shape and dimensions. The reasons for the proposed Standard and its description have been widely discussed in the own contribution [121]. Here the key features are discussed. The developed Standard has been embedded in FreeCAD using Python language as done for all the coded functions and macros related to lattice structures which are described in this Chapter. This new Standard allows to represent lattice structures as conventional components that on the one hand use light and

comprehensive symbols, but on the other provide all the needed information about hierarchic structures.

As described in Section 3.4, International Standards are extremely important to help wider adoption of a certain technology; however, in the AM field, few Standards are approved and available to date due to the constant innovation and exponential improvement of AM technology that does not permit to International Organizations and Associations to keep up the pace. Moreover, the lack of Standards slows also the certification process of structural components in critical applications such as automotive and aerospace.

Moving the attention to 2D drawing Standards, ISO Committee recently focused on the publication of a Standard for part representation in CAD software of composite structures including GD& T system and roughness indication [151]. However, no information is available about how to deal with the 2D representation of parts coming from AM such as lattices or topologically optimized structures.

For this reason, a draft of a simple and user-friendly representation Standard is proposed taking inspiration from the EN 4088-001 regulation about the "Representation of parts made of composite materials" [151]. Similarly, a possible solution to condensate several information about complex structures, such as composite materials and lattices, is the use of simple tables to summarize the main features which describe completely the structure. These tables can be placed over the title block (T/B) section of drawings.

Three different tables are designed to host the main characteristics of lattice structures respectively for uniform non-conformal lattices, graded lattices and conformal periodic structures. However, some features are common to all the developed tables. In particular, only the lattice structures with a cubic shape unit cell, akin to a voxel of dimension v , have been considered, taking the Figure 4.3 as unit type portfolio. Moreover, only struts with square and circular cross-sections are taken into account, whose characteristics dimension is d , while L is the struts element length from one node to the other. However, the same representation Standard could be applied

to other types of lattice structures with small modifications. According to Figure 4.16, where it is shown a list of symbols used in the developed tables, the meaning of these are:

- (a) Unit cell with circular cross-section, which diameter is d in mm;
- (b) Unit cell with square cross-section, which edge dimension is d in mm;
- (c) Voxel-based lattice structure with voxel resolution of v in mm;
- (d) Unit cell with strut length of L mm from node to node;
- (e) Lattice filling orientation in terms of an angle with respect to a datum, in $^\circ$.

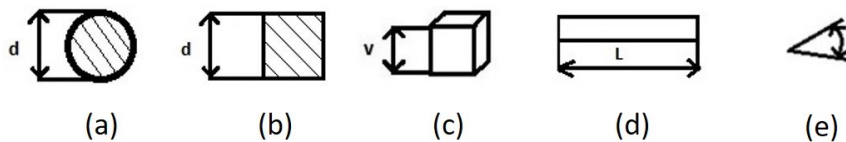


Figure 4.16: Symbols used to describe the struts and unit cell dimensions for the proposed Standard [121]

The three developed tables are shown in Figure 4.17 and will be discussed in the following paragraph. A common feature is a label placed automatically over the table to name and distinguish a lattice structure from the other that may appear in the same drawing. The same label is placed over the corresponding component in the drawing to link the lattice characteristics with the right geometry.

Starting from the simplest type of lattice, namely the uniform and non-conformal periodic structures, a table of 5 rows is developed to contain all the needed information to completely describe the component (Figure 4.17 (a)). In particular, in these types of hierarchic structures, all the unit cells are identical in the three directions and only an infill operation is done, ignoring the external surface shapes. Thus, just the strut type and dimensions (first,

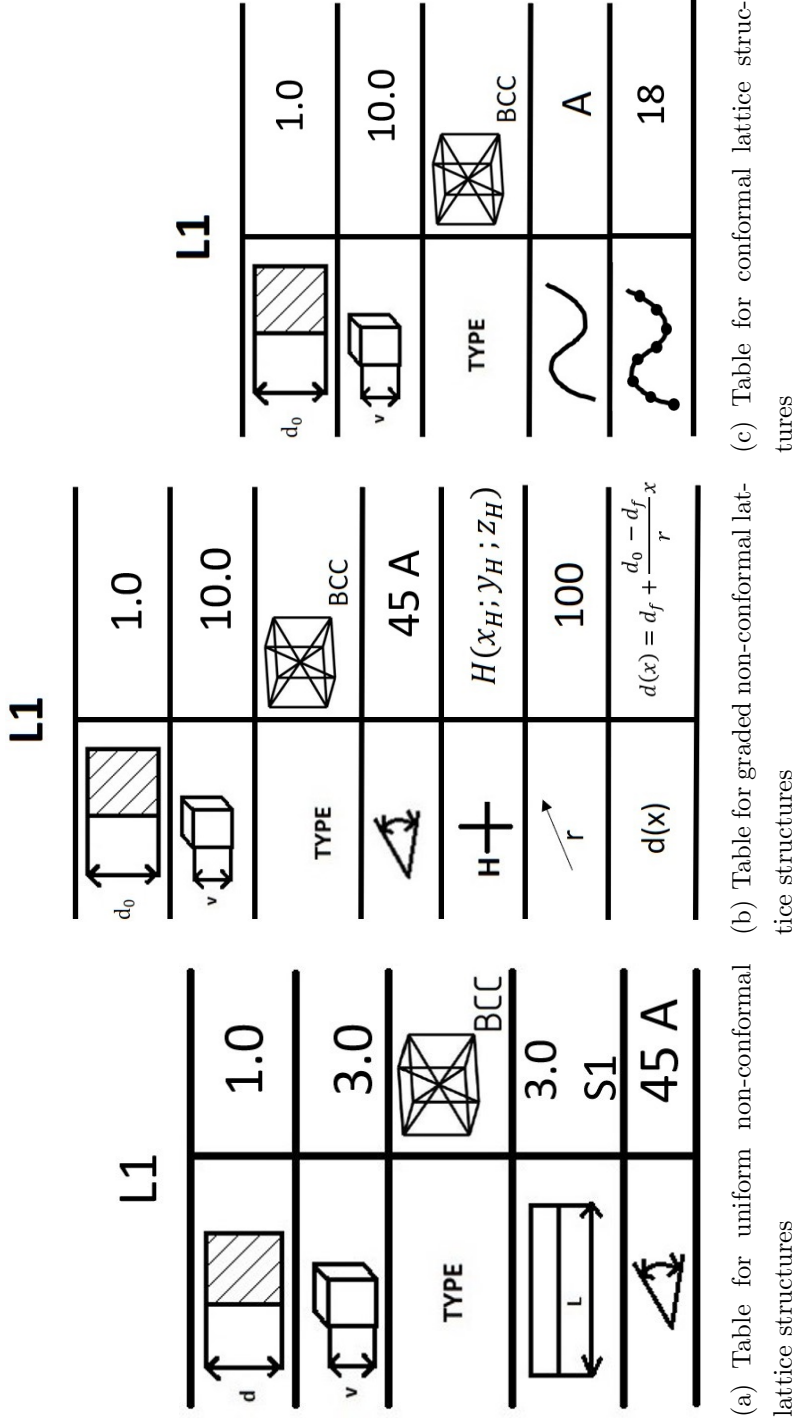


Figure 4.17: Tables used in the proposed representation Standard to describe lattice structures in 2D drawings [121]

second and fourth rows), the unit cell type (third row) and the infill orientation (fifth row) are sufficient to completely describe the structure. Next to each symbol contained in the table, the respective dimension in mm is inserted automatically by the developed framework in FreeCAD. Particular attention is given to the strut length and the possibility to include a sphere or a cube at the intersecting point of several struts to correct the overall shape (Figure 4.8). For this reason, along with the length in mm , an additional label with the indication of S1 states that a sphere of radius 1 mm is added to both endpoints of a strut; respectively a C1 is used for a 1mm edge cube. The last row provides the infill orientation in degrees compared to a datum, in this case, A . The rotation order the designer must follow is z (the axis exiting from the drawing sheet), y (vertical axis) and x (horizontal axis).

Moving to the graded non-conformal lattice structures, in Figure 4.17 (b) a similar table is developed. Compared to uniform lattices, additional rows are added to describe the gradient of change of lattice properties in space. The mathematical formulation of the gradient function of the strut dimension $d(x)$ is included in the seventh row. For the moment, just linear-gradient functions are considered, but a similar approach can be used also for other types of functions. The mathematical formulation of $d(x)$ is

$$d(x) = d_f + \frac{d_0 - d_f}{r}x \quad (4.5)$$

where d_f is the strut dimension at the origin of the sphere of influence, d_0 is the general strut dimension of the uniform lattice and r is the radius of the region of influence. The gradient is centred in the point H whose spatial coordinates are given in the fifth row of the table. As the last parameter, a sphere of influence centred in H of the gradient defines the limited region where the lattice properties variates compared to a uniform one; to completely define it, the radius of the sphere is given in the sixth row in mm .

As the last periodic structure considered in the proposal, the conformal lattices are characterized by a distortion of the unit cells in two dimensions to follow the external surface chosen by the designer. The corresponding table is shown in Figure 4.17 (c) and some differences can be noted if compared

to the previous ones. While the characteristics of struts and unit cell type remain the same, the fourth and fifth rows are replaced with information regarding conformity. In particular, the former describes to which external surface of the object the lattice is conformal using a datum, while the latter contains the number of subdivisions of the conformal surface that is also equal to the number of cells along that surface.

To better distinguish the types of lattice structures inside a complex drawing where multiple period structures may coexist, one of the three symbolic images collected in Table 4.5 is placed inside the contour of the component filled with periodic structure. This is done to increase the readability of 2D drawings and to avoid the use of crosshatches, already employed for cuts and sections (ISO 128-3:2020).

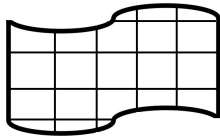
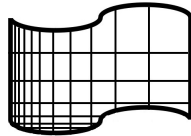
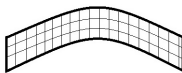
Uniform non-conformal lattice	Graded non-conformal lattice	Conformal lattice
		

Table 4.5: Symbolic image of three different types of periodic structures considered in the proposed Standard [121]

The overall representation proposal has been coded in Python to be included in the *TechDraw* environment of FreeCAD, at the disposal of the user to obtain technical drawings, being available a 3D model. A simple case study involving an assembly made by 2 lattice rods linked with a pin is included to show the effectiveness of the proposed representation Standards. The rods are composed of two thin bosses connected by a lattice structure based on a simple cubic unit cell, as shown in Figure 4.18.

The case study is set up to demonstrate the legibility of this type of assembly in a 2D technical drawing. Being available the same assembly but with the bulk rods, the user is asked to open the *TechDraw* environment and quote the drawing automatically computed by FreeCAD. When it comes the

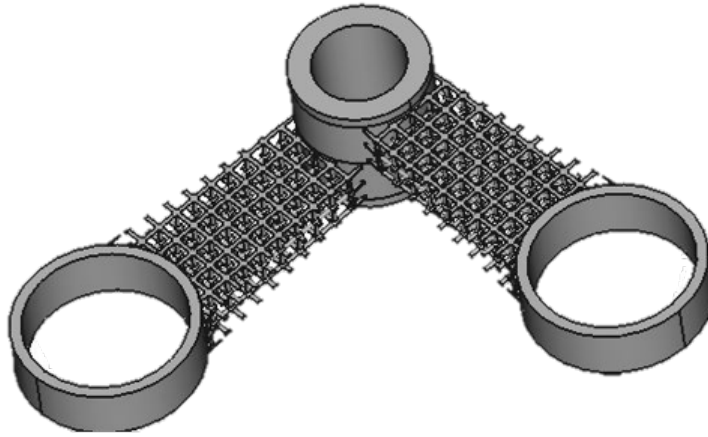


Figure 4.18: Case study to demonstrate the performances of the proposed representation Standard for lattice structure [121]

time to give some specifications about the lattices of the considered assembly, the user launches the own programmed macro, inserts all the lattice geometrical characteristics and places manually the lattice name label and its symbol according to Table 4.5.

In the following, FreeCAD autonomously generates the table previously discussed (Figure 4.17) and places it over the T/B, obtaining a 2D representation that is clear and comprehensive. Thanks to the proposed standard, designers can avoid a complex representation of the lattice components with all the struts and make the drawing representation easy to be understood because of the absence of small details. Moreover, thanks to the developed add-on for lattice structures the quoting process of lattices could be clear and far from being operator-dependant. The corresponding 2D drawing of the considered assembly is shown in Figure 4.19 and it has been obtained applying the proposed standard where both the lattice structures, that are used to fill the rods, are of the uniform non-conformal type.

The advantages of the proposed Standards have been widely discussed in this section, but also some limitations are considered as starting points for future developments. Indeed, the proposed Standard can handle only strut-

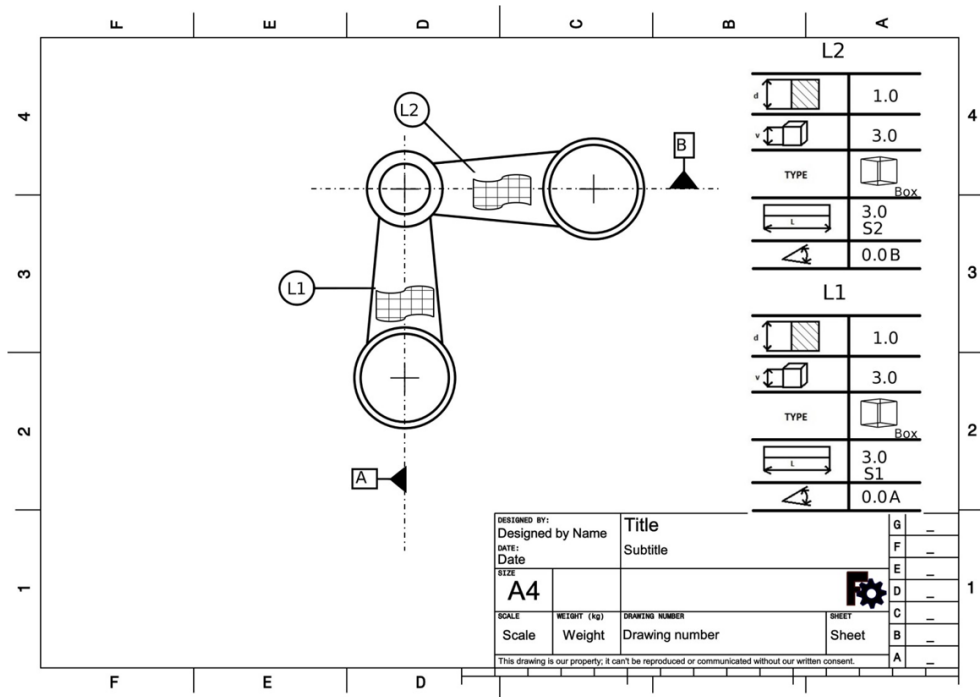


Figure 4.19: Case study to demonstrate the performances of the proposed representation Standard for lattice structure: the considered assembly on the left and the resulting 2D drawing on the right [121]

and-node voxel-based periodic structures, while it is still not able to consider other kinds of lattices, such as the TPMSs. The unit cell type portfolio is still limited but in the future, it can be easily populated with other topologies thanks to the open-source framework used to embed the codes. A similar concept can be applied also to the cross-section topologies, that now are limited to square and circular.

The same concept, here applied for lattices, could be extended for all the components made by AM techniques which should be represented in 2D drawings for the reasons herein listed. Tables placed over the T/B could collect important features about the production process and the main characteristics that are visible with naked eyes to help operators to recognize components in assembly/disassembly operations. Indeed, to date no available standard deals with the 2D representation of topologically optimized

components manufactured with AM, a design process that is skyrocketed in the last years in the automotive and aerospace sector, that will be widely discussed in Chapter 5.

Chapter 5

Topology Optimization and DfAM

As it emerged from the literature review contained in Chapter 2, the flourishing of AM promoted innovative design solutions and optimization approaches in many different sectors. In this context, new design strategies to reach extreme lightweight and exotic structures catch on because of plenty of design flexibility given by AM. A non-inclusive list comprehends the ground structure method, the generative design and the topology optimization which are mainly used in highly efficient industrial applications such as aerospace [152], automotive [153] and biomedicine [154].

The ground structure approach simulates a truss-like structure with a finite number of beam components by deleting unneeded elements from a linked truss structure and freezing nodal locations [155]. Generative design is an iterative process that, given the boundary conditions, generates a set of viable solutions that satisfy the original constraints, with the best option being picked thanks to the designer's assistance [156]. Topology Optimization (TO), as already cited in the previous Chapters, is a numerical design approach that ensures the optimal material distribution by allocating material or void to all discretized volume components without requiring the algorithm to follow pre-designed geometries. Among these structural opti-

mization techniques, TO is the most used in the automotive sector because of its efficiency and robustness; thus, this Chapter will focus on the TO description and all the main achievements in this regard obtained during the PhD project. All the information herein described are picked up from two own contributions [157] and [158].

Regarding the TO, this design tool usually maximizes the global stiffness by minimizing a fitness function that in most situations is represented by total structural compliance. Information on the boundary conditions, the load scenario applied to a preset working volume, the existence of passive features (e.g. holes), and the maximum material volume fraction needed to prevent a dense solution are all required to solve the issue. The design flexibility offered by TO allows for the creation of unique and high-performance solutions while lowering material and structural weight and preserving functionality, as done in [159] for an automotive component to achieve an important weight reduction. Different TO numerical approaches are described in the literature; a non-exhaustive list includes:

- SIMP (Solid Isotropic Material with Penalization): this strategy is mostly used to solve the problem of minimal compliance. It's a gradient-based method that uses a continuous distribution of material density to update the 3D model after each iteration of the structural analysis [160];
- ESO (Evolutionary Structural Optimization technique): this method employs a completely dense control volume and subtracts superfluous material at each iteration until an optimal structure is reached [161]. At each iteration, a characteristic parameter (i.e. Von Mises stress) is evaluated for all the elements and those who have low-stress values become empty elements;
- BESO (Bidirectional ESO): This numerical technique is based on the ESO strategy, but it may also add material if necessary to provide the best results [162].

In the next sections, only the SIMP technique will be discussed, in which the design variable is the density of the material ρ_e of a discrete element e . It gets its name from the power-law dependence of the single e -th element stiffness tensor \mathbf{E}_e on the material density, as stated in eq. 5.1.

$$\mathbf{E}_e = \mathbf{E}(\rho_e) = \rho_e^p \mathbf{E}_o, \rho_e \in [\rho_{min}, 1] \quad (5.1)$$

The penalization factor is p and \mathbf{E}_o is the allocated isotropic material stiffness tensor. The FEA's numerical stability is ensured by setting the lowest permitted relative density value (ρ_{min}) for empty elements with a value larger than zero. The TO issue is known to be poorly posed since the solution is mesh-dependent, although the TO problem can be limited by using a density or a sensitivity filter [163]. As p increases, the relationship between stiffness and density becomes steeper and the severity of the algorithm towards grey elements increases.

During the PhD programme, the author integrated a TO tool in the mentioned open-source CAD software called FreeCAD. The own framework is called ToOp and it was programmed through Python macros. It is based on a SIMP approach using a sensitivity filter to make the problem well-posed. Moreover, the solver uses the continuation method [164], meaning that the penalization value increases with small steps during the optimization iterations until reaching $p = 3$. In this way, the grey elements (relative density between black $\rho_e = \rho_{min}$ and white $\rho_e = 1$ elements) will migrate towards black or white ones without moving away from the optimum value. Unlike other TO open-source codes in the literature limited to rectangular domains [77] or without a user-friendly methodology [165], the ToOp framework is capable of returning an optimized structure after a TO analysis using a user-friendly GUI and an easy workflow from the design of the control volume, simulation settings, meshing and FEA, and post-processing of the 3D model using the same software (Figure 5.1).

In general, the results of the previously cited optimization approaches are connected to the quality of the component mesh of the finite element

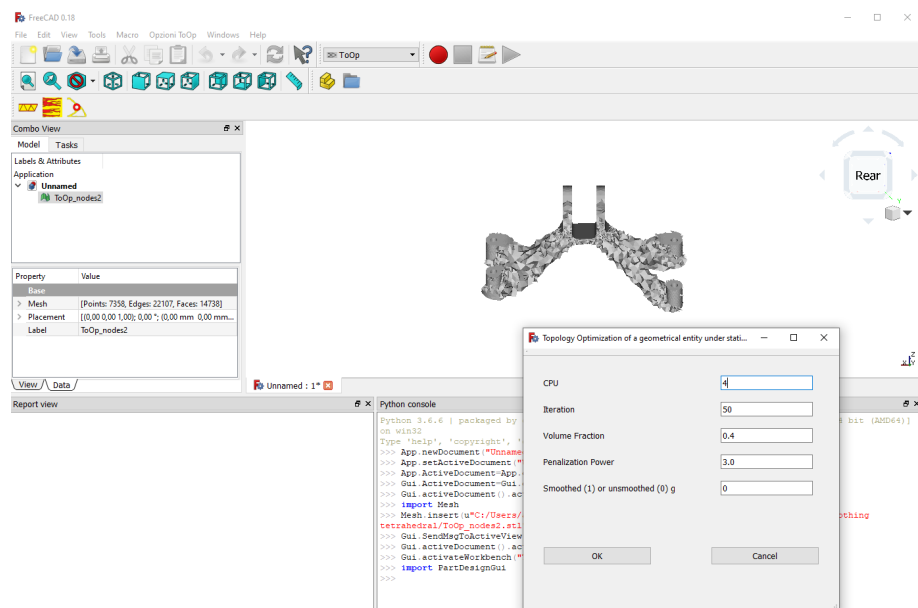


Figure 5.1: GUI of ToOp framework embedded in FreeCAD: view of the dialog window to insert the main parameters for a Topology Optimization simulation

model, regardless of the designer’s optimization methodology. Because of the presence of peaks, cracks, or non-manifold edges in the mesh that discretizes the 3D model, the best solution may be far from manufacturable, as can be seen in Figure 5.2.

At this stage in the design process, you have two options:

- A apply post-processing techniques directly to the ideal solution;
- B re-design the component from scratch, drawing inspiration from the optimal result of the previous phase.

Even if the second option is usually the applied one in commercial design tools, nowadays the research community is striving for the first solution to shorten the design-to-manufacturing cycle, save costs, and improve design workflow efficiency. Although there are various papers in the literature that combine TO and AM ([166] and [167]), the resulting design process is

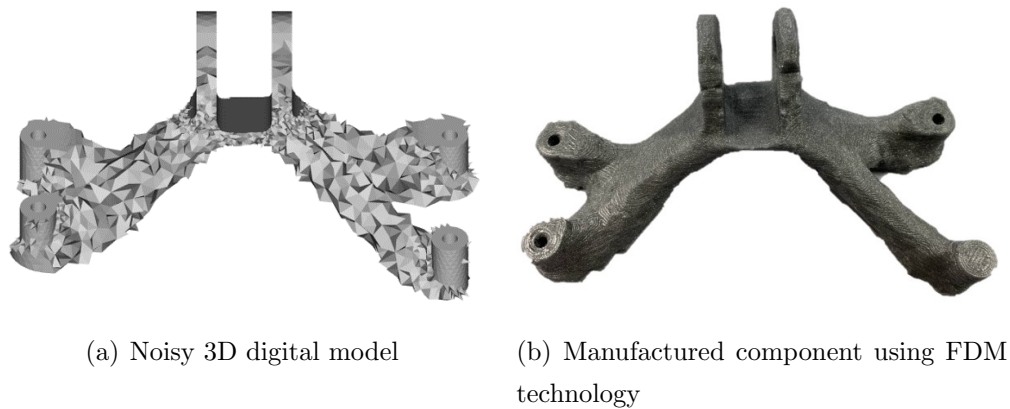


Figure 5.2: Visual comparison between a noisy digital model and the equivalent manufactured component after digital post-processing

still not user-friendly and far from being straightforward. Recently, [168] attempts to bridge the gap by presenting a simple approach for streamlining the last step of producing manufacturable 3D models resulting from structural optimization, but only for a restricted range of scenarios and only for voxel-based models. [169] has combined the TO approach with the Non-Uniform Rational Basis Spline (NURBS) hyper-surfaces framework to offer CAD-compatible descriptors of the structure's topology that are unrelated to the FEM mesh quality. However, when it comes to setting NURBS discrete parameters, this technique is largely dependent on the designer's skill, and it has limited use due to the long calculation time.

To address the aforementioned challenges identified in the literature, the candidate presents an optimized general-purpose surface smoothing post-processing technique, deeply described in its first version in [157] and the final one in [158]. Undoubtedly, TO 3D models require post-processing manipulation before the manufacturing phase to examine and correct non-manifold edges, fractures, and peaks that may arise as a result of the optimization. External surface smoothing, inspired by image denoising approaches [170], is one of the post-processing techniques. Surface smoothing is a numerical approach for detecting and removing noise and spikes from a surface model

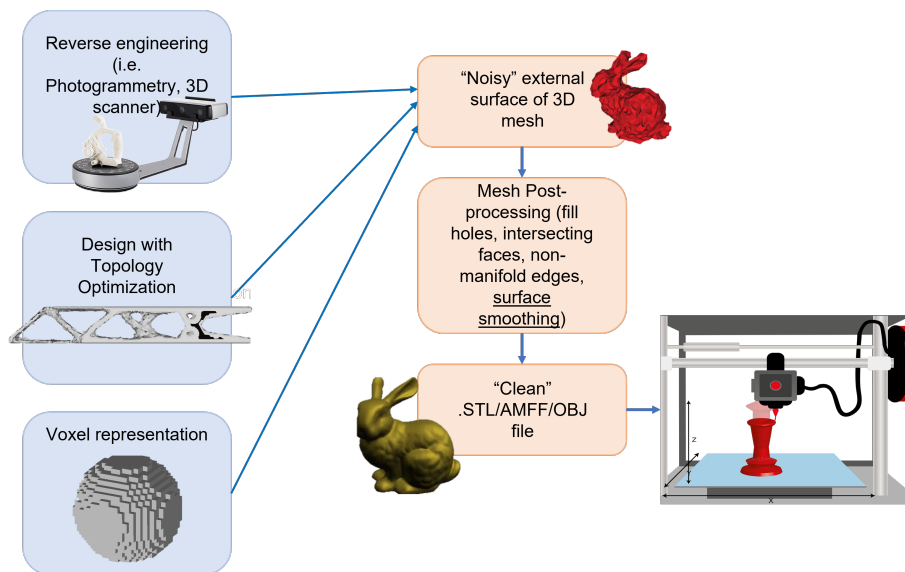


Figure 5.3: The application of digital post-process techniques is required before the production phase

to return a more pleasing geometry by iteratively developing the surface.

The proposed strategy can smooth the exterior surface of meshes derived from a variety of sources, including topology optimization and reverse-engineering from 3D scanning and photogrammetry points clouds (Figure 5.3).

The established methodology is used for 3D models arriving from TO, but the same procedure may be used with any optimization methodology or engineering design approach as long as the 3D model can be exported as an STL surface mesh. Several ways for surface fairing have been proposed in the literature, including:

- mesh modification based on vertice location [171];
- surface smoothing using local curvature of neighbour faces [79];
- mesh optimization based on patch normal filters [172];
- frequency-based surface filtering [173].

Depending on the application, each methodology has pros and limitations, but approaches based on vertex position are known to be simple to build, quick, and perform well. However, some concerns, such as volume reduction throughout iterations, must be taken into account and resolved. Despite the attempts available in the literature, a user-friendly approach for post-processing 3D models employing smoothing algorithms based on mesh alteration of vertices position remains lacking. A suitable smoothing framework that meets the DfAM and TO standards should be able to successfully enhance the model’s exterior form in both voxel and surface mesh cases. Furthermore, volume shrinking during smoothing cycles should be kept to a minimum. Finally, a good smoothing approach should decrease or eliminate the loss of TO model characteristics (e.g. holes or flat surfaces) during the numerical process, so that they do not need to be post-processed (these regions will be referred to as *no-smoothing-space*).

5.1 Vertex-based surface smoothing: state of the art

Vertex-based smoothing techniques available in the literature are the simplest and easiest to apply, even though they suffer from crucial issues such as excessive volume reduction during iterations. To update the mesh, these processes employ neighbourhood information in terms of spatial location, which may be found in STL files. The Laplacian smoothing [171], whose operation may be described as a diffusion problem (eq. 5.2), inspires the majority of the vertex-based techniques, being \mathbf{X} the vertices tensor, L the Laplacian function, λ the diffusion speed ($0 < \lambda < 1$) and ∂t the variation of mesh during the iterations. The mesh connection is preserved and only the position of the vertices changes in this mathematical problem; each vertex is relocated utilizing just the knowledge about its neighbours.

$$\frac{\partial \mathbf{X}}{\partial t} = \lambda L(\mathbf{X}) \quad (5.2)$$

The various vertex-based algorithms available in the literature differ primarily by a distinct representation of the Laplacian operator, which is represented by eq. 5.3 in its linearized version. $N_1(i)$ represents the 1-ring-neighbourhood vertex set, which consists of all vertices related to the i -th vertex by one edge, and x is the spatial position of the i -th vertex's vector of coordinates.

$$L(\mathbf{x}_i) = \sum_{j \in N_1(i)} w_{ij}(\mathbf{x}_j - \mathbf{x}_i) \quad (5.3)$$

Sorkine's traditional Laplacian smoothing method replaces a mesh vertex with the average location of its neighbours at each iteration, using $w_{ij} = 1/n$, where n is the number of one-ring neighbours. This smoothing approach has the benefit of being both simple and fast to compute. As the number of iterations increases, however, it is influenced by significant vertex drifting (vertex movement that is not following the surface normal direction) and mesh shrinkage (mesh volume reduction).

The Scale-Dependent Laplacian smoothing method improves on the previously mentioned technique by using weights proportional to the relative distance between the vertices in the Laplacian operator $w_{ij} = 1/|e_{ij}|$, retaining the size of the triangles and reducing vertex drifting, but still suffering of volume reduction. [174].

The Improved Laplacian Smoothing, often known as the HC-algorithm (HC stands for Humphrey's Classes), is another vertex-based technique being considered [175]. This technique tries to improve the traditional Laplacian method for reducing volume shrinking by adding a second step (push-back) to the standard Laplacian operator to partially push the vertices towards the old location by a value that is the average of its own and its neighbours' difference position vectors weighted by a factor. Furthermore, the new location of a vertex is evaluated not just in terms of its neighbours, but also in terms of its central vertex position. The initial vertex location is, in reality, weighted by a factor and included to aid the algorithm's convergence. Because of these enhancements, the HC method retains mesh characteristics and size better throughout iterations, even though some shrinking still occurs.

Taubin’s method is one of the most effective smoothing techniques ever devised. Because of the application of a two-step smoothing (forward and backwards) to rectify the shrinkage, this technique is comparable to the HC one [173]. This approach permits fine-tuning of both steps by using two scalar values to balance them out.

Though, for complicated shapes resulting from TO studies, where the designer wishes to freeze essential characteristics such as holes or surfaces that should be preserved flat in the ready-to-manufactured digital model, the current techniques are still non-optimized. To address this technological gap, the candidate created the Optimized Humphrey’s Classes — Scale-Dependent Umbrella algorithm (in the following *Optimized HC-SDU algorithm*), which combines the SDU and a modified version of the HC-algorithm to exploit their advantages, as well as several sub-routines to solve the problems mentioned previously.

5.2 Optimized HC-SDU algorithm

The created algorithm is thoroughly discussed in this part. There are two variants of the inventive approach. The first is restricted to voxel-based models and necessitates active user interaction to choose the no-smoothing-space option [157]. The second is a natural progression from the prior version, in which the no-smoothing-space identification is automated and a more advanced form of volume preservation is included in the code [158]. First, all the common features will be analysed and then the distinctive ones will be discussed in two separate sections, along with some results.

The following terminology is used: \mathbf{o}_i stands for the location of the i -th vertex in the noisy mesh, and \mathbf{c}_i stands for the position of the vertex that has not yet been affected by the current iteration of the smoothing process. Finally, \mathbf{s}_i will be used to represent the smoothed mesh. The flowchart containing the overall methodology is shown in Figure 5.4.

Both the developed algorithms use the information contained in an STL

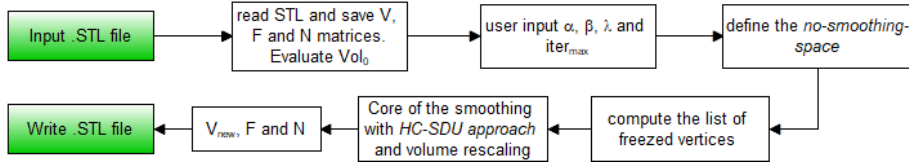


Figure 5.4: *Optimized HC-SDU* flowchart

mesh file, used as input, to save the topological information bits (vertices \mathbf{V} , facets \mathbf{F} , and normal components \mathbf{N}) as matrices. The volume of the STL 3D model is computed and saved in the Vol_0 variable. The algorithm then asks the user to enter numerical values for the four smoothing parameters: α and β weights from the HC-algorithm, λ which controls the process's diffusion speed, and $iter_{max}$, which controls the maximum number of iterations the algorithm can do before stopping if convergence is not achieved (the difference between two consecutive solutions should be less than 0.01).

As previously stated, the core of the *Optimized HC-SDU* smoothing approach is based on two steps phases, similar to the HC-algorithm. However, a substantial shift involves the push-forward phase to update temporarily \mathbf{s}_i , knowing \mathbf{c}_i . This stage is defined by the use of Scale-Dependent weights $1/e_{ij}$ to reduce vertex-drifting by taking into consideration the relative location of the vertices (first equation of 5.4). Then, it is defined the estimation of the vector comprising the relative distance positioning vector \mathbf{diff}_i to the original location by the α weight, as well as the temporary smoothed position of the i -th vertex \mathbf{s}_i . In the standard HC technique and in the 1st version of the developed algorithm, the relative position vector (\mathbf{diff}_i) is a scalar weight function of the original mesh. In the 2nd version, the relative position vector in the new method is determined by the mean position between the original and current meshes, which is weighted by the same scalar value α (second equation of 5.4). This is done to address the HC algorithm's fundamental flaw, which is the mitigation of the largest mesh peaks and surface noise while leaving mild background noise on the smoothed model.

$$\begin{cases} \mathbf{s}_i = \mathbf{c}_i + \frac{2\lambda}{|e_{ij}|} \sum_{j \in N_1(i)} \frac{\mathbf{c}_j - \mathbf{c}_i}{|e_{ij}|} \\ \mathbf{diff}_i = \mathbf{s}_i - \frac{\alpha}{2}(\mathbf{o}_i + \mathbf{c}_i) + (1 - \alpha)\mathbf{c}_i \end{cases} \quad (5.4)$$

Then, to determine the final smoothed location of the i -th vertex \mathbf{s}_i , a push-back step is performed using the same technique used in the HC algorithm:

$$\mathbf{s}_i = \mathbf{s}_i - \beta \mathbf{diff}_i + \frac{1 - \beta}{size(N_1(i))} \sum_{j \in N_1(i)} \mathbf{diff}_j \quad (5.5)$$

With a while cycle, the total procedure is repeated until a sufficient result *smooth enough* is reached, describing the mathematical condition for which the difference in terms of distance between two successive solutions should be less than 0.01 without reaching the maximum number of iterations $iter_{max}$.

To increase the performance of the new smoothing algorithm, a set of functions has been developed to define the *no-smoothing-space* that will be deeply analysed in the following sections. As a common feature, these functions return the list of vertices indices \mathbf{a} within the *no-smoothing-space*. It is feasible to substitute the locations of the original vertices $\mathbf{o}(\mathbf{a})$ into $\mathbf{s}(\mathbf{a})$ to keep the vertices contained in \mathbf{a} . This is done to satisfy one of the goals of a new advanced smoothing algorithm.

To accomplish the second task, namely, to solve the volume shrinkage, the candidate included a volume rescaling step at the end of the *Optimized HC-SDU* codes by comparing the actual mesh volume V_i at the i -th iteration with the initial one. This is done to rescale the volume of the STL during the smoothing process, to keep the STL inner volume constant and equal to the initial one Vol_0 . The volume rescaling operation differs between the first and the second version of the codes and will be discussed in the following.

Once the algorithm reaches convergence, a new matrix containing the vertices' coordinates is returned (V_{new}). Knowing that using a vertex-based approach, the face topology does not change, it is possible to reconstruct the new smoothed mesh in the form of an STL file knowing the new vertices

V_{new} , the facet topology \mathbf{F} and the normal vector components for each face \mathbf{N} . Thus a 3D model that fits the DfAM rules with an appealing external surface is obtained and the design workflow can continue without issues with the production and commercialization of the product.

Once the common features of both versions are described, it is time to deeply analyse the distinctive characteristics of the two developed versions of the *Optimized HC-SDU* algorithm in the two following sections.

5.2.1 1st version

The first version of the *Optimized HC-SDU* algorithm has been developed to be applied only on voxel-based 3D models coming from TO routines. The method aims to both avoid mesh shrinkage and to give the possibility to the user to select and freeze some portions of the digital model during the smoothing process to not modify them during the post-processing. To satisfy these tasks two sub-routines are included in the codes.

5.2.1.1 Volume preservation

The first issue to address is the shrinkage that many diffusion-based smoothing techniques suffer from. The initial mesh is defined by a volume Vol_0 defined by a sequence of triangles called faces. Following the execution of the smoothing operation, at the i -th iteration, the volume is lowered to V_i (due to the diffusion process), which is smaller than Vol_0 . As a result, the smoothed mesh must be rescaled by a factor γ , which is specified in eq 5.6. After each cycle, the γ factor is multiplied by each vertex position [174].

$$\gamma = \sqrt[3]{\frac{Vol_0}{V_i}} \quad (5.6)$$

5.2.1.2 Selection of the *no-smoothing-space*

The identification of critical characteristics that must be kept during optimization can be of extreme importance, such as regions that represent holes

or flat surfaces for functional or manufacturing purposes. To do so, the designer can do an interactive selection utilizing a GUI that depicts the voxel-based geometry. To grasp the 3D body shape, a command has been developed to rotate the mesh in the most appropriate point of view. Then, a closed polyline tool is used to isolate the faces that belong to the *no-smoothing-space*. During the smoothing process, the position of these nodes will be retained, removing them from the list of nodes whose position can be modified.

5.2.1.3 The overall code, the performances and its limitations

The entire approach may be explained using the pseudo-code shown in Figure 5.5, which includes the previously specified sub-routines.

Optimized HC-SDU algorithm	
<pre> Input α, β, λ and n_{iter} while select <i>no_smooth_space</i> = true do select region $a \leftarrow$ save vertices IDs end Vol₀ \leftarrow volume of mesh o_i while not smooth enough do $c \leftarrow s$ for $i \in$ vertices do $n \leftarrow$ neighbours(i).size if $n > 0$ then for $j \in$ neighbours(i) do sumDiff \leftarrow sumDiff + $(c_j - c_i) * 1/ edge_{ij}$ sumWeight \leftarrow sumWeight + $edge_{ij}$ end $s_i \leftarrow c_i + \lambda * \text{sumDiff}/\text{sumWeight}$ end end end </pre>	<pre> diff_i \leftarrow $s_i - (\alpha * o_i + (1 - \alpha) * c_i)$ end for $i \in$ vertices do $n \leftarrow$ neighbours(i).size if $n > 0$ then $s_i \leftarrow s_i - (\beta * \text{diff}_i + (1 - \beta) * n * \sum_{j \in \text{neighbours}(i)} \text{diff}_j)$ end end s(a) \leftarrow o(a) V_i \leftarrow volume of mesh s_i $\gamma \leftarrow (Vol_0/V_i)^{1/3}$ if $\gamma \neq 1$ $s \leftarrow \gamma * s$ end end </pre>

Figure 5.5: Pseudo-code of the 1st version of *Optimized HC-SDU* [157]

The smoothing method was coded in Matlab and evaluated on a digital model generated using an open-source TO technique [77] using voxel representation, as shown in Figure 5.6. Indeed, the 3D model returned by the TO function can't be manufactured due to the evident stair-effect on its external surfaces. This is the perfect context where to apply the developed smoothing approach. During the post-processing, the suggested method is compared against existing algorithms to assess its performance, such as classic Laplacian, SDU Laplacian and HC-algorithm. The variations in total volume, total

surface area, and "total change" of the triangulated model during iterations are used to assess the performances. The Euclidian distance between \mathbf{o}_i and \mathbf{s}_i after smoothing is defined as the model's change. The sum of the changes for the entire surface is the total change.

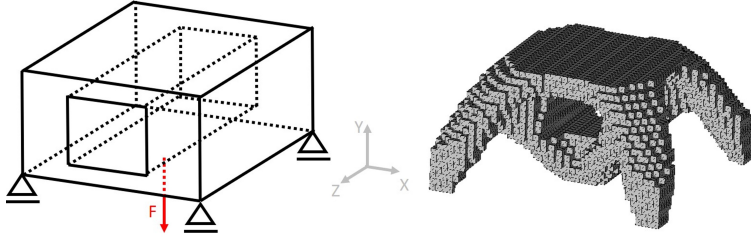


Figure 5.6: The case study used to test and compare the performances of the 1st version of *Optimized HC-SDU* [157]

To properly set the simulations, the diffusion parameter λ , which must lay in the range $[0, 1]$, has been set as $\lambda = 0.6307$ since research shows that this value represents a suitable trade-off for improved mesh volume preservation with a small number of iterations [174]. To get a satisfying outcome, the weight factor values (α and β) used in the novel algorithm and the HC-one must be set following the criteria in the literature [175]. Pre-set values are proposed after multiple tries to attain a satisfactory qualitative result: $\alpha = 0.15$, $\beta = 0.4$, $\lambda = 0.6307$ and $iter_{max} = 50$. To protect the four supports at the bottom of the model and the squared hole in the centre of the 3D model from the smoothing process, the *no-smoothing-space* has been graphically configured to include them.

A computer with a 4-core 3.1 GHz CPU and 32 GB of RAM was used to run the smoothing simulations on the 3D model. Figure 5.7 provides for a qualitative comparison of the outcomes of the applied smoothing methods. Furthermore, the computing time spent for each technique to complete the 50 iterations is equivalent, and a smoothed solution for a mesh with 6428 vertices, 19284 edges, and 12856 triangular faces may be discovered in less than a minute.

Figure 5.8 (a) shows the changes in mesh volume throughout smoothing

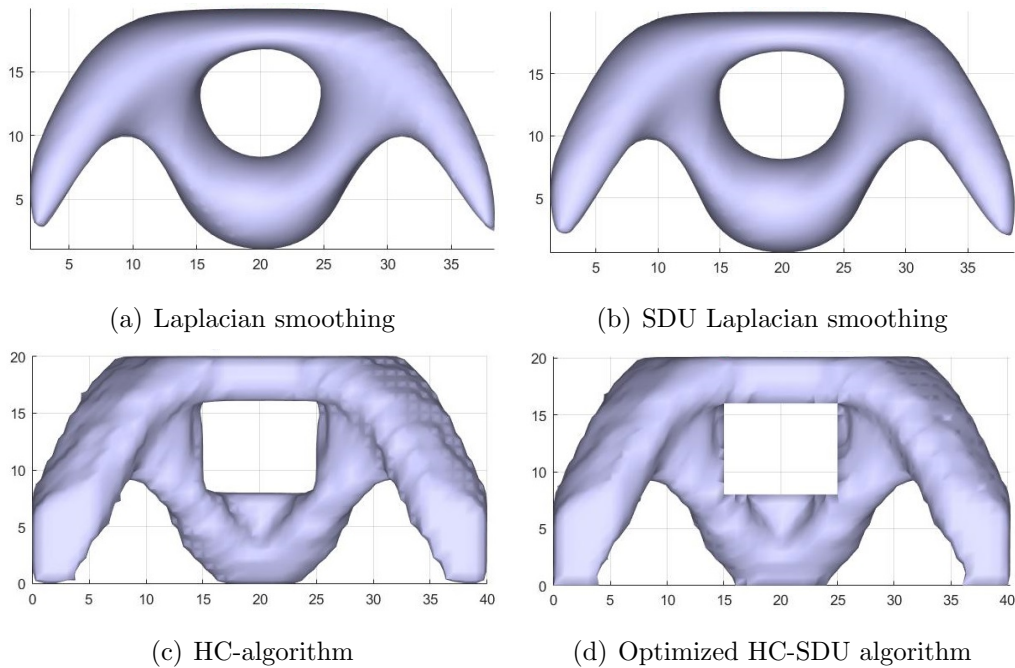


Figure 5.7: The 3D smoothed model after 50 iterations

operation cycles for a quantitative comparison. Due to the diffusion process impact, which reflects on mesh shrinkage, the mesh volume decreases as the number of iterations increases. The only approach that keeps the original volume is the Optimized HC-SDU algorithm, which employs a volume preservation sub-routine to keep the volume constant throughout the iterations. Finally, the total change parameter must strike a balance between a pleasing and smoothed appearance, and a model that does not collapse on itself. As a consequence, the best results have a high total change and a tiny or non-existent total volume drop. When compared to the other algorithms, the *Optimized HC-SDU* method performs better on this scale. On the one hand, it keeps the *no-smoothing-space* and maintains the initial mesh volume, while, on the other, it has a high total change value (Figure 5.8 (b)).

The SDU and traditional Laplacian methods produce good total change figures and a pleasing exterior surface. However, the respectively models collapsed on themselves, and the shrinkage impact is significant. Last but not

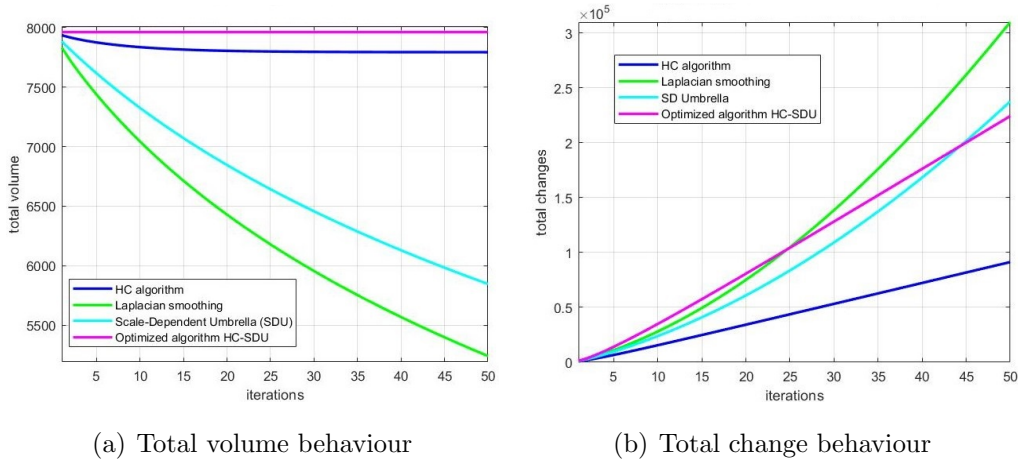


Figure 5.8: Quantitative comparison of smoothing algorithms after 50 iterations with $\alpha = 0.15$, $\beta = 0.4$ and $\lambda = 0.6307$ [157]

least, the HC-algorithm provides middle-of-the-road results, with minimal mesh alterations but restricted volume shrinking.

To summarize, the outcomes imply that the two key requirements that prompted the development of the new algorithm have been adequately met. Compared to the literature, the initial volume is kept constant during the iterations, with a sufficient total change value and computing time. However, several flaws in the no-smoothing-space specification have been identified, and it is planned to detect these regions automatically in the second version. Furthermore, the new version addresses the issue of light background noise that persists on the smoothed model, while the largest mesh peaks and surface noise are reduced.

5.2.2 2nd version

This section offers a description of the candidate’s novel vertex-based smoothing technique, which is widely detailed here in its second edition and extensively discussed in [158]. The goal of this new version is to complete the same duties as the previous one, specifically the need to post-process 3D models generated by TO analysis to preserve significant characteristics

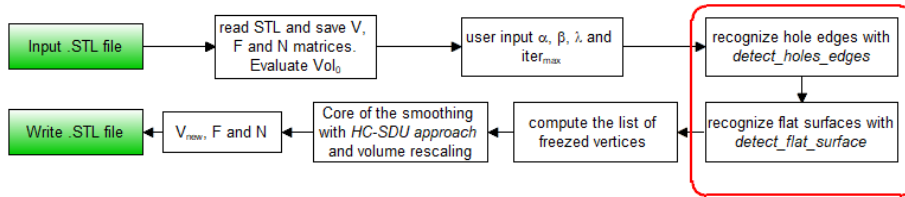


Figure 5.9: Flowchart of the *Optimized HC-SDU* 2nd version

while avoiding volume shrinking. However, the new version may be used to clean up any sort of noisy STL surface meshes, including those generated by TO tools and reverse engineering methodologies. The updated flowchart is shown in Figure 5.9 with the main modifications, focused on the automatic detection of the *no-smoothing-space*, highlighted in red.

As it happens for the first version, the input file is an STL one, and the information containing the vertices and face topology are saved in the respective matrices. Then the user is asked to enter the input values for the four parameters and weights that drive the smoothing parameters. To have a more flexible algorithm, applicable to both TO and RE models, the following pre-set values, in accordance with literature, are suggested: $\alpha = 0.27$, $\beta = 0.51$, $\lambda = 0.6307$ and $iter_{max} = 150$.

Then, the updated version of own developed sub-routines is used to detect and freeze features of the 3D model. A Matlab function named *detect-flat-surface* is used to find the vertices of a flat surface by examining the components of the selected facet's normal vector and those of its neighbours. The second subroutine searches for holes in the digital model using a function called *detect-holes-edges*, which looks for closed-loop sharp edges that correspond to the summit of holes, based on the methods provided in [176]. The IDs of the vertices that belong to a flat surface or a hole's edge are returned by both of the cited sub-routines. The approach produces an array containing the vertices belonging to the *no-smoothing-space* by combining these two ID lists, which is supplied to the algorithm's core function, as done also in the previous version. The detailed description of these functions is postponed to the following sections.

Other innovations involve the *forward-step* of the *Optimized HC-SDU* approach, wherein the updated version, the mean position between the original and the current mesh will be used to compute the difference vector, instead of the original one alone:

$$\begin{aligned}
 \mathbf{diff}_i &= \mathbf{s}_i - \alpha \mathbf{o}_i + (1 - \alpha) \mathbf{c}_i \\
 &\Downarrow \\
 \mathbf{diff}_i &= \mathbf{s}_i - \frac{\alpha}{2} (\mathbf{o}_i + \mathbf{c}_i) + (1 - \alpha) \mathbf{c}_i
 \end{aligned} \tag{5.7}$$

Indeed, this is done to remove the background noise of smoothed models compared to the original HC algorithm, which is a behaviour that impacts that smoothing approach.

Furthermore, the position of geometric limitations such as the size of the bounding box or the required location of supports is preserved in the new version of the volume rescaling sub-routine, differently from what was implemented in the first version. To solve this problem, the volume rescaling is performed by multiplying the vertices' matrix by \mathbf{B} , which is defined as an identity matrix multiplied by the factor γ of eq. 5.6. However, there are certain identical elements in the main diagonal, such as $\mathbf{B}(i, i) = 1$ if index i is a member of vector \mathbf{a} , the array that contains the IDs of all the nodes belonging to holes or flat surfaces that do not need a smoothing process. As a result, the i -th node will avoid the volume rescaling procedure, ensuring that constraining positions are preserved (eq. 5.8).

$$\mathbf{B} = \begin{bmatrix} \gamma & 0 & 0 & & & \\ 0 & \gamma & 0 & \cdots & & 0 \\ 0 & 0 & 1 & & & \\ & \vdots & & \ddots & & \vdots \\ & & & & \gamma & 0 & 0 \\ & 0 & & \cdots & 0 & 1 & 0 \\ & & & & 0 & 0 & \gamma \end{bmatrix} \tag{5.8}$$

5.2.2.1 Automatic flat surface detection

From the first version, it was undoubted that a faster and more automated function able to recognize the flat surfaces of the noisy model was necessary. To fill this task, a function called *detect-flat-surfaces* is coded and requires as input the topology information previously collected from the STL file. The function compares the components of the normal vector of each facet of the surface mesh with the neighbour triangles. The subroutine counts the number of neighbour facets having the same normal as the considered facet.

To capture facets that correspond to a planar surface that are near a sharp edge of the component, a threshold value L is placed on the function and has to be defined by the user at the beginning. If the number of facets with the same normal as the i -th facet is more than $x - L$ and the i -th facet has x neighbours, the i -th facet belongs to a planar surface, and the three vertices are recorded in the array of the *no-smoothing-space* \mathbf{a}_1 . For the case studies that will be provided in the following, a threshold value of $L = 2$ was determined after multiple experiments (Figure 5.10). Indeed, if $L > 2$, the function begins to choose triangles that no longer belong to the planar surface, and if $L = 0$, many planar surface facets are lost throughout the process if they are near a sharp edge. Figure 5.11 contains the pseudo-code of the described function.

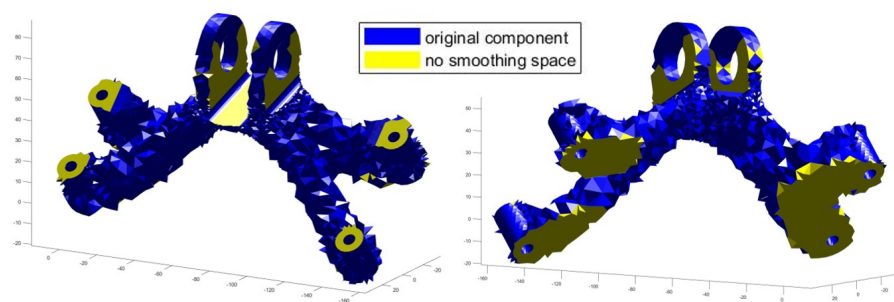


Figure 5.10: Flat surfaces recognized by the *detect-flat-surface* function, using $L = 2$ [158]

Detect flat surface	
<pre> Input F, N and L a ← [] for i ∈ F do n ← N(i) q ← unique list of ID faces of neighbours of F(i) for j ∈ q do if N(q(j)) - n < 1e-4 then N(q(j)) and F(i) same normal -> z(j) = 1 else N(q(j)) and F(i) different normal -> z(j) = 0 end end </pre>	<pre> end z ← sum(z) if z > (length(q) - L) for k ∈ q do a ← [a ; q(k)] end end end output a </pre>

Figure 5.11: Pseudo-code of the *detect-flat-surface* function [158]

5.2.2.2 Automatic hole detection

Another important feature in 3D models that should be preserved is the position and the shape of holes, needed for assembly purposes. For this reason, *detect-holes-edges* is a new function that detects the existence of holes and cavities in the digital model. With the topology information coming from the mesh file (faces \mathbf{F} , normals \mathbf{N} , edges \mathbf{E} , and face adjacency \mathbf{ADJ}), the function can discover all the sharp edges $\mathbf{S_E}$. When an edge is shared by two neighbouring facets (common edge) and the angle between the two normal vectors is around 90 degrees, it is said to be sharp. The add-on then explores each mesh edge to search for a simple closed loop of sharp edges, namely a edges' closed loop with no crossings. The methodology is inspired by [176] and the overall methodology is shown in the flowchart available in Figure 5.12, while the pseudo-code is reported in Figure 5.13.

Finally, the method returns the number of sharp edges closed loops identified in the model, as well as an array containing the IDs of the vertices affected by the selected sharp edges $\mathbf{a_2}$. This array is merged with $\mathbf{a_1}$ coming from the *detect-flat-surfaces* to identify all the vertices belonging to the *no-smoothing-space* which will be fixed during the smoothing and rescaling processes.

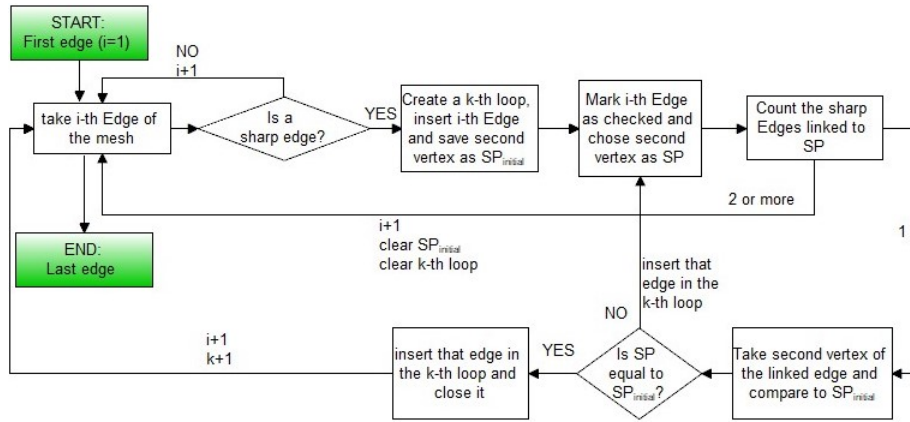


Figure 5.12: Methodology flowchart of the *detect-holes-edges* function [158]

Find hole vertices	
<pre> Input F, N, ADJ, E S_E ← [] for i ∈ ADJ do neigh ← ADJ(i) for j ∈ neigh do common_edge ← F(i) ∩ F(neigh(j)) if common_edge ≠ ∅ do θ ← angle between N(i) and neigh(j) if 85° < θ < 95° do S_E ← [S_E; common_edge] end end end end for i ∈ E do index ← E(i) ∩ S_E if index=0 do check_edge(i)=1 end end loops ← [] n_loops=1; SP=0; for i ∈ E do if check_edge(i)=0 then loops ← [loops; E(i)] SP_{init} ← E(i,2) </pre>	<pre> count=1 index ← i SP ← E(index,2) while SP ≠ SP_{init} & SP≠0 count=1 do check_edge(i)=1 link_edge ← find linked edges to SP ∈ SE if length(link_edge) = 1 then ind ← link_edge ∩ E SP ← E(ind,2) loops ← [loops; E(ind)] count +1 else for m ∈ link_edge index ← link_edge(m) ∩ E check_edge(index) = 1 end SP ← 0 clear current loop count ← 0 n_loops - 1 end end n_loops + 1 end a ← list of unique vertices ∈ loops output a </pre>

Figure 5.13: Pseudo-code of the *detect-holes-edges* function [158]

5.2.2.3 The overall code, the performances and its limitations

Once the sub-routines compose the \mathbf{a} array, this is passed to the core of the algorithm previously described that can evaluate the new vertex position. At

each iteration, the updated and smoothed vertex matrix is multiplied by the \mathbf{B} matrix of the volume rescaling function to keep constant the overall mesh volume still preserving the bounding box dimensions and the constraining positions. The pseudo-code of the overall algorithm is visible in Figure 5.14.

Optimized HC-SDU algorithm	
<pre> Input α, β, λ and $iter_{max}$ \mathbf{a}_1:=detect_flat_surfaces(V,F,N,L) \mathbf{a}_2:=detect_holes_edges(V,F,N) $\mathbf{a}=\mathbf{a}_1+\mathbf{a}_2$ $V_0 \leftarrow$ volume of mesh \mathbf{a} while not smooth enough & iter < $iter_{max}$ do $c \leftarrow s$ for $i \in V$ do $n \leftarrow$ neighbours(i).size if $n > 0$ then for $j \in$ neighbours(i) do $sumDiff \leftarrow sumDiff + (c_i - c_j) * 1/ edge_{ij}$ $sumWeight \leftarrow sumWeight + edge_{ij}$ end $s_i \leftarrow c_i + \lambda * sumDiff/sumWeight$ end end $diff_i \leftarrow s_i - (\alpha/2 * (o_i + c_i) + (1 - \alpha) * c_i)$ end </pre>	<pre> for $i \in V$ do $n \leftarrow$ neighbours(i).size if $n > 0$ then $s_i \leftarrow s_i - (\beta * diff_i + (1 - \beta) * n * \sum_{j \in neighbours(i)} diff_j)$ end end $\mathbf{S}(\mathbf{a}) \leftarrow \mathbf{O}(\mathbf{a})$ $V_{new} \leftarrow$ volume of mesh s_i $\gamma \leftarrow (V_0/V_{new})^{1/3}$ if $\gamma \neq 1$ then: $\mathbf{B} \leftarrow \gamma * \mathbf{I}$ for $i \in \mathbf{a}$ $\mathbf{B}(\mathbf{a}(i), \mathbf{a}(i))=1$ end $\mathbf{S} \leftarrow \mathbf{B} * \mathbf{S}$ end end </pre>

Figure 5.14: Pseudo-code of the *Optimized HC-SDU* algorithm [158]

The *Optimized HC-SDU* technique is compared against the standard Laplacian smoothing, the Laplacian smoothing utilizing SDU weights, the HC-algorithm, and the Taubin’s approach to better comprehend the algorithm’s performance. Following literature recommendations, the weights α and β were set after a sensitivity analysis to discover the ideal values. The optimal situation is one in which the algorithm converges and the total change is maximized. The remaining parameters, such as λ and $iter_{max}$, are selected for ease of use: the diffusion speed is set to match literature benchmarks, and the maximum number of iterations is designed to keep the computational time and cost to a minimum.

A first case study, deeply described in [158], refers to a cantilever beam used for validation purposes. To do not lengthen the discussion too much, only a significant case study of a real component is reported here. The 3D model of the GE bracket [95] is used for this purpose. The model is first topologically optimized in the own ToOp environment. The following

boundary conditions have been applied: the four holes in the component's base are constrained, and a shear load of 4525 N is applied at 45° to the basement on the two upper wings; a volume fraction of 50%, an initial volume mesh size of 2 mm, and the Ti6Al4V material are chosen, with a penalization factor of 3.

The STL model of the optimized structure is utilized as an input file to the smoothing algorithms with $\alpha = 0.27$, $\beta = 0.51$, $\lambda = 0.6307$, and $iter_{max} = 150$ as input parameters coming from the sensitivity analysis. The no-smoothing regions that the created algorithm detects automatically can be seen in Figure 5.15 with encouraging results; the list of vertices belonging to both regions is then passed to the core of the algorithm as previously described.

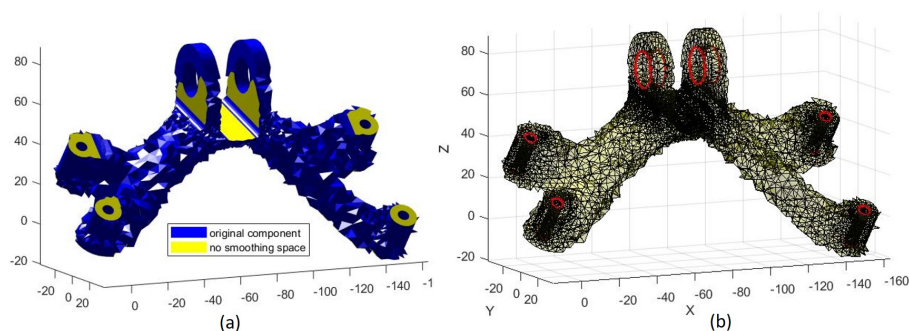


Figure 5.15: Visual result of the automatic detection of the *no-smoothing-space*: (a) detection of flat surfaces (in yellow) and (b) detection of holes' edges (in red) [158]

A qualitative (Figure 5.16) and quantitative comparison (by means of total volume and total change monitoring during the iterations shown in Figure 5.17) of the smoothing process is undertaken, as it was for the prior version of the algorithm. Table 5.1 also includes the time it takes to execute all of the smoothing methods, the number of iterations required to attain convergence, and a comparison with the model's dimensions to explain the *no-smoothing-space* performance detection.

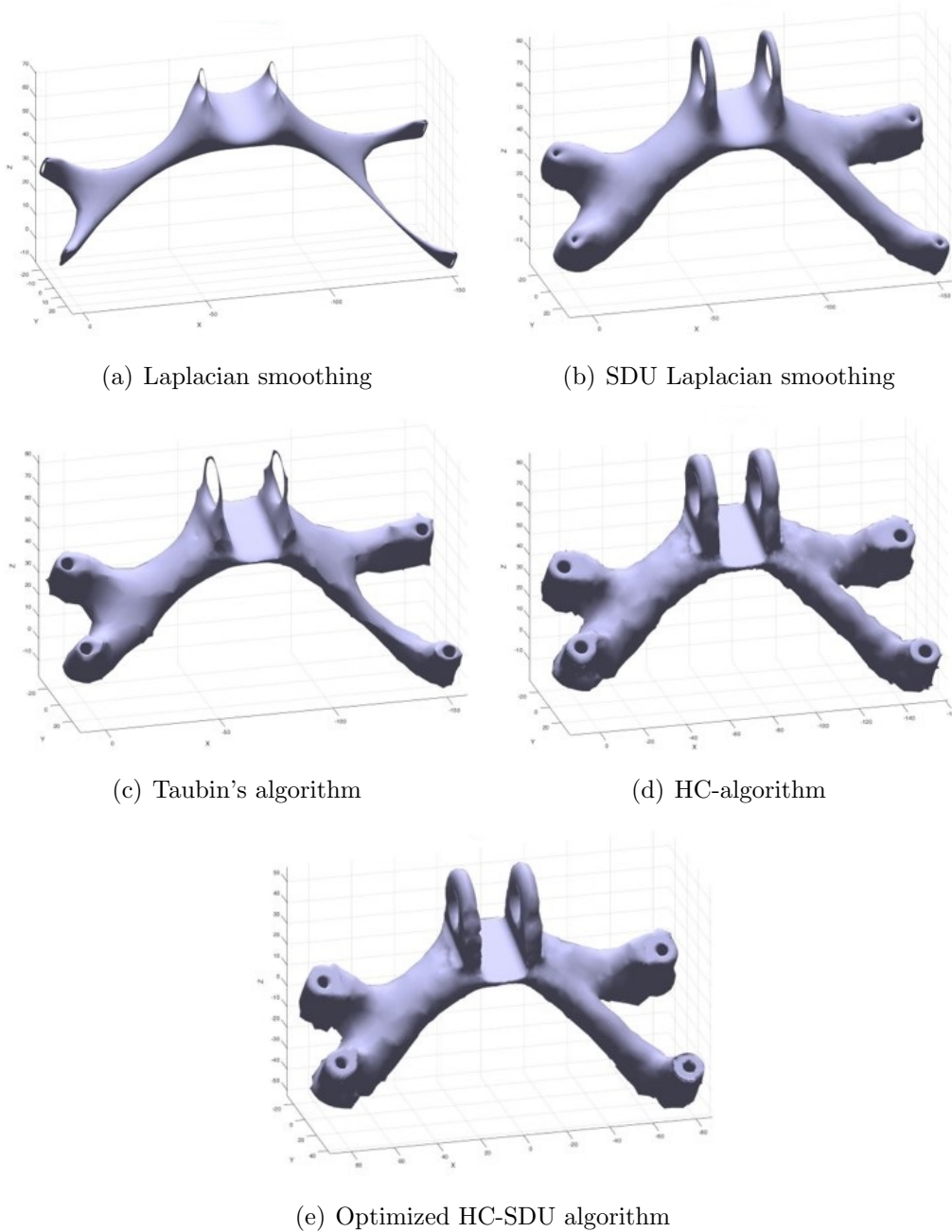


Figure 5.16: The 3D smoothed models of GE bracket [158]

5.2.3 Discussion of the results

From the results collected in the previous section, it emerges that, even though large values of total changes are attained for both geometries, Lapla-

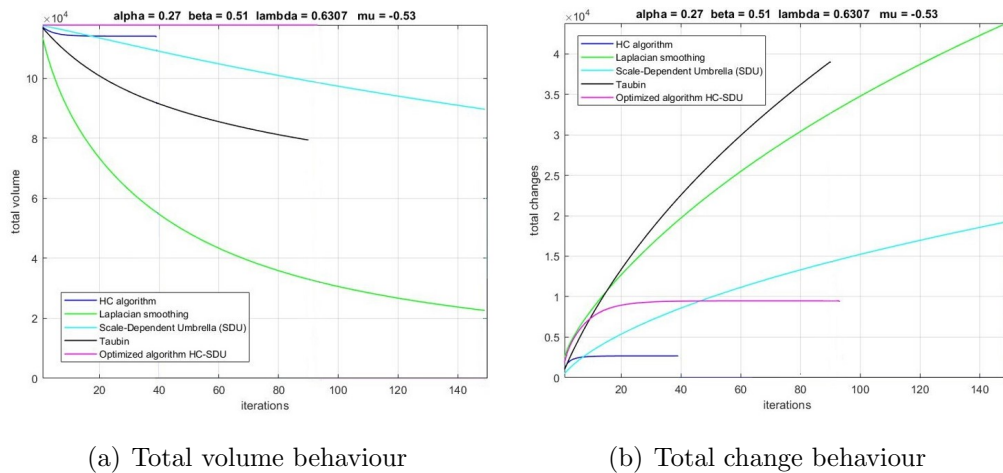


Figure 5.17: Quantitative comparison of the *Optimized-HC-SDU* smoothing algorithm applied to the GE bracket [157]

cian smoothing with classic weights and SDU weights yields poor quality results due to substantial volume shrinkage. Furthermore, after 150 iterations, neither of them achieves convergence, and the *no-smoothing-space* is significantly altered. For all of the aforementioned reasons, these two smoothing techniques are deemed unsuitable for post-processing complicated geometries before production. Moreover, on the one hand, Taubin’s method has a middle-of-the-road behaviour: it is quick, meets convergence conditions, but suffers from a small degree of size shrinkage and no feature preservation. On the other hand, even if the volume shrinkage level and feature degradations are low, the HC method converges quickly but with little alterations and no major improvements on the final mesh shape, making it nearly useless.

Finally, with the maximum of total change and matching of convergence requirements, *Optimized HC-SDU* algorithms decisively perform better, attaining satisfying results. The volume rescaling sub-routine in the *Optimized HC-SDU* method precisely retains the starting volume value, and the hole dimensions match exactly between the original and optimized models. This is an important consideration in a real-world design workflow: for example, if certain holes used to link components are changed in shape or dimension,

Smoothing approach	Volume change [%]	2 loaded holes change [%]	4 holes in the base change [%]	time [s]	Iters
Laplacian	-82	-37	-100	145	150
SDU	-26	+10	-73	139	150
HC	-4	-3	-2	74	40
Taubin	-33	+19	-24	22	91
Optimized HC-SDU	+0	+0	+0	19	94

Table 5.1: Dimensional and computational results of smoothing approaches applied to the GE bracket; the % refers to a comparison with the original model [158]

the assembly cannot be finished, and the component must be rejected and redesigned. However, while β can be chosen near the lower boundary suggested by Vollmer, α is not as simple to choose as the previous parameter because it has been discovered that it is dependent on the number of vertices in the *no-smoothing-space*: a higher α value is required to place more emphasis on the original mesh topology if high % of the vertices lies in that region. In conclusion, when compared to previous systems, the implemented functionalities of feature identification and volume rescaling that drive the algorithm throughout iterations do not affect the computing cost.

As the last test, the innovative algorithm is compared to the Taubin’s one coupled with the two developed functions to isolate the *no-smoothing-space* to see if the main smoothing improvements are due to the application of the *detect-flat-surface* and *detect-holes-edges* functions before the surface smoothing or the actual *Optimized HC-SDU* algorithm itself in its completeness. Figure 5.18 (b) illustrates that when compared to the innovative technique, the modified version of Taubin does not generate suitable results with a slower and less performant approach. Indeed, the final geometry is deformed and far worse than the *Optimized HC-SDU* process (Figure 5.18

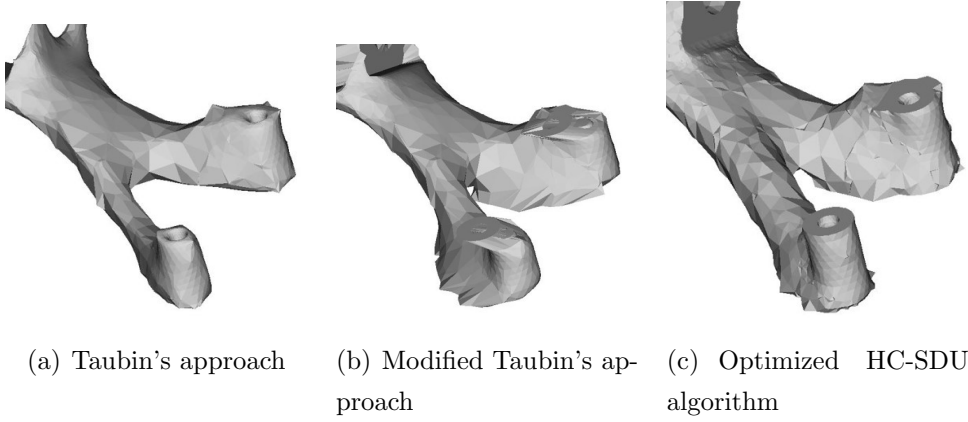


Figure 5.18: Detailed view comparison of the smoothed GE bracket model

(c)). To conclude, the developed smoothing technique is the best of the approaches considered since both high frequency and background disturbances are smoothed with promising outcomes.

From a denoising standpoint, the novel technique appears to deliver good results. However, further tests focus on the smoothed component's structural performance: the smoothed GE bracket's compliance was computed and compared to that of the equivalent noisy model. Following the technique outlined in [177], let c be the structure's compliance, \mathbf{U} the nodal generalized displacement, \mathbf{K} the global stiffness matrix, and \mathbf{F} the matrix of the nodal generalized external forces, ρ_e the element density, and \mathbf{K}_e the element stiffness matrix; the compliance can be computed as:

$$\begin{cases} c = \mathbf{U}^T \mathbf{K} \mathbf{U} \\ \mathbf{K} = \sum_{i=1}^{N_e} \rho_e \mathbf{K}_e \\ \mathbf{K} \mathbf{U} = \mathbf{F} \end{cases} \quad (5.9)$$

Because it comes straight from the topology optimization study, the structural compliance of the noisy mesh is chosen as a benchmarking value. It was calculated using the displacement values obtained from the topology optimization analysis, as well as the load circumstances previously mentioned for the GE bracket. Structure compliance is, in fact, the fitness function

that the TO process strives to decrease throughout optimization cycles. By comparing the compliance of the noisy and smoothed models, the structure compliance slightly increases in the second one (2%), but the smoothing approach returns a 3D model that is ready to be built without the requirement to create the optimized component from scratch in CAD software. Even if a slight approximation in terms of compliance should be permitted, this speeds up the design-to-manufacturing cycle and minimizes the designer's effort.

To summarize, the suggested results show that the *Optimized HC-SDU* smoothing approach meets the key objectives that pushed the algorithm design. This methodology might aid in the creation of optimized structures suited for Additive Manufacturing, perfectly fitting the Topology Optimization process' output. This avoids the time-consuming CAD drawing from scratch of the optimized component where the output of TO is replicated, resulting in a significant decrease in time to market, operator effort, and precision.

Chapter 6

Voxel-based approach for fluid-dynamics analysis

To increase the potentiality of the developed set of tools, an innovative fluid-dynamics tool based on voxel representation is elaborated. Indeed, as the dissertation title states, the PhD project aims to develop a modelling tool based on V-rep for Fluid-Structure Interaction (FSI) simulations.

6.1 Fluid-Structure Interaction analysis

The interaction between the principles controlling fluid dynamics and the structural mechanics of a body is significant in the design of components for applications where fluid-dynamic loads will be able to deform the structure. Fluid-dynamic loads arise when a moving body is submerged in a fluid, which can deform and move structural parts. The deformations of the structure produce a change in the geometry of the body, which modifies the distribution of pressure across the object and, as a result, the loads operating on the structure will change. This kind of interaction might be either steady or oscillatory. The study of this phenomenon has a wide range of applications, ranging from aeronautics and automotive to industrial processes and biomedicine [178]. As a result, numerical calculations using software suited

for both CFD and FEM investigations are used to investigate the interplay between the structure's mechanical and fluid-dynamic behaviour. There are three simulation approaches used by the FSI [179]:

- FSI of rigid bodies: because the structure has no deformations, just the structure's motion, of primary interest, in the fluid is evaluated, and only a CFD software is required;
- 1-Way FSI: Because the deformations are negligible, the pressure distribution on the body and the fluid dynamic loads stay similar; all that is required is to import the CFD results into the FEM program and there is no need to update and solve again the flow field;
- 2-way FSI: Due to the significant deformations, it is important to connect the CFD and FEM software iteratively.

For the scope of this project, small deformations have been considered and just the 1-way FSI is taken into account. While a simple voxel-based tool for structural analysis is described in Chapter 4 for periodic structures, there is the need to develop a fluid-dynamic tool based on V-rep that can be combined or used as stand-alone software to solve the flow field around objects, especially in the automotive field.

6.1.1 A solution for the aerodynamic problem

Indeed, nowadays different ways of evaluating aerodynamic loads are available to designers. Real-life component testing is the most precise method, but it requires the creation of a new prototype each time a change is made, making it the most expensive method in terms of time to market and money. It may also be unsustainable during the conceptual and preliminary design stages when a large number of configurations must be tested and evaluated. Another frequent method employed by aerodynamic engineers is to test a small-scale device in a wind tunnel; however, even this method is costly and

time-consuming, especially in the early phases of design. To acquire consistent results, wind tunnel measurements need a lengthy and arduous setup and calibration process. As a result, at the conceptual design stage, fluid dynamics numerical techniques are frequently employed to analyse the velocity and pressure fields surrounding objects.

The panel technique is one of the easiest methodologies for solving the potential flow among the numerical approaches to determine the aerodynamic loads. It rose to prominence in the 1970s, particularly in the aerospace industry [180], and it is based on strong flow assumptions such as inviscid, incompressible, irrotational, and steady flow [181]. Because of the inviscid flow assumption, the panel method's resultant flow field is free of viscous effects, which have a significant impact on drag. As a result, in recent decades, this numerical technique has been overlooked in favour of CFD approaches, which are now regarded as the most valuable, accurate, rapid, and inexpensive solution for solving aerodynamic issues. CFD, on the one hand, use volumetric discretization, whereas the panel approach employs a surface subdivision of the object into basic pieces known as panels. The difference is due to the computing time necessary to find a solution: even though the CFD technique is more accurate than the panel method, it takes longer to solve the problem. As a result, the panel technique remains a powerful approach for evaluating aerodynamic loads and moments during the early phases of design, when several configurations should be studied as quickly as possible to identify the best one that justifies future development. Once the ideal design has been identified, the CFD method may be used to precisely estimate the object's aerodynamic performance. Wind tunnel testing might therefore be conducted only after the exact design has been finalized to confirm the CFD results. As the last step in the design workflow, to keep R&D expenses as low as feasible, experimental tests might be undertaken just on the final design of produced prototypes (Figure 6.1).

On the one hand, the panel method's computational lightness makes it extremely appealing, but on the other hand, the 'panelization' procedure,

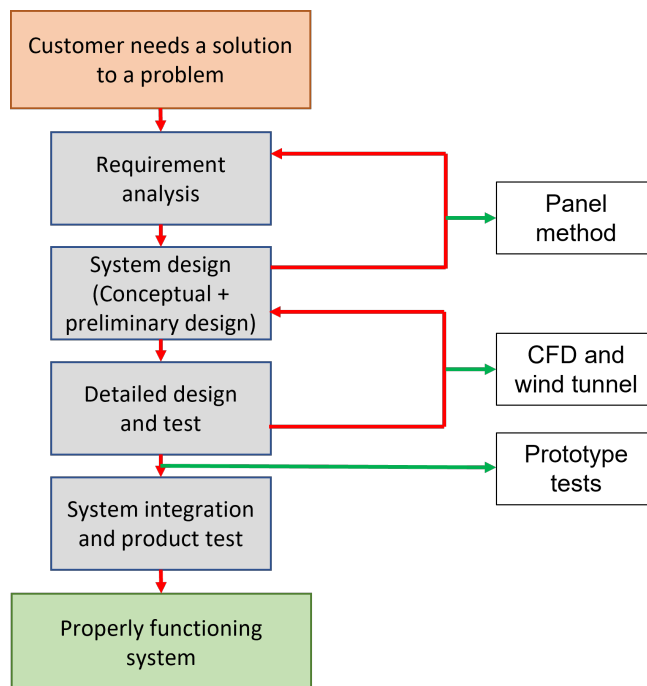


Figure 6.1: Different approaches to solve the flow can be used at different stages of a typical design workflow

namely the distribution of discrete 2D elements over the outer surfaces of the CAD model of the component to be evaluated, is crucial. Indeed, the designer has no prior knowledge of where the four vertices of each rectangular panel are located, especially in the case of complicated free forms. As a result, the user must create a cloud of points that are consistent with the object's surface from scratch. Indeed, this process is time-consuming and difficult, and it needs to be tailored to each case study.

To get over this issue, voxel discretization may be useful for fixing the location of the panel's vertices. Indeed, the exterior voxelized surface (EV-model) may be simply retrieved once the voxel model of the item of interest (V-model) is established. The panelization process can then be accelerated by matching each panel to the square surface of each voxel in the EV-model. However, the use of cubic cells on aerodynamic bodies, causes a stair-effect on the exterior surface, that might lead to artificial peaks and valleys in the

pressure distribution field, which must be thoroughly investigated. Furthermore, the application of V-rep to fluid-dynamic issues is novel since, to the author's knowledge, there are still few scholarly contributions on the subject ([182] and [183]), particularly with the ability to investigate the ease of prospective flow solutions. Only a few contributions believe voxel discretization to be relevant for fluid dynamics, but only for niche applications rather than building a general-purpose tool.

To close the highlighted technological gap, the candidate investigates the feasibility of using voxels as a discretization unit to easily and automatically panelize objects for numerical potential-flow solutions, intending to determine whether such a methodology could provide consistent results to the user. Two of my papers, widely discussed in the following, address this topic: the first discusses the novel approach and validates it using simple case studies [184], while the second applies the voxel-based panel method to the Ahmed Body [185], a popular benchmark body in the aerodynamics area [186]. The aerodynamic performance of this shape has been studied extensively in the literature. As a consequence, the novel technique provided in this study may be reviewed and tested by comparing the Lift and Drag estimation findings with data from the literature.

6.2 Voxel-based panel methodology

The ray-tracing voxelization discussed in Chapter 4 is utilized to voxelize the 3D model and then automatically match panels along the EV-model of the body to achieve the scope of this research. Once the panels' placement is defined, the authors adapted the APAME open-source panel method software to be integrated with the technique and to compute the aerodynamic loads [187]. It's worth mentioning that while there are various open-source panel technique tools available, the most of them are limited to simple 2D geometries (i.e. [188] and [189]). On the other hand, panel approaches established for 3D models, such as Boeing's Panair [180], do not allow for straight-

forward voxel discretization integration. Other packages, such as [190], are still in the early stages of development. To be consistent with APAME panel placement, described in detail in the following section, the developed approach up to now can only be automated for 3D models that may be regarded as a group of 2.5D bodies (2D shapes that are extruded in width). Despite this, many real-life bodies may be separated into a collection of 2.5D bodies, as it is shown in the following.

Because of its robustness and clear coding, the authors chose APAME, which was written in MATLAB, as the foundation for the construction of a panel code for use in the study. APAME was created to assess the aerodynamic loads and moments operating on aircraft structures. It's a tool that can come in handy at the preliminary/conceptual design stage when time is limited and a basic estimate of aerodynamic lift and induced drag force/coefficient would suffice. An overall drag calculation is not attainable owing to the strong flow assumptions underlying this technique, such as inviscid flow: the induced drag can be computed, but the skin drag is dependent on viscous factors and is not captured by the panel methodology. Furthermore, the form drag (which is taken into account in the case of blunt bodies) is not recorded by the panel approaches. All potential flow methodologies should not be used to predict drag due to flow assumptions unless geometrical modifications based on similar flat plate skin and drag form are incorporated.

However, because the discretization happens just on the exterior surface of the body rather than subdividing the entire volumetric flow domain, the computing requirement to resolve potential flow is significantly smaller than CFD techniques. As a result, a panel technique, embedding a V-rep, has been chosen as the best choice for developing a code that can be used to replace CFD programs for subsonic attached regimes in the early design context to estimate the lift and induced drag of simple bodies.

To solve the flow, the APAME tool uses the simplified version of the Navier Stokes equations, where the continuity equation becomes the Laplace ones (eq. 6.1), after the simplification due to flow assumptions:

$$\begin{cases} \frac{\partial^2 \phi}{\partial x_i^2} = 0 \\ \frac{\partial \phi}{\partial x_i} = \mathbf{v}_i \end{cases} \quad (6.1)$$

The scalar speed potential ϕ of the velocity field \mathbf{v}_i may be recognized as the problem's solution. Furthermore, it is important to predict the pressure distribution p to fully solve a flow around an object. The pressure distribution may be approximated using the Euler-Bernoulli equation (eq. 6.2) after the velocity field is known, thanks to the simplified methodology provided by the panel technique, where ρ represents the density of the medium.

$$\frac{v^2}{2} + \frac{p}{\rho} + gz = cost \quad (6.2)$$

Once the pressure distribution has been calculated, APAME may compute the aerodynamic loads and moments by integrating them across the tested body's exterior surface. To avoid delving into the debate, which is beyond the scope of this thesis, more information on the panel method theory and technique employed in APAME may be found in [191].

The voxel-based fluid-dynamics methodology, whose flowchart can be seen in Figure 6.2, combines the voxel-based modelling and the APAME software, previously described.

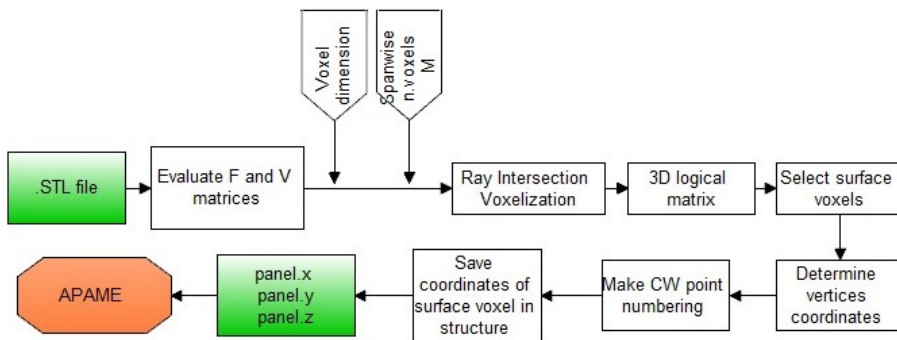


Figure 6.2: Voxel-based panel method flowchart [184]

The proposed technique begins with the existence of a 3D model of the item of interest saved in the STL format, which may be obtained using any

commercial CAD program. The technique then extracts the matrices in the STL file that describe the triangulated mesh discretization. The matrices of vertices \mathbf{V} , facets \mathbf{F} , and the matrix of normal vector components, in particular, are constructed. The imported 3D model should be oriented in the following way: the 2D profile belongs to the XZ plane, while the spanwise direction follows the Y-axis. Then, the user is asked to actively participate to choose the voxel resolution vox_{dim} along with the X and Z directions, as well as the resolution in the spanwise Y direction M (Figure 6.3).

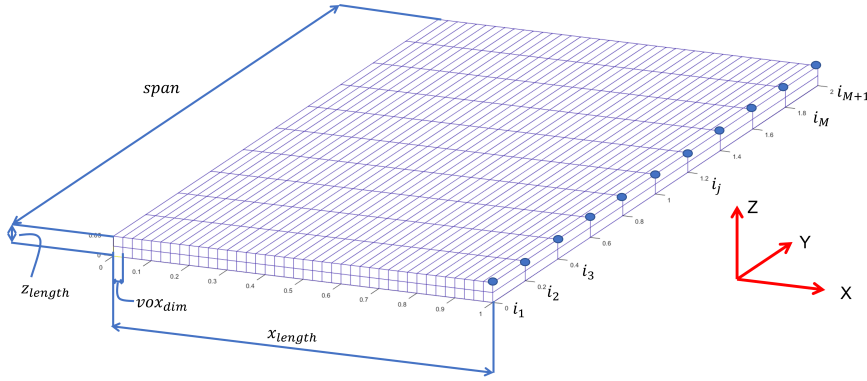


Figure 6.3: Discretization explanation of a Voxel-based model of a flat plate

The number of lateral panels N is affected by vox_{dim} in the X and Z directions, whereas the number of longitudinal panels M is affected by the resolution in the Y direction. Indeed, eq. 6.3 may be used to calculate the voxelization resolution in all three directions.

$$\begin{cases} \Delta y = \frac{span}{M} \\ vox_{dim} = \Delta x = \Delta z \end{cases} \quad (6.3)$$

These input parameters are provided to the voxelization function, which implements the ray-tracing intersection process, once the voxel resolution is defined. The function discretizes and converts the 3D model to a V-model,

yielding a logical 3D matrix of dimensions $n \times m \times M$, where:

$$\begin{cases} n = \frac{x_{length}}{\Delta x} \\ m = \frac{z_{length}}{\Delta z} \\ M = \frac{span}{\Delta y} \end{cases} \quad (6.4)$$

The EV-model is derived from the V-model using a MATLAB function available to the developer community [192], which gives the matrix of vertices coordinates of square surface elements. Before transmitting the EV-model to the APAME program, each square element must be assigned to a panel, the fundamental discretization unit required to solve the potential-flow problem. The spatial positions of the vertices belonging to the panels become the input of the APAME open-source software after the exterior surface panel structure is established according to the APAME needs. The pressure coefficient and velocity distributions, as well as the aerodynamic loads and moments operating in all three directions, are all returned by this tool. It is critical to properly set the free stream velocity module v_∞ , the density of the medium ρ , and the direction of the flow in terms of angle of attack α and sideslip angle β , as well as the reference surface S_{ref} that should be used to compute the aerodynamic load coefficients, with q being the reference dynamic pressure. Once the flow is solved, the lift and drag coefficient of the V-model can be computed. For a numerical problem where only the longitudinal loads are investigated ($\beta = 0^\circ$), the eq. 6.5 are valid.

$$\begin{cases} C_X = \frac{F_X}{qS_{ref}} \\ C_Z = \frac{F_Z}{qS_{ref}} \\ C_L = C_Z \cos(\alpha) - C_X \sin(\alpha) \\ C_D = C_Z \sin(\alpha) + C_X \cos(\alpha) \end{cases} \quad (6.5)$$

Thanks to the proposed methodology, the user automatically achieves the distribution of panels conformal to the exterior surface of the body he or she wishes to investigate thanks to the linkage of APAME software with the voxelization method. As a result, the arduous procedure of constructing a cloud

of points coherent with the surface of the geometry from scratch in a CAD is automated, making the new technique advantageous in the basic design phases due to the drastically reduced computing time. As previously stated, the computational reduction of time spent analysing several configurations, to discover the optimal one, is critical in the early phases of design.

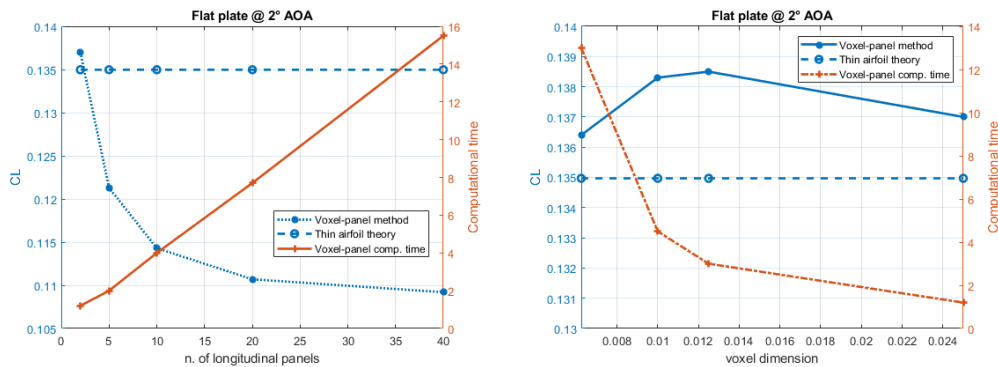
6.3 Results

A simple case study is built up to evaluate the suggested technique and to investigate how voxel discretization may alter numerically the aerodynamic performances of a 3D body. The simplest geometry covered in every aerodynamic text, a flat plate, is tested initially. Two finite span wings with NACA 0024 and NACA 2412 airfoils are explored in the following. Finally, the Ahmed body [186] is examined using a simplified 3D model. To prevent flow separation and turbulent phenomena, the simulations are conducted using a boundary condition of a free stream velocity with a modest angle of attack. In the following the lift coefficient C_L value returned by APAME is compared to the lift coefficient for the 3D model available in the scientific literature or evaluated by xFoil software [193], correcting the results of 2D airfoil characteristics keeping into consideration the aspect ratio AR (namely the ratio between the spanwise and chord dimension):

$$C_{L_{3D}} = \frac{C_{L_{2D}}}{1 + \frac{C_{L_{2D}}}{\pi AR}} \quad (6.6)$$

The initial geometry selected to test the voxel-based panel approach is a flat plate, which was chosen for its geometrical simplicity and ease of voxelization process to understand the impact of input parameters and develop a sensitivity analysis. Furthermore, according to aerodynamic theory, the lift coefficient for a flat plate at a small angle of attack (AOA) may be assumed to be equal to $C_L = 2\pi\alpha$ using a Joukowski mapping and the Kutta-Joukowski Lift Theorem [194]. A sensitivity analysis is carried out by running numerous simulations with different voxel parameters, such as the number of longitudi-

nal panels M and the voxel dimension vox_{dim} , to determine the best accuracy trade-off (Figure 6.4).



(a) Sensitivity study for different discretization along the spanwise direction (b) Sensitivity study for different voxel dimension along X direction

Figure 6.4: Sensitivity analysis on voxel resolution for the flat plate lift coefficient at $\alpha = 2^\circ$ [184]

The first sensitivity analysis involves the number of longitudinal panels used, which has an impact on C_L as shown in Figure 6.4 (a). It may be concluded that a low M value indicates a more precise lift coefficient prediction that is extremely near to the theoretical outcome. The best results are obtained when $M = 2$ (1.46% error) and the processing power required is significantly reduced. This might be explained by the fact that the overall matrix that describes panel interaction has lower dimensions. To determine the flow solution, this matrix must be inverted so that numerical inaccuracies might grow with the size. Increasing M may introduce singularities in the solution of the flow field, which may have an impact on the outcome. Regarding the best voxel resolution in the chord direction, the results reveal that an intermediate vox_{dim} value should be chosen as a trade-off between high geometry quality and the simulation's speed (Figure 6.4 (b)).

Bearing in mind the outcomes from the sensitivity study, the $C_L(\alpha)$ graph can be generated, with a confined mean error for the selected AOA interval $\alpha = [0, 2, 4, 6]$ that increases as one approaches the boundary layer separation

(Figure 6.5).

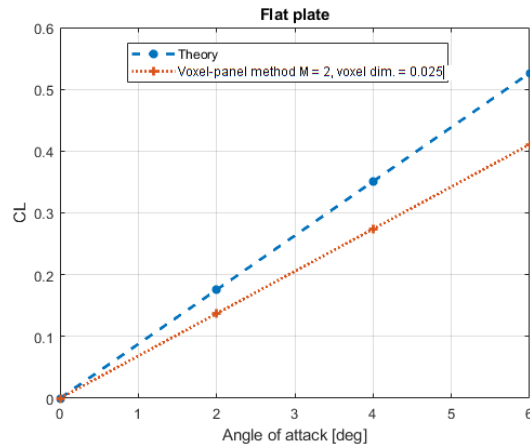


Figure 6.5: Lift coefficient vs AOA behaviour comparison using $M = 2$ and $vox_{dim} = 0.025$ [184]

To evaluate the performance of the voxel-based panel method even in real-life components, two finite wings using the NACA 0024 and NACA 2412 are then evaluated, which are frequently used for low-speed aircraft wings. To compute realistic lift coefficients for use as a reference, the xFoil code is employed. The case study features a finite span wing, and xFoil computes the aerodynamics of the 2D airfoil. A correction for 3D finite wings has been performed based on the aspect ratio (eq. 6.6).

The lift coefficients for both NACA airfoils derived from simulations conducted at different AOAs using different discretization criteria are shown in Figure 6.6. The lift coefficient behaviour has been successfully captured by the innovative technique owing to a thoughtful choice of voxel resolution, based on these findings. A lesser number of longitudinal panels translates to a more precise solution that is quite similar to xFoil but with fewer processing expenses. Using a workstation with a 4core 3.1 GHz CPU and 32 GB of RAM, it took less than half a minute to simulate both finite wings in whole, a result extremely encouraging in terms of computational resources and results' accuracy if compared to classic CFD, wind tunnel and on-the-field experimental approaches.

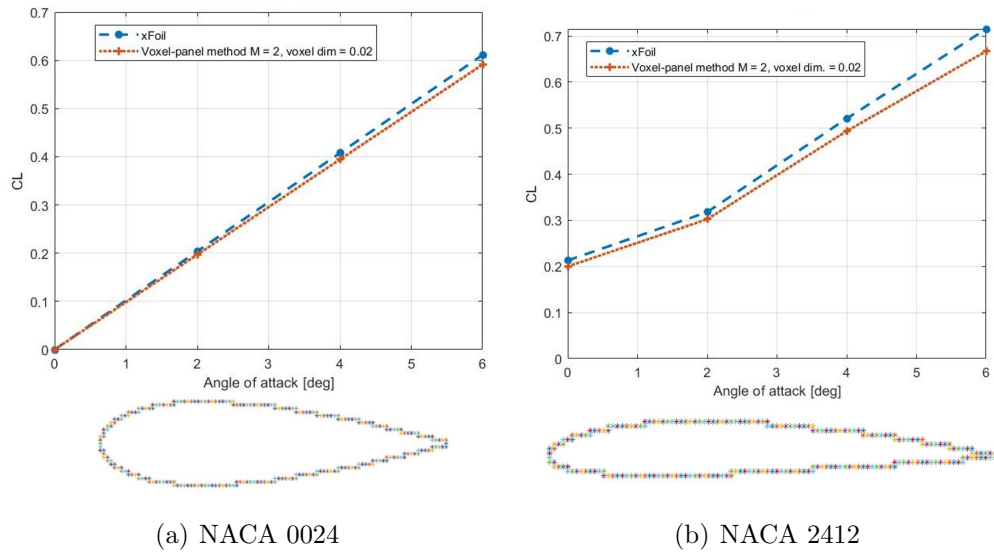


Figure 6.6: Lift coefficient plots for finite wings and the 2D airfoil silhouettes

6.3.1 The Ahmed body case study

In comparison to earlier case studies, which were characterized by basic geometries and 2.5D modelling (2D silhouette extruded in the third dimension), the suggested technique is validated to attain the aerodynamic performances of a real-life 3D body. Because various aerodynamic studies are accessible in the scientific literature, the authors chose the Ahmed Body as the major case study to analyze: Ahmed body is frequently used as a standard for aerodynamic research in the automotive field.

Only the novel methodology's capacity to estimate the lift force has been explored so far. However, the goal is to provide a comprehensive tool that can calculate a reasonable estimate of the entire drag force using geometrical adjustments for both skin friction and form drag sources. To accomplish this goal, the authors used Dobrev and Massouh's [195] work as a reference for the Ahmed body's aerodynamic performance. In this source, there are numerical references for both lift and drag aerodynamic coefficients, which were determined through numerical and experimental studies. Indeed, the voxel-based panel method's performance is measured in terms of estimating aerodynamic

efficiency E , which is defined as the ratio of lift to overall drag loads. It's crucial to remember that the total drag is described in aerodynamics as the sum of three contributions:

- skin friction drag, which is produced by the viscosity of the medium;
- form drag, which is caused by the shape of the body;
- induced drag, which is created by the object's motion, which redirects the airflow arriving at it. It has an impact on all bodies that create lift and downforce.

Only the simulation results for the Ahmed Body with a 25° slant angle are used to validate the suggested technique given in this contribution among all the sets of results for different slant angles investigated in [195]. The following are the boundary conditions utilized in Dobrev and Massouh's work, which are also used in the voxel-based methodology:

- 30 m/s free stream velocity;
- 0° angle of attach of the free-stream flow field;
- 1,225 kg/m^3 air density;
- the reference area is set to be the cross-section of the Ahmed body.

Only the experimental aerodynamic values of [195] will be used as a reference value in the following to evaluate the correctness of the technique described in this Chapter. The performance comparison will be calculated as a percentage discrepancy between the results from Dobrev's research and those calculated using the approach described here.

Even for the Ahmed body, a similar sensitivity analysis, as done in the previous case studies, is performed to choose the best set of voxel resolution inputs. The main results are collected in Figure 6.7. According to Figure 6.7 (b), a suitable result may be reached with less computing work even with a smaller number of spanwise panels. However, the optimal discretization

resolution is a compromise between accuracy, computational load, and geometry consistency. Indeed, the designer should double-check that the voxel resolution is accurate enough to represent the model's features. According to the authors' calculations, $M = 30$ is the lowest threshold that allows for a consistent geometry with the original, particularly in the lower portion of the body where the four cylinders represent the car's wheels. Moreover, the presented CFD approach is size-dependent in the sense that the solution is highly reliant on the discretization step, which might result in artefacts linked to the approximate representation of the boundary layer, which may be difficult to comprehend for non-expert fluid-dynamics designers.

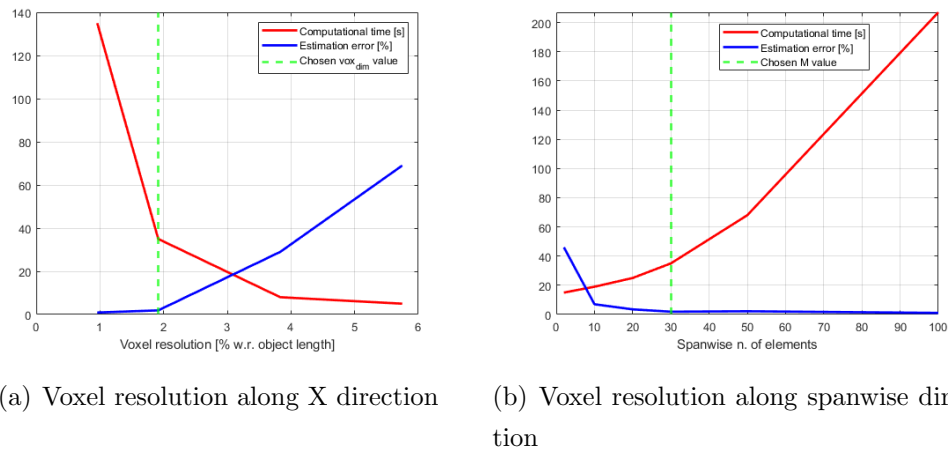


Figure 6.7: Sensitivity analysis of voxel resolution for the Ahmed body case study: the computation time (in red) and estimation error (in blue) for the Ahmed body's lift coefficient are shown

The fluid dynamics simulation is built up using the identical boundary conditions established in Dobrev's study after the voxel grid input values are fixed. The panelization stage of the 3D model took 14 seconds for MATLAB to automatically distribute the panels around the exterior surface. This outcome is encouraging when contrasted to traditional panel technique approaches described in the literature, in which the designer must create a panel distribution that is consistent with the exterior surface of a 3D model

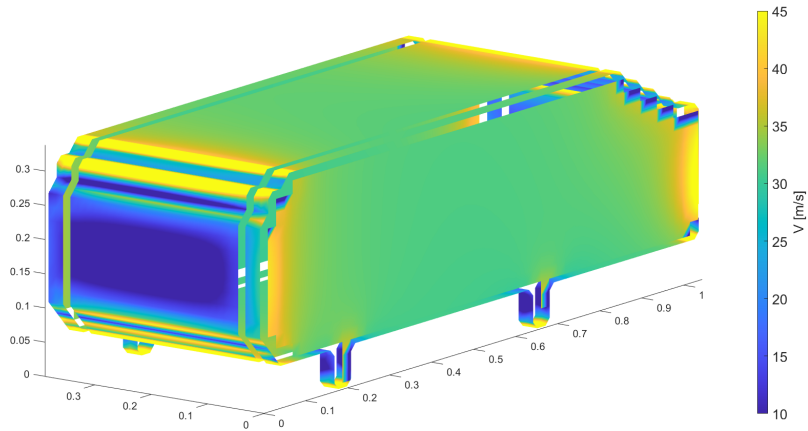
for which a CAD model is provided from scratch. After then, the APAME routine took 21 seconds to calculate the influence matrix of the many singularities spread around the body and 2 seconds to solve the numerical problem. Summing up all the timings, a preliminary solution may be obtained in less than a minute, which is far faster than studies conducted in wind tunnel facilities, which might take weeks to set up and evaluate the data. Furthermore, using CFD, the meshing process frequently necessitates extensive human involvement, with many hours spent detecting inconsistent mesh zones. As a result, if adequate accuracy results can be attained, the suggested voxel-based panel approach might be extremely useful.

The fluid dynamic simulation is run with the best voxel resolution detected from Figure 6.7, and the pressure and velocity field distributions are retrieved and graphically shown in Figure 6.8. As it can be seen, the complex 3D model can be seen as the sum of 2.5 elementary bodies assembled coherently.

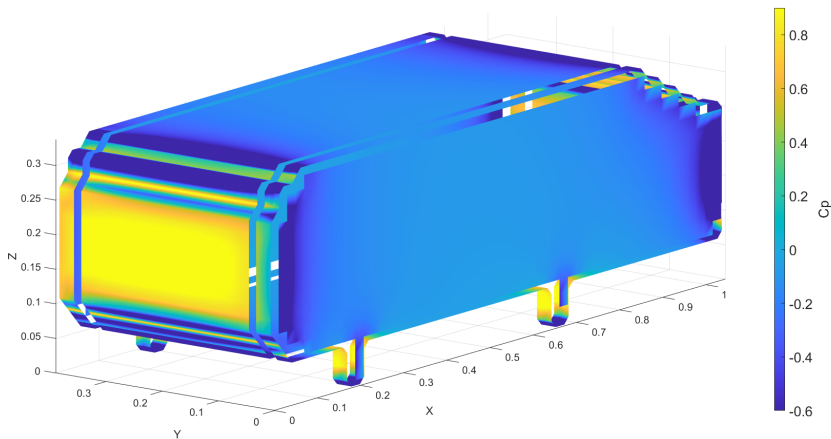
The overall lift and induced drag loads may be computed using the voxel-based panel code by integrating the pressure distribution over the model's surface. Furthermore, using the Prandtl's power-law for turbulent flows [196], it is feasible to determine the skin friction drag coefficient C_f approximately using geometrical shape adjustments. The predicted friction drag is dependent on the Reynolds number Re_x , which may be calculated using the free stream velocity module V , the characteristic dimension of the 3D model x , the medium density ρ , and the kinematic viscosity μ for the given case study.

$$\begin{cases} C_f = 0.0592Re_x^{-1/5} \\ Re_x = \frac{Vx\rho}{\mu} \end{cases} \quad (6.7)$$

The form drag coefficient may be determined using the publicly accessible blunt bodies drag coefficient tables, assuming the Ahmed body is near to a long cylinder [197]. Straightforwardly, the total drag and lift loads, as well as the aerodynamic efficiency, may be calculated by multiplying the aerodynamic coefficients by the dynamic pressure and the reference area, thanks



(a) Velocity distribution



(b) Pressure coefficient distribution

Figure 6.8: Velocity and pressure distribution over the Ahmed body

to the prior assumptions. In terms of aerodynamic efficiency, the result produced by the voxel-based panel method after the geometrical corrections is encouragingly near to the literature reference value. Indeed, as an alternative approach to geometrical corrections for drag estimation, the lift may be estimated using the voxel-based technique, while the entire drag may then be calculated by dividing the lift times the aerodynamic efficiency value taken

from the literature [195], but the single skin and form drag contributions remain unknown (Figure 6.9).

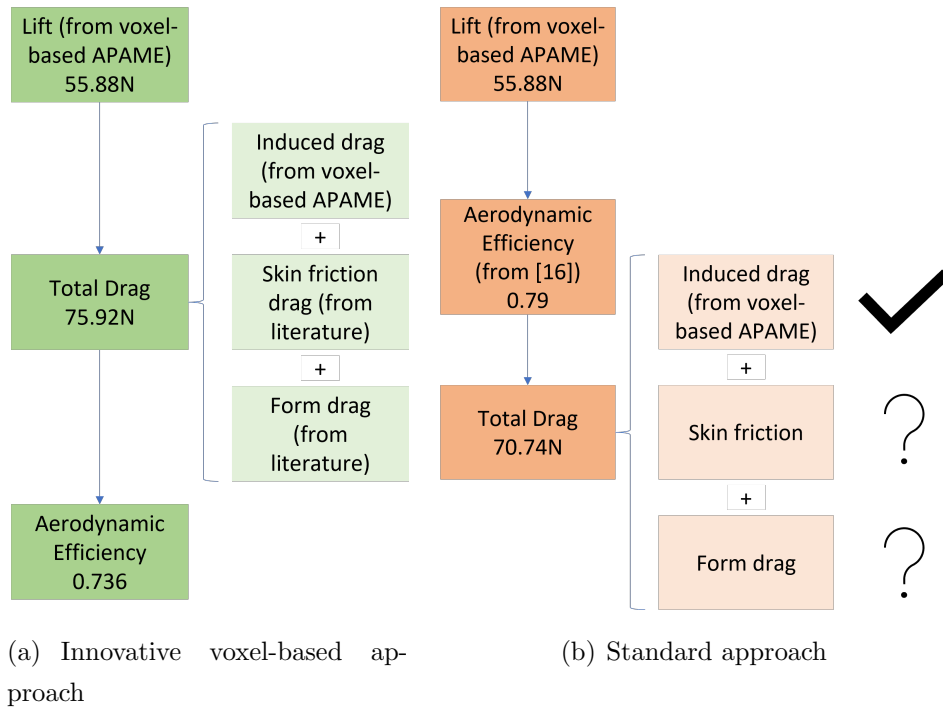


Figure 6.9: Comparison of estimation approaches for lift, drag and aerodynamic efficiency

When comparing the more rigorous and conventional technique to the new approach described in this Chapter, an acceptable evaluation error is achieved (less than 7%) when the lift, total drag and aerodynamic efficiency should be determined. Indeed, at the conceptual design stage, it is critical to compute both lift and drag aerodynamic forces with as little computational effort as feasible.

Thus, based on the combination of the panel technique and voxel discretization, a novel quick and simple to implement strategy has been designed. Indeed, voxelization mitigates the drawbacks of a time-consuming and labour-intensive panelization approach. Furthermore, a simple approach for calculating the total drag force is described: just the produced lift load

is required since geometrical corrections compensate for the lack of a panel method in the computation of skin and form drag. The results reveal a high level of agreement with literature-based reference values. Furthermore, this work proposes and investigates a novel voxel application that might lead to new research in this sector.

6.4 Discussion

Thanks to the innovative methodology described here, the panel method is a valuable numerical method for estimating aerodynamic forces and moments for subsonic flows in the conceptual and preliminary design stages, thanks to lower computational costs compared to CFD-based approaches. Furthermore, the novel and hitherto unexplored combination of the panel technique with voxelization solves the tiresome problem of the panelization process, allowing for rapid and fully automated panelling of the object's exterior surface. When the lift is taken into account, there is a good agreement (less than 6% inaccuracy in the coefficient estimation). In the context of a preliminary design stage, when a large number of configurations must be tried in a short amount of time to discover the design solution to bring to the preliminary and detailed design phases, this level of inaccuracy should be regarded as acceptable.

The first drawback is the formulation's exclusive use of flows potentials. In the proposed case studies, the candidate did not deepen the method for a 2-way FSI modelling. Thus, the computational drawbacks of volumetric discretization may result in an unnecessary and costly design stage, particularly valid for shapes with low surface/volume ratios. In any case, the proposed implementation discussed in this chapter is meant to be a rapid tool for early analyses which must eventually be followed by more accurate CFD simulations.

Moreover, because of the strong flow assumption on which the panel technique is based, this approach is known to have limits in terms of total drag

estimation. To address the second issue, a method based on basic calculations is provided for calculating the total drag in a simplified manner utilizing adjustments for skin drag and form drag derived from literature tables. This method is valid in terms of results accuracy compared to literature values (less than 10% error in total drag estimation) and computational speed compared to traditional CFD analyses. Furthermore, without the requirement for operators knowledgeable in meshing and CFD studies, fluid dynamics evaluations may be performed directly from aesthetic/conceptual 3D models (just an STL file is required) generated by design departments.

However, on the one hand, the panelization procedure is currently automated for bodies that can be approximated with a set of 2.5D bodies (2D shapes that are extruded in width), but tailored algorithms to translate complex panels distribution into a format that can be read by the panel method algorithms must be developed for 3D bodies. On the other hand, numerous real-life bodies may be decomposed into a group of 2.5D bodies (as the Ahmed body example shows), allowing the approach to be used to complex-shaped objects in their current form.

Further research into the voxel-based panel approach should be conducted to enhance the capability of the novel voxel-based fluid dynamic approach to mimic complicated and completely 3D structures, such as a full racing car visible in Figure 6.10, to better understand how automated voxel panelization operates in increasingly difficult situations. When literature reference values are unavailable, the findings should be compared to other numerical approaches (e.g. CFD).

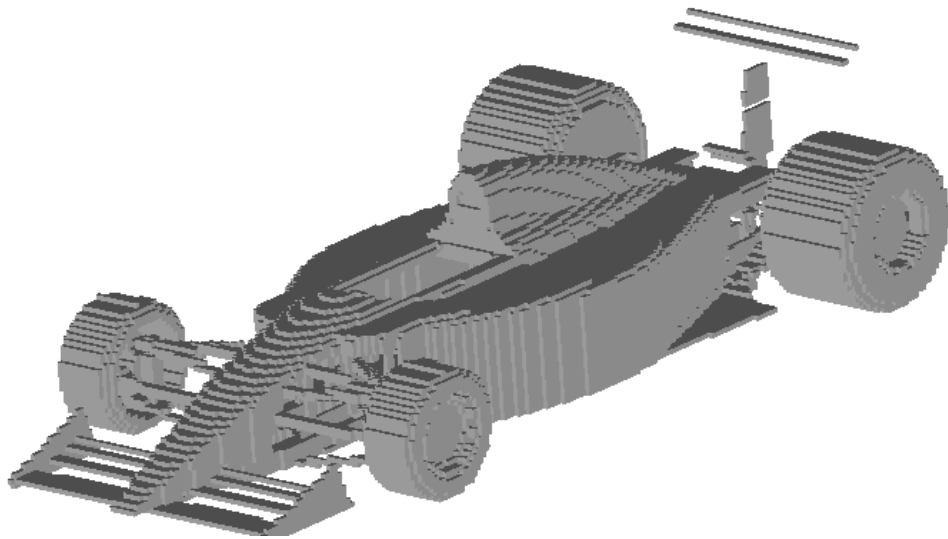


Figure 6.10: 3D voxel-based model of a complete racing car

Chapter 7

Conclusions

Volumetric Representation approaches, such as voxelization, are a type of CAD modelling that uses volumes to represent geometries. Among the several approaches, the voxelization method can aid in the display of tri-dimensional (3D) objects in CAD. This type of visualization is based on the use of voxels, which are small hexahedral volumes. Compared to common 3D representation techniques, such as the widely used Boundary Representation (B-rep), voxel-based modelling can handle more data, store the details of intricate interiors of 3D models, and speed up geometry manipulations and operations such as boolean operations, rotations, and so on.

However, the advantages of such modelling techniques are not well exploited in the available literature to represent exotic shapes for the automotive field, mainly coming from Additive Manufacturing processes, such as lattice structures and topologically optimized models. Furthermore, the application of V-rep to fluid-dynamic simulation is innovative, since the author is aware of few scientific contributions on the subject, particularly with the capacity to explore the ease of flow solutions. Nowadays, only a few contributors feel that voxel discretization could be useful for fluid dynamics, but only in specific situations rather than as a general-purpose tool. Despite the existence of simple tools based on voxel representation, these have limited capabilities and there is still a lack of a unique framework that could em-

bed all the necessary tools to simplify and expedite the design workflow for automotive components.

To address these gaps, highlighted through an objective literature review, the candidate developed several design tools that exploit the V-rep geometric modelling throughout his PhD program. At first, a thorough study of the advantages and disadvantages of Additive Manufacturing procedures that yield intricate models, such as lattices and topologically optimized structures, was prioritized, for which voxel-based modelling may be highly useful. Some of the constraints of Additive Manufacturing methods, such as restricted construction volumes, are addressed, and solutions are proposed in-depth.

The focus then shifted to the first form of complicated geometry outlined earlier. Lattice structures, widely used in high-performance automotive applications due to high strength-to-weight ratios, are investigated in-depth, and the voxel-based representation is used to aid in the structural simulation of periodic structures using 1D modelling. The promising findings demonstrate that the novel technique successfully calculates structural deformations while requiring little processing resources. It allows understanding of the mechanical reaction even at the lattice's unit cell, which is not possible with homogenization approaches.

In the following, particular emphasis was given to the topology optimization design technique that allows the creation of highly optimized intricate shapes. However, often these models can't be directly built due to defects that affect the external surface, or due to the stair-effect of voxels if V-rep is employed. So, an enhanced surface smoothing technique has been developed and analysed in this dissertation. In comparison to existing techniques, the novel methodology is capable of automatically recognizing particular features (i.e. holes, planar surfaces) of optimized models that should be preserved during post-processing without degrading the structure's mechanical response.

Finally, the voxel representation is used to provide a simple tool for estimating aerodynamic loads quickly at the early design stage, when several configurations must be analyzed to determine the best one (for example, the

best airfoil for a race car's wing). Voxelization is used in conjunction with a panel method code to automatically discretize 3D objects. The unique approach has been tested on well-known components, and the findings show that the methodology is both resilient and accurate when compared to literature benchmarking values.

All the contents described in this document have been collected in several scientific contributions submitted and published in international conferences and journals. Moreover, all the developed tools were programmed by own using Python or Matlab language to be highly customizable. Pseudo-codes and methodology flowcharts have been provided in this dissertation to help the comprehension of the tools. An open-source CAD software, called FreeCAD has been selected to host all the routines herein described. However, due to the Covid19 Pandemia, the research activity has inevitably slowed down and for this reason, the embedding phase has not been accomplished yet. However, soon, this task will be achieved to give a personal contribution to the research activity in this field.

Appendix A

List of scientific publications

1. Bacciaglia A., Ceruti, A., Liverani A. (2019) *Lattice structures representation in 2D drawings: a proposal for a standard*, Extended abstract in: Mechanics and Materials in Design Conference M2D2019, September 4-6, 2019, Bologna, Italy;
2. Bacciaglia A., Ceruti, A., Liverani A. (2019) *Additive manufacturing in automotive: advantages and criticalities*, Extended abstract in: Mechanics and Materials in Design Conference M2D2019, September 4-6, 2019, Bologna, Italy;
3. Bacciaglia A., Ceruti A., Liverani A. (2019) *A systematic review of Vox- elization Method in Additive Manufacturing*, Mechanics & Industry Journal 20(6), 630;
4. Bacciaglia A., Ceruti A., Liverani A. (2020) *Additive Manufacturing Challenges and Future Developments in the Next Ten Years*. In: Rizzi C., Andrisano A.O., Leali F., Gherardini F., Pini F., Vergnano A. (eds) Design Tools and Methods in Industrial Engineering. ADM 2019. Lecture Notes in Mechanical Engineering. Springer, Cham;
5. Bacciaglia A., Ceruti A., Liverani A. (2020) *Photogrammetry and Additive Manufacturing Based Methodology for Decentralized Spare Part Production in Automotive Industry*. In: Ahram T., Karwowski W., Vergnano A., Leali

- F., Taiar R. (eds) Intelligent Human Systems Integration 2020. IHSI 2020. Advances in Intelligent Systems and Computing, vol 1131. Springer, Cham;
6. Bacciaglia A., Ceruti A., Liverani A. (2020) *Evaluation of 3D printed mouthpieces for musical instruments*, Rapid Prototyping Journal, 26(3), pp. 577-584;
 7. Bacciaglia A., Ceruti A., Liverani A. (2020) *Proposal of a standard for 2D representation of bio-inspired lightweight lattice structures in drawings*, Proceedings of the Institution of Mechanical Engineers, Part C: Journal of Mechanical Engineering Science;
 8. Bacciaglia A., Ceruti A., Liverani A. (2020) *Advanced Smoothing for Voxel-based Topologically Optimized 3D Models*, 2020 IEEE 10th International Conference Nanomaterials: Applications & Properties (NAP), pp. 1-5;
 9. Bacciaglia A., Ceruti A., Liverani A. (2021) *Controllable pitch propeller optimization through meta-heuristic algorithm*, Engineering with Computers 37, pp. 2257–2271;
 10. Bacciaglia A., Ceruti A., Liverani A. (2021) *A design of experiment approach to 3D-printed mouthpieces sound analysis*, Progress in Additive Manufacturing 6, pp. 571–587;
 11. Bacciaglia A., Ceruti A., Liverani A. (2021) *Structural Analysis of Voxel-Based Lattices Using 1D Approach*, 3D Printing and Additive Manufacturing. Ahead of print;
 12. Bacciaglia A., Ceruti A., Liverani A. (2021) *Surface smoothing for topological optimized 3D models*, Structural and Multidisciplinary Optimization 64(6), pp. 3453–3472;
 13. Bacciaglia A., Ceruti A., Liverani A. (2022) *Towards Large Parts Manufacturing in Additive Technologies for Aerospace and Automotive applications*, Procedia Computer Science 200, pp. 1113-1124;
 14. Bacciaglia A., Ceruti A., Liverani A. (2022) *A voxel-based 2.5D panel method for fluid-dynamics simulations*, In: Rizzi C., Campana F., Bici M., Gherar-

dini F., Ingrassia T., Cicconi P. (eds) Design Tools and Methods in Industrial Engineering II. ADM 2021. Lecture Notes in Mechanical Engineering. Springer, Cham;

15. Bacciaglia A., Ceruti A., Liverani A. (2022) *A 3D Voxel-based approach for fast aerodynamic analyses in conceptual design phases*, Computer-Aided Design & Applications, 19(6), pp. 1236-1254.

Bibliography

- [1] B. Wassermann, S. Kollmannsberger, S. Yin, L. Kudela, and E. Rank, “Integrating CAD and numerical analysis: ‘Dirty geometry’ handling using the Finite Cell Method,” *Computer Methods in Applied Mechanics and Engineering*, vol. 351, pp. 808–835, 2019.
- [2] G. Jense, “Voxel-based methods for CAD,” *Computer-Aided Design*, vol. 21, no. 8, pp. 528–533, 1989.
- [3] Luca Grigolato, Stefano Rosso, Roberto Meneghello, Gianmaria Concheri, and Gianpaolo Savio, “Heterogeneous objects representation for Additive Manufacturing: a review,” *Instant Journal of Mechanical Engineering*, pp. 14–23, 2019.
- [4] B. Wassermann, T. Bog, S. Kollmannsberger, and E. Rank, “A design-through-analysis approach using the finite cell method,” in *Proceedings of the VII European Congress on Computational Methods in Applied Sciences and Engineering (ECCOMAS Congress 2016)*, (Crete Island, Greece), pp. 2601–2613, Institute of Structural Analysis and Antiseismic Research School of Civil Engineering National Technical University of Athens (NTUA) Greece, 2016.
- [5] S. Kwon, H. Kim, and D. Mun, “Multiobjective evolutionary optimization for feature-based simplification of 3D boundary representation models,” *The International Journal of Advanced Manufacturing Technology*, vol. 110, no. 9-10, pp. 2603–2618, 2020.
- [6] T. Torigaki and K. Fujitani, “Power of a voxel approach to structural analysis and topology-shape optimization in automobile industries,” *Japan Journal of Industrial and Applied Mathematics*, vol. 17, no. 1, pp. 129–147, 2000.
- [7] M. P. Bendsøe and O. Sigmund, *Topology optimization: theory, methods, and applications*. Engineering online library, Berlin Heidelberg: Springer, second edition, corrected printing ed., 2011.

- [8] A. Nordin, “Challenges in the industrial implementation of generative design systems: An exploratory study,” *Artificial Intelligence for Engineering Design, Analysis and Manufacturing*, vol. 32, no. 1, pp. 16–31, 2018.
- [9] T. Grimm, *User’s guide to rapid prototyping*. Dearborn, Mich: Society of Manufacturing Engineers, 2004.
- [10] A. Lerebours, F. Marin, S. Bouvier, C. Egles, A.-C. Masquelet, and A. Rassineux, “A voxel-based method for designing a numerical biomechanical model patient-specific with an anatomical functional approach adapted to additive manufacturing,” *Computer Methods in Biomechanics and Biomedical Engineering*, vol. 22, no. 3, pp. 304–312, 2019.
- [11] M. Lengsfeld, J. Schmitt, P. Alter, J. Kaminsky, and R. Leppek, “Comparison of geometry-based and CT voxel-based finite element modelling and experimental validation,” *Medical Engineering & Physics*, vol. 20, no. 7, pp. 515–522, 1998.
- [12] J. Ashburner and K. Friston, “Voxel Based Morphometry,” in *Encyclopedia of Neuroscience*, pp. 471–477, Elsevier, 2009.
- [13] S. W. Wang and A. E. Kaufman, “Volume Sampled Voxelization of Geometric Primitives,” in *Proceedings of the 4th Conference on Visualization ’93, VIS ’93, (USA)*, pp. 78–84, IEEE Computer Society, 1993. event-place: San Jose, California.
- [14] Z. Duan, Q. Yang, X. Meng, and J. Li, “Detailed Voxel-Based Implicit Modeling With Local Boolean Composition of Discrete Level Sets,” *IEEE Access*, vol. 8, pp. 48376–48385, 2020.
- [15] F. Nooruddin and G. Turk, “Simplification and repair of polygonal models using volumetric techniques,” *IEEE Transactions on Visualization and Computer Graphics*, vol. 9, no. 2, pp. 191–205, 2003.
- [16] A. Kolb, L. John, and T. Q. Algorithm, “Volumetric Model Repair for Virtual Reality Applications,” *The Eurographics Association*, 2001.
- [17] G. Marmitt, A. Kleer, I. Wald, H. Friedrich, and P. Slusallek, “Fast and Accurate Ray-Voxel Intersection Techniques for Iso-Surface Ray Tracing,” in *Proceedings of the Vision, Modeling, and Visualization Conference 2004*, (Stanford, California, USA), pp. 429–435, 2004.
- [18] S. Mantovani, S. Barbieri, M. Giacomini, A. Croce, A. Sola, and E. Bassoli, “Synergy between topology optimization and additive manufacturing in the automotive field,” *Proceedings of the Institution of Mechanical Engineers, Part B: Journal of Engineering Manufacture*, 2020.

- [19] L. Zhu, N. Li, and P. Childs, “Light-weighting in aerospace component and system design,” *Propulsion and Power Research*, vol. 7, no. 2, pp. 103–119, 2018.
- [20] G. Machado and L. Trabuco, “Some results in topology optimization applied to biomechanics,” *Computers & Structures*, vol. 82, no. 17-19, pp. 1389–1397, 2004.
- [21] G. I. N. Rozvany, “A critical review of established methods of structural topology optimization,” *Structural and Multidisciplinary Optimization*, vol. 37, no. 3, pp. 217–237, 2009.
- [22] I. Gibson, D. W. Rosen, and B. Stucker, *Additive manufacturing technologies: 3D printing, rapid prototyping, and direct digital manufacturing*. New York, NY: Springer, 2. ed ed., 2015.
- [23] A. H. Azman, F. Vignat, and F. Villeneuve, “Design Configurations and Creation of Lattice Structures for Metallic Additive Manufacturing,” in *14 e Colloque National AIP-Priméca*, (La Plagne, France), 2015.
- [24] M. Rashed, M. Ashraf, R. Mines, and P. J. Hazell, “Metallic microlattice materials: A current state of the art on manufacturing, mechanical properties and applications,” *Materials & Design*, vol. 95, pp. 518–533, 2016.
- [25] O. M. Querin, V. Toropov, D. Liu, H. Lohse-Busch, C. Hühne, S. Niemann, and B. Y. Kolesnikov, “Topology and parametric optimization of a lattice composite fuselage structure,” 2013.
- [26] S. Arabnejad and D. Pasini, “Mechanical properties of lattice materials via asymptotic homogenization and comparison with alternative homogenization methods,” *International Journal of Mechanical Sciences*, vol. 77, pp. 249–262, 2013.
- [27] R. Guinovart-Diaz, J. Bravo-Castillero, R. Rodriguez-Ramos, R. Martinez-Rosado, F. Serrania, and M. Navarrete, “Modeling of elastic transversely isotropic composite using the asymptotic homogenization method. Some comparisons with other models,” *Materials Letters*, vol. 56, no. 6, pp. 889–894, 2002.
- [28] S. Rosso, F. Uriati, L. Grigolato, R. Meneghello, G. Concheri, and G. Savio, “An Optimization Workflow in Design for Additive Manufacturing,” *Applied Sciences*, vol. 11, no. 6, p. 2572, 2021.
- [29] A. Booth, D. Papaioannou, and A. Sutton, *Systematic approaches to a successful literature review*. Los Angeles ; Thousand Oaks, Calif: Sage, 2012.
- [30] A. Bacciaglia, A. Ceruti, and A. Liverani, “A systematic review of voxelization method in additive manufacturing,” *Mechanics & Industry*, vol. 20, no. 6, p. 630, 2019.

- [31] S. Rosso, G. Savio, F. Uriati, R. Meneghello, and G. Concheri, “Optimization Approaches in Design for Additive Manufacturing,” *Proceedings of the Design Society: International Conference on Engineering Design*, vol. 1, no. 1, pp. 809–818, 2019.
- [32] W. Gao, Y. Zhang, D. Ramanujan, K. Ramani, Y. Chen, C. B. Williams, C. C. Wang, Y. C. Shin, S. Zhang, and P. D. Zavattieri, “The status, challenges, and future of additive manufacturing in engineering,” *Computer-Aided Design*, vol. 69, pp. 65–89, 2015.
- [33] A. E. Kaufman, “Volume visualization,” *ACM Computing Surveys*, vol. 28, no. 1, pp. 165–167, 1996.
- [34] B. Kitchenham, O. Pearl Brereton, D. Budgen, M. Turner, J. Bailey, and S. Linkman, “Systematic literature reviews in software engineering – A systematic literature review,” *Information and Software Technology*, vol. 51, no. 1, pp. 7–15, 2009.
- [35] F42 Committee, “Terminology for Additive Manufacturing Technologies,” tech. rep., ASTM International.
- [36] T. D. Ngo, A. Kashani, G. Imbalzano, K. T. Nguyen, and D. Hui, “Additive manufacturing (3D printing): A review of materials, methods, applications and challenges,” *Composites Part B: Engineering*, vol. 143, pp. 172–196, 2018.
- [37] A. Krishnakumar, K. Suresh, and A. Chandrasekar, “Towards Assembly-Free Methods for Additive Manufacturing Simulation,” in *Volume 1A: 35th Computers and Information in Engineering Conference*, (Boston, Massachusetts, USA), American Society of Mechanical Engineers, 2015.
- [38] N. Boddeti, Z. Ding, S. Kaijima, K. Maute, and M. L. Dunn, “Simultaneous Digital Design and Additive Manufacture of Structures and Materials,” *Scientific Reports*, vol. 8, no. 1, 2018.
- [39] A. Verma and R. Rai, “Computational Geometric Solutions for Efficient Additive Manufacturing Process Planning,” in *Volume 1A: 34th Computers and Information in Engineering Conference*, (Buffalo, New York, USA), American Society of Mechanical Engineers, 2014.
- [40] S. E. Ghiasian, P. Jaiswal, R. Rai, and K. Lewis, “From Conventional to Additive Manufacturing: Determining Component Fabrication Feasibility,” in *Volume 2A: 44th Design Automation Conference*, (Quebec City, Quebec, Canada), American Society of Mechanical Engineers, 2018.

- [41] Y.-S. Leung, H. Mao, and Y. Chen, “Approximate Functionally Graded Materials for Multi-Material Additive Manufacturing,” in *Volume 1A: 38th Computers and Information in Engineering Conference*, (Quebec City, Quebec, Canada), American Society of Mechanical Engineers, 2018.
- [42] U. S. Venkatesan and S. S. Pande, “Efficient Process Planning Strategies for Additive Manufacturing,” in *Volume 2: Additive Manufacturing; Materials*, (Los Angeles, California, USA), American Society of Mechanical Engineers, 2017.
- [43] J. Martinez, J. Dumas, and S. Lefebvre, “Procedural voronoi foams for additive manufacturing,” *ACM Transactions on Graphics*, vol. 35, no. 4, pp. 1–12, 2016.
- [44] G. A. da Silva, A. T. Beck, and O. Sigmund, “Stress-constrained topology optimization considering uniform manufacturing uncertainties,” *Computer Methods in Applied Mechanics and Engineering*, vol. 344, pp. 512–537, 2019.
- [45] G. Sossou, F. Demoly, G. Montavon, and S. Gomes, “Design for 4D printing: rapidly exploring the design space around smart materials,” *Procedia CIRP*, vol. 70, pp. 120–125, 2018.
- [46] G. Moroni, S. Petrò, and W. Polini, “Geometrical product specification and verification in additive manufacturing,” *CIRP Annals*, vol. 66, no. 1, pp. 157–160, 2017.
- [47] E. Shchurova and A. Shchurova, “A New File Format to Describe Fiber-reinforced Composite Workpiece Structure for Additive Technology Machines,” *Procedia Engineering*, vol. 129, pp. 105–110, 2015.
- [48] M. K. Thompson and M. Mischkot, “Design of Test Parts to Characterize Micro Additive Manufacturing Processes,” *Procedia CIRP*, vol. 34, pp. 223–228, 2015.
- [49] S.-i. Park and D. W. Rosen, “Quantifying effects of material extrusion additive manufacturing process on mechanical properties of lattice structures using as-fabricated voxel modeling,” *Additive Manufacturing*, vol. 12, pp. 265–273, 2016.
- [50] E. Doubrovski, E. Tsai, D. Dikovskiy, J. Geraedts, H. Herr, and N. Oxman, “Voxel-based fabrication through material property mapping: A design method for bitmap printing,” *Computer-Aided Design*, vol. 60, pp. 3–13, 2015.
- [51] G. Retsin and M. J. Garcia, “Discrete Computational Methods for Robotic Additive Manufacturing,” 2016.
- [52] O. Formoso, G. Trinh, S. Hu, and K. Cheung, “Development and Robustness Characterization of a Digital Material Assembly System,” *Procedia Manufacturing*, vol. 26, pp. 1003–1013, 2018.

- [53] F. Craveiro, H. Bartolo, A. Gale, J. Duarte, and P. Bartolo, “A design tool for resource-efficient fabrication of 3d-graded structural building components using additive manufacturing,” *Automation in Construction*, vol. 82, pp. 75–83, 2017.
- [54] J. Wu, N. Aage, R. Westermann, and O. Sigmund, “Infill Optimization for Additive Manufacturing—Approaching Bone-Like Porous Structures,” *IEEE Transactions on Visualization and Computer Graphics*, vol. 24, no. 2, pp. 1127–1140, 2018.
- [55] A. Ahsan, R. Xie, and B. Khoda, “Heterogeneous topology design and voxel-based bio-printing,” *Rapid Prototyping Journal*, vol. 24, no. 7, pp. 1142–1154, 2018.
- [56] S.-K. Ueng, L.-G. Chen, and S.-Y. Jen, “Voxel-based virtual manufacturing simulation for three-dimensional printing,” *Advances in Mechanical Engineering*, vol. 10, no. 6, 2018.
- [57] S.-I. Park and D. W. Rosen, “Homogenization of Mechanical Properties for Material Extrusion Periodic Lattice Structures Considering Joint Stiffening Effects,” *Journal of Mechanical Design*, vol. 140, no. 11, 2018.
- [58] A. Gleadall, I. Ashcroft, and J. Segal, “VOLCO: A predictive model for 3D printed microarchitecture,” *Additive Manufacturing*, vol. 21, pp. 605–618, 2018.
- [59] A. Aremu, J. Brennan-Craddock, A. Panesar, I. Ashcroft, R. Hague, R. Wildman, and C. Tuck, “A voxel-based method of constructing and skinning conformal and functionally graded lattice structures suitable for additive manufacturing,” *Additive Manufacturing*, vol. 13, pp. 1–13, 2017.
- [60] A. Ripetskiy, S. Zelenov, E. Kuznetsova, and L. Rabinskiy, “Evaluation of the Thermal Processes and Simulation Methods for Additive Manufacturing Based on the Geometry Voxel Representation,” *Key Engineering Materials*, vol. 771, pp. 91–96, 2018.
- [61] S. Dinda, D. Modi, T. W. Simpson, S. Tedia, and C. B. Williams, “Expediting Build Time, Material, and Cost Estimation for Material Extrusion Processes to Enable Mobile Applications,” in *Volume 2A: 43rd Design Automation Conference*, (Cleveland, Ohio, USA), American Society of Mechanical Engineers, 2017.
- [62] 3DHubs, “Additive manufacturing technologies.”
- [63] S. N. Reddy K., V. Maranan, T. W. Simpson, T. Palmer, and C. J. Dickman, “Application of Topology Optimization and Design for Additive Manufacturing Guidelines on an Automotive Component,” in *Volume 2A: 42nd Design Automation Conference*, (Charlotte, North Carolina, USA), American Society of Mechanical Engineers, 2016.

- [64] Z. Wang, C. Jiang, P. Liu, W. Yang, Y. Zhao, M. F. Horstemeyer, L.-Q. Chen, Z. Hu, and L. Chen, “Uncertainty quantification and reduction in metal additive manufacturing,” *npj Computational Materials*, vol. 6, no. 1, p. 175, 2020.
- [65] O. Sigmund, “A 99 line topology optimization code written in Matlab,” *Structural and Multidisciplinary Optimization*, vol. 21, no. 2, pp. 120–127, 2001.
- [66] D. Pham and R. Gault, “A comparison of rapid prototyping technologies,” *International Journal of Machine Tools and Manufacture*, vol. 38, no. 10-11, pp. 1257–1287, 1998.
- [67] P. Ferretti, C. Leon-Cardenas, G. M. Santi, M. Sali, E. Ciotti, L. Frizziero, G. Donnici, and A. Liverani, “Relationship between FDM 3D Printing Parameters Study: Parameter Optimization for Lower Defects,” *Polymers*, vol. 13, no. 13, p. 2190, 2021.
- [68] C. R. Deckard and J. J. Beaman, “Selective laser sintering with assisted powder handling,” 1990. Publisher: United States Patent and Trademark Office.
- [69] F. Uriati, F. Da Rin Betta, P. Ferro, S. Rosso, G. Savio, G. Concheri, and R. Meneghello, “High Density AlSi10Mg Aluminium Alloy Specimens Obtained by Selective Laser Melting,” in *Design Tools and Methods in Industrial Engineering* (C. Rizzi, A. O. Andrisano, F. Leali, F. Gherardini, F. Pini, and A. Vergnano, eds.), pp. 871–878, Cham: Springer International Publishing, 2020. Series Title: Lecture Notes in Mechanical Engineering.
- [70] K. Cooper, *Rapid Prototyping Technology*. CRC Press, 2001.
- [71] Y. L. Yap, C. Wang, S. L. Sing, V. Dikshit, W. Y. Yeong, and J. Wei, “Material jetting additive manufacturing: An experimental study using designed metrological benchmarks,” *Precision Engineering*, vol. 50, pp. 275–285, 2017.
- [72] M. L. Griffith, L. D. Harwell, J. T. Romero, E. Schlienger, C. L. Atwood, and J. E. Smugeresky, “Multi-material processing by LENS,” in *1997 International Solid Freeform Fabrication Symposium*, 1997.
- [73] L. J. Hornbeck, “Digital Light Processing for high-brightness high-resolution applications,” (San Jose, CA), pp. 27–40, 1997.
- [74] E.-A. Karabassi, G. Papaioannou, and T. Theoharis, “A Fast Depth-Buffer-Based Voxelization Algorithm,” *Journal of Graphics Tools*, vol. 4, no. 4, pp. 5–10, 1999.
- [75] P. Hurtik, P. Hodakova, and I. Perfilieva, “Fast String Searching Mechanism:,” (Gijón, Spain.), 2015.

- [76] D. J. Munk, T. Kipouros, G. A. Vio, G. T. Parks, and G. P. Steven, “Multiobjective and multi-physics topology optimization using an updated smart normal constraint bi-directional evolutionary structural optimization method,” *Structural and Multidisciplinary Optimization*, vol. 57, no. 2, pp. 665–688, 2018.
- [77] K. Liu and A. Tovar, “An efficient 3D topology optimization code written in Matlab,” *Structural and Multidisciplinary Optimization*, vol. 50, no. 6, pp. 1175–1196, 2014.
- [78] A. Ceruti, R. Ferrari, and A. Liverani, “Design for Additive Manufacturing Using LSWM: A CAD Tool for the Modelling of Lightweight and Lattice Structures,” in *Sustainable Design and Manufacturing 2017* (G. Campana, R. J. Howlett, R. Setchi, and B. Cimatti, eds.), vol. 68, pp. 756–765, Cham: Springer International Publishing, 2017. Series Title: Smart Innovation, Systems and Technologies.
- [79] A. Belyaev and Y. Ohtake, “A comparison of mesh smoothing methods,” in *Israel-Korea Bi-National Conference on Geometric Modeling and Computer Graphics*, (Tel Aviv, Israel), pp. 83 – 87, Tel Aviv University, 2003.
- [80] M. Boruciński and M. Królikowski, “Design of non-uniform truss structures for improved part properties,” *Advances in Manufacturing Science and Technology*, vol. 37, no. 4, 2013.
- [81] J. D. Hiller and H. Lipson, “Stl 2.0: A proposal for a universal multi-material additive manufacturing file format,” in *In Mechanical and Aerospace Engineering*, pp. 266–278, 2009.
- [82] A. Bacciaglia, A. Ceruti, and A. Liverani, “Additive Manufacturing Challenges and Future Developments in the Next Ten Years,” in *Design Tools and Methods in Industrial Engineering* (C. Rizzi, A. O. Andrisano, F. Leali, F. Gherardini, F. Pini, and A. Vergnano, eds.), pp. 891–902, Cham: Springer International Publishing, 2020. Series Title: Lecture Notes in Mechanical Engineering.
- [83] A. Bacciaglia, A. Ceruti, and A. Liverani, “Photogrammetry and Additive Manufacturing Based Methodology for Decentralized Spare Part Production in Automotive Industry,” in *Intelligent Human Systems Integration 2020* (T. Ahram, W. Karwowski, A. Vergnano, F. Leali, and R. Taiar, eds.), vol. 1131, pp. 796–802, Cham: Springer International Publishing, 2020. Series Title: Advances in Intelligent Systems and Computing.
- [84] A. Bacciaglia, A. Ceruti, and A. Liverani, “Towards Large Parts Manufacturing in Additive Technologies for Aerospace and Automotive applications,” *Procedia Computer Science*, vol. 200, pp. 1113–1124, 2022.

- [85] B. Redwood, B. Garrett, and F. Schöffner, *The 3D printing handbook: technologies, design and applications*. Amsterdam: 3D Hubs, 2017.
- [86] D. Systems, “StereoLithography Interface Specification,” 1988.
- [87] M. C. Shellabear and O. J. Nyrhilae, “DMLS - Development history and state of the art,” (Erlangen, Germany), 2004.
- [88] E. Eilam and E. J. Chikofsky, *Reversing: secrets of reverse engineering*. Indianapolis, IN: Wiley, 2005.
- [89] J. Holmström, J. Partanen, J. Tuomi, and M. Walter, “Rapid manufacturing in the spare parts supply chain: Alternative approaches to capacity deployment,” *Journal of Manufacturing Technology Management*, vol. 21, no. 6, pp. 687–697, 2010.
- [90] P. Liu, S. H. Huang, A. Mokasdar, H. Zhou, and L. Hou, “The impact of additive manufacturing in the aircraft spare parts supply chain: supply chain operation reference (scor) model based analysis,” *Production Planning & Control*, vol. 25, no. 13-14, pp. 1169–1181, 2014.
- [91] Y. Li, Y. Cheng, Q. Hu, S. Zhou, L. Ma, and M. K. Lim, “The influence of additive manufacturing on the configuration of make-to-order spare parts supply chain under heterogeneous demand,” *International Journal of Production Research*, vol. 57, no. 11, pp. 3622–3641, 2019.
- [92] S. H. Khajavi, J. Holmström, and J. Partanen, “Additive manufacturing in the spare parts supply chain: hub configuration and technology maturity,” *Rapid Prototyping Journal*, vol. 24, no. 7, pp. 1178–1192, 2018.
- [93] F. Pérès and D. Noyes, “Envisioning e-logistics developments: Making spare parts in situ and on demand,” *Computers in Industry*, vol. 57, no. 6, pp. 490–503, 2006.
- [94] K. Schindler, “Mathematical foundations of photogrammetry,” tech. rep., ETH Zurich, Switzerland.
- [95] “GE jet engine bracket challenge.”
- [96] R. Leal, F. M. Barreiros, L. Alves, F. Romeiro, J. C. Vasco, M. Santos, and C. Marto, “Additive manufacturing tooling for the automotive industry,” *The International Journal of Advanced Manufacturing Technology*, vol. 92, no. 5-8, pp. 1671–1676, 2017.
- [97] M. Dumas, P. Terriault, and V. Brailovski, “Modelling and characterization of a porosity graded lattice structure for additively manufactured biomaterials,” *Materials & Design*, vol. 121, pp. 383–392, 2017.

- [98] Y. Kok, X. Tan, P. Wang, M. Nai, N. Loh, E. Liu, and S. Tor, “Anisotropy and heterogeneity of microstructure and mechanical properties in metal additive manufacturing: A critical review,” *Materials & Design*, vol. 139, pp. 565–586, 2018.
- [99] M. L. McMillan, M. Jurg, M. Leary, and M. Brandt, “Programmatic generation of computationally efficient lattice structures for additive manufacture,” *Rapid Prototyping Journal*, vol. 23, no. 3, pp. 486–494, 2017.
- [100] I. Campbell, D. Bourell, and I. Gibson, “Additive manufacturing: rapid prototyping comes of age,” *Rapid Prototyping Journal*, vol. 18, no. 4, pp. 255–258, 2012.
- [101] ANSI, “Standardization Roadmap for Additive Manufacturing,” 2018.
- [102] C. Ferro, R. Grassi, C. Seclì, and P. Maggiore, “Additive Manufacturing Offers New Opportunities in UAV Research,” *Procedia CIRP*, vol. 41, pp. 1004–1010, 2016.
- [103] L. Frizziero, G. M. Santi, G. Donnici, C. Leon-Cardenas, P. Ferretti, A. Liverani, and M. Neri, “An Innovative Ford Sedan with Enhanced Stylistic Design Engineering (SDE) via Augmented Reality and Additive Manufacturing,” *Designs*, vol. 5, no. 3, p. 46, 2021.
- [104] “3dWasp.”
- [105] U. Klaeger and A. Telesh, “Novel Robotic 3D Printing Technology for the Manufacture of Large Parts,” in *Progress in Digital and Physical Manufacturing* (H. A. Almeida and J. C. Vasco, eds.), (Cham), pp. 40–45, Springer International Publishing, 2020.
- [106] G. Savio, R. Meneghello, and G. Concheri, “Optimization of lattice structures for Additive Manufacturing Technologies,” in *Advances on Mechanics, Design Engineering and Manufacturing* (B. Eynard, V. Nigrelli, S. M. Oliveri, G. Peris-Fajarnes, and S. Rizzuti, eds.), pp. 213–222, Cham: Springer International Publishing, 2017. Series Title: Lecture Notes in Mechanical Engineering.
- [107] A. B. Naveed, S. I. Butt, A. Mubashar, F. N. Chaudhry, N. u. Qadir, and Z. Faping, “Design and verification of enhanced CFRTPCs fabrication technique using fused deposition modeling,” *Journal of Thermoplastic Composite Materials*, 2020.
- [108] J. Laureto and J. Pearce, “Open Source Multi-Head 3D Printer for Polymer-Metal Composite Component Manufacturing,” *Technologies*, vol. 5, no. 2, p. 36, 2017.
- [109] BCN3D, “BCN3D’s signature IDEX Technology: Doubling productivity while halving costs.”

- [110] C. Duran, V. Subbian, M. T. Giovanetti, J. R. Simkins, and F. R. Beyette Jr, “Experimental desktop 3D printing using dual extrusion and water-soluble polyvinyl alcohol,” *Rapid Prototyping Journal*, vol. 21, no. 5, pp. 528–534, 2015.
- [111] P. Pecho, V. Ažaltovič, B. Kandra, and M. Bugaj, “Introduction study of design and layout of UAVs 3D printed wings in relation to optimal lightweight and load distribution,” *Transportation Research Procedia*, vol. 40, pp. 861–868, 2019.
- [112] W. Associates, ed., *Wohlers report 2021: 3D printing and additive manufacturing state of the industry annual worldwide progress report*. Fort Collins (Colo.): Wohlers Associates, 2021.
- [113] L. Frizziero, G. M. Santi, C. Leon-Cardenas, G. Donnici, A. Liverani, P. Papaleo, F. Napolitano, C. Pagliari, G. L. Di Gennaro, S. Stallone, S. Stilli, G. Trisolino, and P. Zarantonello, “In-House, Fast FDM Prototyping of a Custom Cutting Guide for a Lower-Risk Pediatric Femoral Osteotomy,” *Bioengineering*, vol. 8, no. 6, p. 71, 2021.
- [114] S. K. Moon, Y. E. Tan, J. Hwang, and Y.-J. Yoon, “Application of 3D printing technology for designing light-weight unmanned aerial vehicle wing structures,” *International Journal of Precision Engineering and Manufacturing-Green Technology*, vol. 1, no. 3, pp. 223–228, 2014.
- [115] M. Heppa, “The impact of direct digital manufacturing on supply chain operations, cost and environmental performance in an aerospace application,” Master’s thesis, Concordia University, 2018.
- [116] Safran, “Safran unveils Add+, an engine demonstrator built using 30% 3D-printed components,” 2019.
- [117] EDAG, “EDAG Insights 1/15 - EDAG Light Cocoon,” 2015.
- [118] S. Cottrell and J. Howell, “Reproducing musical instrument components from manufacturers’ technical drawings using 3D printing: Boosey & Hawkes as a case study,” *Journal of New Music Research*, vol. 48, no. 5, pp. 449–457, 2019.
- [119] A. Bacciaglia, A. Ceruti, and A. Liverani, “Evaluation of 3D printed mouthpieces for musical instruments,” *Rapid Prototyping Journal*, vol. 26, no. 3, pp. 577–584, 2019.
- [120] A. Bacciaglia, A. Ceruti, and A. Liverani, “A design of experiment approach to 3D-printed mouthpieces sound analysis,” *Progress in Additive Manufacturing*, vol. 6, no. 3, pp. 571–587, 2021.

- [121] A. Bacciaglia, A. Ceruti, and A. Liverani, “Proposal of a standard for 2D representation of bio-inspired lightweight lattice structures in drawings,” *Proceedings of the Institution of Mechanical Engineers, Part C: Journal of Mechanical Engineering Science*, 2020.
- [122] A. Bacciaglia, A. Ceruti, and A. Liverani, “Structural Analysis of Voxel-Based Lattices Using 1D Approach,” *3D Printing and Additive Manufacturing*, 2021.
- [123] S. Llorente, “Honeycomb sandwich primary structure applications on the Boeing model 360 helicopter,” in *International SAMPE Symposium and Exhibition*, vol. 34 (1), pp. 824 – 838, SAMPE, Covina, CA, United States, 1989.
- [124] G. Campo, A. Vettorello, and M. Giacalone, “Optimization Methodology for Continuous Heterogeneous Structures: A Preliminary Design of an Engine Mounting Bracket,” *Key Engineering Materials*, vol. 827, pp. 116–121, 2019.
- [125] I. Maskery, L. Sturm, A. Aremu, A. Panesar, C. Williams, C. Tuck, R. Wildman, I. Ashcroft, and R. Hague, “Insights into the mechanical properties of several triply periodic minimal surface lattice structures made by polymer additive manufacturing,” *Polymer*, vol. 152, pp. 62–71, 2018.
- [126] S. Rosso, A. Curtarello, F. Basana, L. Grigolato, R. Meneghello, G. Concheri, and G. Savio, “Modeling Symmetric Minimal Surfaces by Mesh Subdivision,” in *Advances on Mechanics, Design Engineering and Manufacturing III* (L. Roucoules, M. Paredes, B. Eynard, P. Morer Camo, and C. Rizzi, eds.), pp. 249–254, Cham: Springer International Publishing, 2021. Series Title: Lecture Notes in Mechanical Engineering.
- [127] F. Tamburrino, S. Graziosi, and M. Bordegoni, “The Design Process of Additively Manufactured Mesoscale Lattice Structures: A Review,” *Journal of Computing and Information Science in Engineering*, vol. 18, no. 4, 2018.
- [128] E. Dragoni and V. A. Ciace, “Mechanical design and modelling of lightweight additively manufactured lattice structures evolved from regular three-dimensional tessellations,” *Proceedings of the Institution of Mechanical Engineers, Part C: Journal of Mechanical Engineering Science*, vol. 235, no. 10, pp. 1759–1773, 2021.
- [129] D. S. Nguyen and F. Vignat, “A method to generate lattice structure for Additive Manufacturing,” in *2016 IEEE International Conference on Industrial Engineering and Engineering Management (IEEM)*, pp. 966–970, 2016.
- [130] D. W. Rosen, “Computer-Aided Design for Additive Manufacturing of Cellular Structures,” *Computer-Aided Design and Applications*, vol. 4, no. 5, pp. 585–594, 2007.

- [131] S. Y. Choy, C.-N. Sun, K. F. Leong, and J. Wei, “Compressive properties of Ti-6Al-4V lattice structures fabricated by selective laser melting: Design, orientation and density,” *Additive Manufacturing*, vol. 16, pp. 213–224, 2017.
- [132] J. Austermann, A. J. Redmann, V. Dahmen, A. L. Quintanilla, S. J. Mecham, and T. A. Osswald, “Fiber-Reinforced Composite Sandwich Structures by Co-Curing with Additive Manufactured Epoxy Lattices,” *Journal of Composites Science*, vol. 3, no. 2, p. 53, 2019.
- [133] M. Mazur, M. Leary, M. McMillan, S. Sun, D. Shidid, and M. Brandt, “Mechanical properties of Ti6Al4V and AlSi12Mg lattice structures manufactured by Selective Laser Melting (SLM),” in *Laser Additive Manufacturing*, pp. 119–161, Elsevier, 2017.
- [134] M. McMillan, M. Jurg, M. Leary, and M. Brandt, “Programmatic Lattice Generation for Additive Manufacture,” *Procedia Technology*, vol. 20, pp. 178–184, 2015.
- [135] L. J. Gibson and M. F. Ashby, *Cellular solids: structure and properties*. Cambridge solid state science series, Cambridge: Cambridge Univ. Press, 2. ed., 1. paperback ed. (with corr.), transferred to digital printing ed., 2001.
- [136] R. Hutchinson and N. Fleck, “The structural performance of the periodic truss,” *Journal of the Mechanics and Physics of Solids*, vol. 54, no. 4, pp. 756–782, 2006.
- [137] J. Chen, “Fracture analysis of cellular materials: A strain gradient model,” *Journal of the Mechanics and Physics of Solids*, vol. 46, no. 5, pp. 789–828, 1998.
- [138] R. V. Craster, J. Kaplunov, and A. V. Pichugin, “High-frequency homogenization for periodic media,” *Proceedings of the Royal Society A: Mathematical, Physical and Engineering Sciences*, vol. 466, no. 2120, pp. 2341–2362, 2010.
- [139] C. Florence and K. Sab, “A rigorous homogenization method for the determination of the overall ultimate strength of periodic discrete media and an application to general hexagonal lattices of beams,” *European Journal of Mechanics - A/Solids*, vol. 25, no. 1, pp. 72–97, 2006.
- [140] C.-M. Chen, N. Kikuchi, and F. Rostam-Abadi, “An enhanced asymptotic homogenization method of the static and dynamics of elastic composite laminates,” *Computers & Structures*, vol. 82, no. 4-5, pp. 373–382, 2004.
- [141] A. L. Kalamkarov, I. V. Andrianov, and V. V. Danishevs’kyi, “Asymptotic Homogenization of Composite Materials and Structures,” *Applied Mechanics Reviews*, vol. 62, no. 3, 2009.
- [142] P. r. manual, “The neutral file,” 2018.

- [143] A. Vigliotti and D. Pasini, “Stiffness and strength of tridimensional periodic lattices,” *Computer Methods in Applied Mechanics and Engineering*, vol. 229-232, pp. 27–43, 2012.
- [144] E. Andreassen and C. S. Andreasen, “How to determine composite material properties using numerical homogenization,” *Computational Materials Science*, vol. 83, pp. 488–495, 2014.
- [145] G. Dong, Y. Tang, and Y. F. Zhao, “A 149 Line Homogenization Code for Three-Dimensional Cellular Materials Written in matlab,” *Journal of Engineering Materials and Technology*, vol. 141, no. 1, 2019.
- [146] A. Vigliotti and D. Pasini, “Mechanical properties of hierarchical lattices,” *Mechanics of Materials*, vol. 62, pp. 32–43, 2013.
- [147] Renishaw, “Ti6Al4V ELI-0406 powder for additive manufacturing Datasheet,” 2017.
- [148] R. D. Cook, *Finite element modeling for stress analysis*. New York: Wiley, 1995.
- [149] S. Mantovani, G. Campo, and M. Giacalone, “Steering column support topology optimization including lattice structure for metal additive manufacturing,” *Proceedings of the Institution of Mechanical Engineers, Part C: Journal of Mechanical Engineering Science*, 2020.
- [150] A. Ceruti, P. Marzocca, A. Liverani, and C. Bil, “Maintenance in aeronautics in an Industry 4.0 context: The role of Augmented Reality and Additive Manufacturing,” *Journal of Computational Design and Engineering*, vol. 6, no. 4, pp. 516–526, 2019.
- [151] “DIN EN 4408-001:2007-06, Aerospace series - Technical drawings - Representation of parts made of composite materials - Part 1: General rules,” tech. rep., ASD-STAN - Aerospace, 2005.
- [152] J. Wong, L. Ryan, and I. Y. Kim, “Design optimization of aircraft landing gear assembly under dynamic loading,” *Structural and Multidisciplinary Optimization*, vol. 57, no. 3, pp. 1357–1375, 2018.
- [153] M. Cavazzuti, A. Baldini, E. Bertocchi, D. Costi, E. Torricelli, and P. Moruzzi, “High performance automotive chassis design: a topology optimization based approach,” *Structural and Multidisciplinary Optimization*, vol. 44, no. 1, pp. 45–56, 2011.
- [154] G. Percoco, A. E. Uva, M. Fiorentino, M. Gattullo, V. M. Manghisi, and A. Boccaccio, “Mechanobiological Approach to Design and Optimize Bone Tissue Scaffolds 3D Printed with Fused Deposition Modeling: A Feasibility Study,” *Materials*, vol. 13, no. 3, p. 648, 2020.

- [155] M. Ohsaki, *Optimization of finite dimensional structures*. Boca Raton: CRC Press/-Taylor & Francis, 2011.
- [156] S. Krish, “A practical generative design method,” *Computer-Aided Design*, vol. 43, no. 1, pp. 88–100, 2011.
- [157] A. Bacciaglia, A. Ceruti, and A. Liverani, “Advanced Smoothing for Voxel-based Topologically Optimized 3D Models,” in *2020 IEEE 10th International Conference Nanomaterials: Applications & Properties (NAP)*, (Sumy, Ukraine), pp. 1–5, IEEE, 2020.
- [158] A. Bacciaglia, A. Ceruti, and A. Liverani, “Surface smoothing for topological optimized 3D models,” *Structural and Multidisciplinary Optimization*, 2021.
- [159] S. Mantovani, G. A. Campo, and A. Ferrari, “Additive manufacturing and topology optimization: A design strategy for a steering column mounting bracket considering overhang constraints,” *Proceedings of the Institution of Mechanical Engineers, Part C: Journal of Mechanical Engineering Science*, vol. 235, no. 10, pp. 1703–1723, 2021.
- [160] M. P. Bendsøe, “Optimal shape design as a material distribution problem,” *Structural Optimization*, vol. 1, no. 4, pp. 193–202, 1989.
- [161] Y. Xie and G. Steven, “Evolutionary structural optimization for dynamic problems,” *Computers & Structures*, vol. 58, no. 6, pp. 1067–1073, 1996.
- [162] Q. Li, G. Steven, and Y. Xie, “A simple checkerboard suppression algorithm for evolutionary structural optimization,” *Structural and Multidisciplinary Optimization*, vol. 22, no. 3, pp. 230–239, 2001.
- [163] O. Sigmund, “On the Design of Compliant Mechanisms Using Topology Optimization*,” *Mechanics of Structures and Machines*, vol. 25, no. 4, pp. 493–524, 1997.
- [164] X. Gao, L. Li, and H. Ma, “An Adaptive Continuation Method for Topology Optimization of Continuum Structures Considering Buckling Constraints,” *International Journal of Applied Mechanics*, vol. 09, no. 07, 2017.
- [165] M. Denk, “ToOptix.”
- [166] A. T. Gaynor, N. A. Meisel, C. B. Williams, and J. K. Guest, “Multiple-Material Topology Optimization of Compliant Mechanisms Created Via PolyJet Three-Dimensional Printing,” *Journal of Manufacturing Science and Engineering*, vol. 136, no. 6, 2014.
- [167] R. Rezaie, M. Badrossamay, A. Ghaie, and H. Moosavi, “Topology Optimization for Fused Deposition Modeling Process,” *Procedia CIRP*, vol. 6, pp. 521–526, 2013.

- [168] T. Zegard and G. H. Paulino, “Bridging topology optimization and additive manufacturing,” *Structural and Multidisciplinary Optimization*, vol. 53, no. 1, pp. 175–192, 2016.
- [169] G. Costa, M. Montemurro, and J. Pailhès, “NURBS hyper-surfaces for 3D topology optimization problems,” *Mechanics of Advanced Materials and Structures*, vol. 28, no. 7, pp. 665–684, 2021.
- [170] A. Buades, B. Coll, and J. M. Morel, “A Review of Image Denoising Algorithms, with a New One,” *Multiscale Modeling & Simulation*, vol. 4, no. 2, pp. 490–530, 2005.
- [171] O. Sorkine, “Laplacian Mesh Processing,” *Eurographics 2005 - State of the Art Reports*, p. 18 pages, 2005. Artwork Size: 18 pages Publisher: The Eurographics Association.
- [172] M. Wei, J. Huang, X. Xie, L. Liu, J. Wang, and J. Qin, “Mesh Denoising Guided by Patch Normal Co-Filtering via Kernel Low-Rank Recovery,” *IEEE Transactions on Visualization and Computer Graphics*, vol. 25, no. 10, pp. 2910–2926, 2019.
- [173] G. Taubin, “A signal processing approach to fair surface design,” in *Proceedings of the 22nd annual conference on Computer graphics and interactive techniques - SIGGRAPH '95*, pp. 351–358, ACM Press, 1995.
- [174] M. Desbrun, M. Meyer, P. Schröder, and A. H. Barr, “Implicit fairing of irregular meshes using diffusion and curvature flow,” in *Proceedings of the 26th annual conference on Computer graphics and interactive techniques - SIGGRAPH '99*, pp. 317–324, ACM Press, 1999.
- [175] J. Vollmer, R. Mencl, and H. Muller, “Improved Laplacian Smoothing of Noisy Surface Meshes,” *Computer Graphics Forum*, vol. 18, no. 3, pp. 131–138, 1999.
- [176] X. Qu and B. Stucker, “Circular hole recognition for STL-based toolpath generation,” *Rapid Prototyping Journal*, vol. 11, no. 3, pp. 132–139, 2005.
- [177] G. Costa, M. Montemurro, and J. Pailhès, “A 2D topology optimisation algorithm in NURBS framework with geometric constraints,” *International Journal of Mechanics and Materials in Design*, vol. 14, no. 4, pp. 669–696, 2018.
- [178] F. Sotiropoulos and X. Yang, “Immersed boundary methods for simulating fluid–structure interaction,” *Progress in Aerospace Sciences*, vol. 65, pp. 1–21, 2014.
- [179] M. Ezkurra, J. A. Esnaola, M. Martinez-Agirre, U. I. Etxeberria, U. Lertxundi, L. Colomo, M. Begiristain, and I. Zurutuza, “Analysis of One-Way and Two-Way FSI Approaches to Characterise the Flow Regime and the Mechanical Behaviour

- during Closing Manoeuvring Operation of a Butterfly Valve,” *World Academy of Science, Engineering and Technology, International Journal of Mechanical, Aerospace, Industrial, Mechatronic and Manufacturing Engineering*, vol. 12, pp. 313–319, 2018.
- [180] R. Carmichael and L. Erickson, “PAN AIR - A higher order panel method for predicting subsonic or supersonic linear potential flows about arbitrary configurations,” in *14th Fluid and Plasma Dynamics Conference*, (Palo Alto, CA, U.S.A.), American Institute of Aeronautics and Astronautics, 1981.
- [181] J. Katz and A. Plotkin, *Low-speed aerodynamics: from wing theory to panel methods*. McGraw-Hill series in aeronautical and aerospace engineering, New York: McGraw-Hill, 1991.
- [182] K. Kobayashi, H. Shimizu, and M. Kaiho, “Numerical Simulation of Unsteady Turbulent Flow by Voxel Method,” *JSME International Journal Series B*, vol. 47, no. 3, pp. 477–482, 2004.
- [183] K. Onishi, R. Bale, and M. Tsubokura, “Assessment of Rotating Wheel Vehicle Aerodynamics Simulation Using Cartesian Grid Method and Open-Grill Full Vehicle Models,” 2019.
- [184] A. Bacciaglia, A. Ceruti, and A. Liverani, “A Voxel-Based 2.5D Panel Method for Fluid-Dynamics Simulations,” in *Design Tools and Methods in Industrial Engineering II* (C. Rizzi, F. Campana, M. Bici, F. Gherardini, T. Ingrassia, and P. Cicconi, eds.), pp. 13–26, Cham: Springer International Publishing, 2022. Series Title: Lecture Notes in Mechanical Engineering.
- [185] A. Bacciaglia, A. Ceruti, and A. Liverani, “A 3D Voxel-based Approach for Fast Aerodynamic Analyses in Conceptual Design Phases,” *Computer-Aided Design and Applications*, vol. 19, no. 6, pp. 1236–1254, 2022.
- [186] S. Ahmed, G. Ramm, and G. Faltin, “Some Salient Features Of The Time-Averaged Ground Vehicle Wake,” 1984.
- [187] D. Filkovic and Z. Virag, *Apame 3D Panel Method*. PhD thesis, University of Zagreb, 2008.
- [188] S. Bilal, “Source Panel Method applied to Flow around Cylinder.”
- [189] VBBV, “2D panel method for Cp distribution on airfoils.”
- [190] C. C. GmbH, “OpenAPAME.”
- [191] H. W. M. Hoeijmakers, “Panel Methods in Aerodynamics; Some Highlights,” in *Panel Methods in Fluid Mechanics with Emphasis on Aerodynamics: Proceedings of*

- the Third GAMM-Seminar Kiel, January 16 to 18, 1987* (J. Ballmann, R. Eppler, and W. Hackbusch, eds.), pp. 1–34, Wiesbaden: Vieweg+Teubner Verlag, 1988.
- [192] A. Adam, “Converting a 3D logical array into an STL surface mesh,” 2021.
- [193] M. Drela, “XFOIL: An Analysis and Design System for Low Reynolds Number Airfoils,” in *Low Reynolds Number Aerodynamics* (C. A. Brebbia, S. A. Orszag, J. H. Seinfeld, P. Spanos, A. S. Cakmak, P. Silvester, C. S. Desai, G. Pinder, R. McCrory, S. Yip, F. A. Leckie, A. R. S. Ponter, K.-P. Holz, K.-J. Bathe, J. Connor, W. Wunderlich, J. Argyris, and T. J. Mueller, eds.), vol. 54, pp. 1–12, Berlin, Heidelberg: Springer Berlin Heidelberg, 1989. Series Title: Lecture Notes in Engineering.
- [194] J. D. Anderson, *Fundamentals of aerodynamics*. McGraw-Hill series in aeronautical and aerospace engineering, Singapore: McGraw-Hill, 5. ed. in si units ed., 2011.
- [195] I. Dobrev and F. Massouh, “Investigation of relationship between drag and lift coefficients for a generic car model,” in *BULTRANS-2014 Proceedings*, (Sozopol, Bulgaria).
- [196] H. Schlichting and K. Gersten, *Boundary-Layer Theory*. Berlin, Heidelberg: Springer Berlin Heidelberg, 2017.
- [197] W. E. Baker, P. A. Cox, J. J. Kulesz, R. A. Strehlow, and P. S. Westine, *Explosion Hazards and Evaluation*. Saint Louis: Elsevier Science, 2014.